

Losi 5ive wheel analysis

Federico Fornerone

Politecnico di Torino, Department of Mechanical and Aerospace Engineering
Corso Duca degli Abruzzi, 24 – 10129 Torino, Italy

Index

Index.....	1
Abstract	3
Introduction	4
1. Studied vehicle.....	5
1.1 Wheel.....	5
2. Static stiffness evaluation	7
2.1 Introduction.....	7
2.2 Experimental setup	8
2.3 Structure building.....	8
2.4 Components weighting.....	11
2.5 Measurement.....	12
2.6 Wire study.....	15
3. Tyre test-rig	19
3.1 Test-rig project.....	19
3.2 Wheel support building	23
3.3 Counterweight system	25
3.4 Feasibility study	26
3.4.1 Wheel support mass.....	26
3.4.2 Angular plate fixing.....	27
3.5 Test-rig assembly	29
4. Dynamic stiffness evaluation.....	37
4.1 Setup.....	37
4.1.1 Hardware setup.....	37
4.1.2 Software setup	38
4.2 Data acquisition.....	40
4.3 Raw data	42
4.4 Post-processing	50
4.5 Natural frequencies (first attempt)	52
4.6 Dynamic stiffness calculation (first attempt).....	54
4.7 Simulation.....	57
4.7.1 Solidworks simulation	57
4.7.2 LUPOS simulation.....	59
4.7.3 Frequencies comparison.....	63
4.8 Natural frequencies.....	63
4.9 Dynamic stiffness estimation.....	64

5. Wheel simulation	68
5.1 Model structure	68
5.1.1 Structure points.....	72
5.2 Parametric analysis.....	78
5.3 Free real modal analysis	81
5.3.1 Rim and disc real modal analysis	89
5.3.2 Foam insert real modal analysis	97
5.3.3 Tyre real modal analysis	105
5.4 Pinned real modal analysis	113
5.5 Results comparison.....	120
Conclusions	122
Reference.....	123

Abstract

The main objective of the experiment is the evaluation of the dynamics of the wheels of a car model (the radio controlled Losi 5ive-T 2.0 1:5).

This study requires some laboratory tests in order to obtain stiffness characteristic. The first test to be done is a static test, in order to evaluate the static stiffness of the tire. Then a dynamic test is required to evaluate the dynamic behaviour.

After the experimental tests a FEM simulation is done to investigate the dynamics in a numeric way.

As it will be explained, this kind of wheel has several components that can modify the wheel dynamics. For this reason, multiple tests must be done with all the possible configurations of these components.

Introduction

The first part of this thesis is the static study. This preliminary study consents the determination of the static stiffness of the wheel in all the possible configurations. To do this a simple idea is used: some known weights are applied to the wheel and the deformation is measured. Then, knowing the applied force and the deformation the stiffness could be easily calculated.

With this test it is possible to have an idea of the wheel stiffness and these first results will be useful for the dynamic test. The static test will be better explained in chapter two.

For the dynamic test a special testrig is needed. In this thesis the project of this testrig and its construction is shown in chapter three.

Chapter four explain the dynamic test. The basic idea is to apply a known force and measuring the resulting accelerations and displacement with some appropriate sensors. Knowing the system response, the wheel stiffness can be estimated.

In the final chapter, a wheel simulation is studied. This study consists in the modelling and some real modal analysis to know the wheel frequencies. In the future, this wheel model could be integrated in an entire car model in order to analyse the whole car frequencies.

1. Studied vehicle

The studied vehicle is the Losi 5ive-T 2.0 [4] (Figure 1.1 and Figure 1.2).



Figure 1.1 – Losi 5ive-T 2.0 [4].



Figure 1.2 – Wheel detail of Losi 5ive-T 2.0 [4].

This vehicle is a radio controlled 1:5 model. It is powered by a 32cc air cooled gasoline engine with a 4WD transmission.

This model has been chosen thanks to its many possibility in terms of components choices. In fact, it is possible to replace a lot of components including the dampers oil, the suspensions springs, the tyre and the tyres inserts.

1.1 Wheel

The studied component of this model is the wheel (Figure 1.1.1).

This wheel is composed by numerous parts. As it is possible to see in Figure 1.1.2 and Figure 1.1.3 the base is the wheel rim on which the foam insert, and the tire are mounted. On the sides two plastic supports are screwed on the rim to keep all the components together.



Figure 1.1.1 – Wheel



Figure 1.1.2 – Wheel rim and the lateral supports.



Figure 1.1.3 – Tyres and foam inserts.

2. Static stiffness evaluation

2.1 Introduction

The wheel components are shown in Figure 2.1.1.



Figure 2.1.1 – Wheel

As it is possible to see from Figure 2.1.1 the wheel is composed by many parts. The disc (1) is the main support, it is in fact the base for the other components and also the connection point of the wheel on the hub. On the disc there is the rim, and on the rim the foam insert (2) is located (which has the purpose of increasing the stiffness and the damping of the tire) and the tire (3) are mounted. Then two lateral supports (4 and 5) are mounted to hold both tire and foam in the right axial position.

The objective of this experiment is the estimation of the tire stiffness in all the four different cases (two type of tyre with and without insert) using an appropriate experimental set-up. In the following sections the structure and the measurement method are explained. Then the results are reported and analysed. In Figure 2.1.2 the two type of tyre are shown, they are recognisable mainly for the different tyre profile.



Figure 2.1.2 – Tyre type LOS 45023 (left) and LOSB 7240 (right)

2.2 Experimental setup

The basic idea of this experiment is a static test, in which several weights are used in order to obtain a tyre deformation. Then, knowing the applied forces and the resultant deformations, the static stiffness can be calculated.

The starting scheme is shown in Figure 2.2.1.

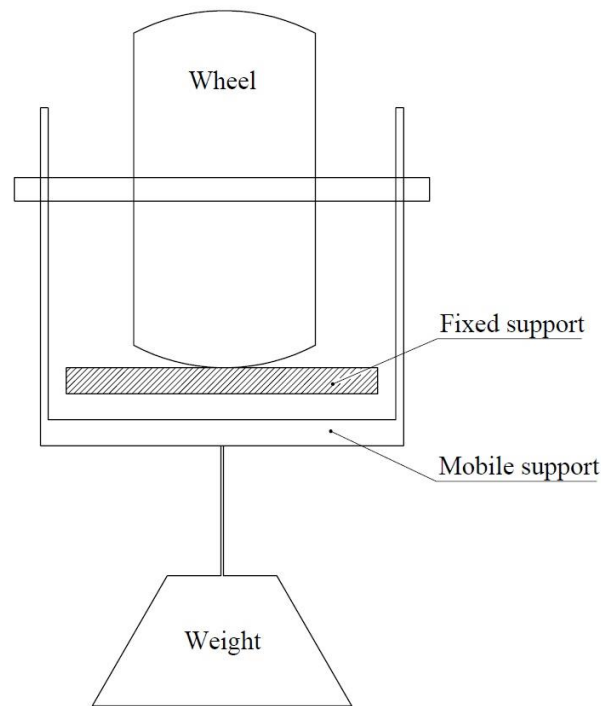


Figure 2.2.1 – Starting scheme of the experiment.

The scheme shows the wheel placed over a fixed support. A mobile support is required to hold the wheel in position. On the lower side of the mobile support the weight is fixed.

Knowing the values of the applied weights and the deformation of the tyre (that can be measured looking at the distance between the fixed and the mobile supports) the tyre stiffness can be calculated using:

$$k = \frac{F}{x} \quad (2.2.1)$$

$$F = mg \quad (2.2.2)$$

where the mass m includes all the weights mass and the mobile support mass.

So, after the defining of the basic scheme the real components must be found. In particular two things have to be defined: the building of the structures and the measuring process.

2.3 Structure building

The main structures that must be built are mainly the fixed support and the mobile support.

For the mobile support the easiest way is the use of the exact same support projected for the dynamic tests. The process of designing and building of this support are explained in the next chapters. The mobile support with the wheel is shown in Figure 2.3.1.



Figure 2.3.1 – Wheel mounted on the mobile support.

For the fixed support, an aluminium bar fixed on the workbench is used. The aluminium bars are perfect for this use because of the strength that are capable of and the fixing easiness. The problem with the aluminium bars is that the lateral surface is not plane. This could bring errors in the measuring phase. To solve this a thin steel plate is fixed on the aluminium bar using two clamps. In Figure 2.3.2 and Figure 2.3.3 the overall structure (mobile and fixed support) is shown.

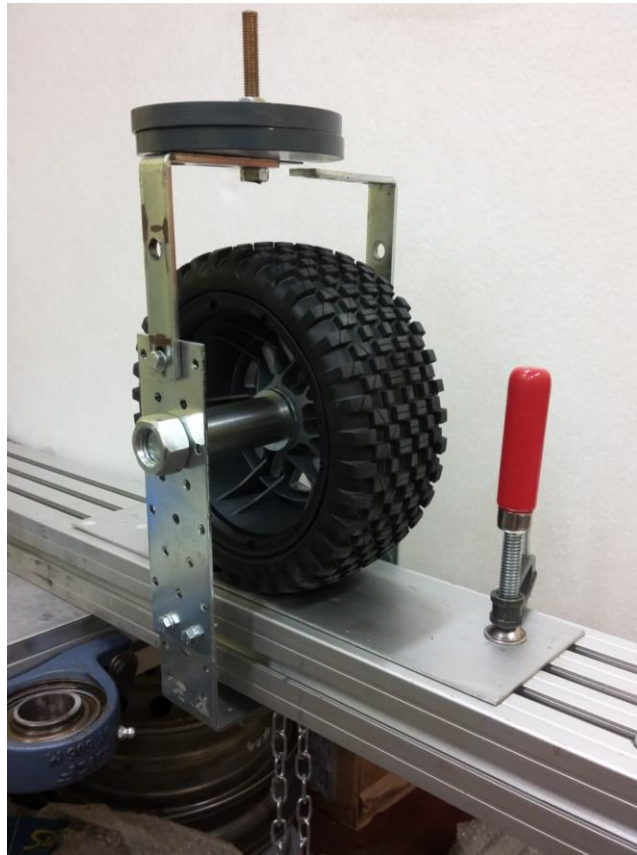


Figure 2.3.2 – Mobile support detail.

In Figure 2.3.2 it is possible to see the mobile support above the aluminium bar fixed on the workbench. Between the tyre and the bar, the thin steel plate is visible. On the lower part of the figure, there is the chain that support the weights. On the upper part there is a modify of the mobile structure occurred during the test with a pair of weights fixed on it. That weights have the function of balancing the structure and keeping the centre of gravity and the application point of the test weight perfectly vertical. The wheel and the mobile support in fact do not present a perfect symmetry and this could lead to an inclination of the wheel during the test.

In Figure 2.3.3 it is possible to see the applied weights and on the floor the laser meter.

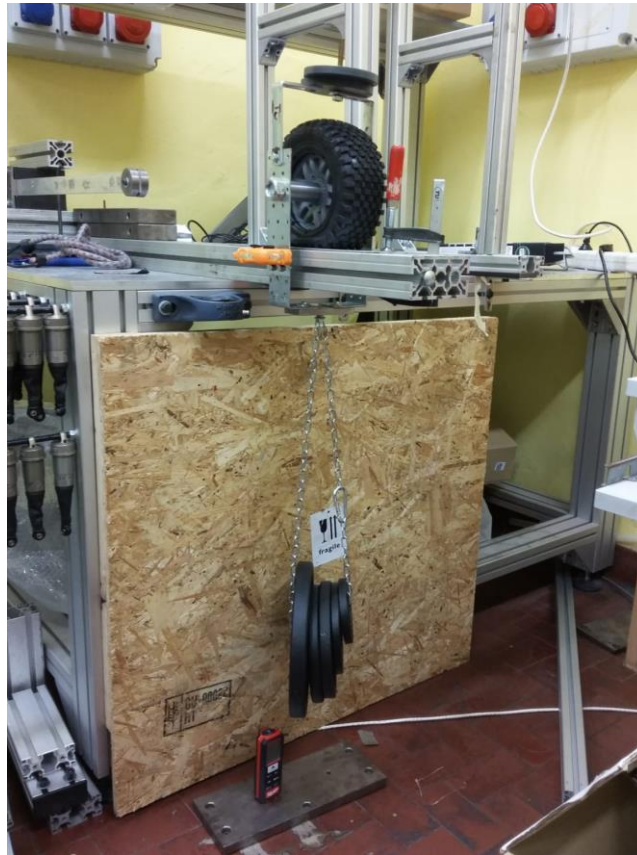


Figure 2.3.3 – Overall test structure.

2.4 Components weighting

After the definition of the structure all the single components of the mobile structure have to be weighted in order to correct the values of the applied weights during the calculation of the tyre stiffness.

The Table 2.4.1 shown all the mobile support component weights.

Table 2.4.1 – Mobile support components weight.

Component	Weight [kg]
Weight screw	0.0061
Carabiner	0.0206
Chain	0.0926
Screw M18	0.3492
Spacer 1	0.1262
Spacer 2	0.1223
Washer 1	0.0141
Washer 2	0.0139
Nut 18	0.0416
Angular plate 1	0.0878
Angular plate 2	0.0877
Plain plate 1	0.1526

Plain plate 2	0.1548
Main Stirrup	0.2523
Weights screw	0.0375
Level tool	0.045
Lateral plate	0.0876
Balance weight 1	0.5002
Balance weight 2	0.501
Total	2.6931

2.5 Measurement

The measurement is done with a laser meter Figure 2.5.1.

During the measurement the laser meter is placed down to the ground and the measured parameter is the distance between the ground and the mobile support. Increasing the applied weight, the tyre deformation increases and the distance of the mobile support from the ground decrease. The starting measurement is done without weights applied, so only the mobile support weights in considered. Then the next measurements are done with an increment of 0.5 kg each time up to a maximum of 10.5 kg excluding the support weight. In Figure 2.5.2 some of the weights are shown.



Figure 2.5.1 – Laser meter.



Figure 2.5.2 – Weights.

The measurements for all the possible combination of tyre and insert are reported in Table 2.5.1.

Table 2.5.1 – Displacement, mass and force values for all the configurations.

m [kg]	F [N]	Δx [m]			
		LOS 45023	LOS 45023 without insert	LOSB 7240	LOSB 7240 without insert
2.693	26.419	0	0	0	0
3.169	31.091	0.001	0.001	0	0.001
3.707	36.361	0.001	0.002	0	0.001
4.183	41.032	0.001	0.002	0	0.002
4.670	45.813	0.001	0.003	0.001	0.003
5.146	50.484	0.001	0.004	0.001	0.003
5.683	55.754	0.002	0.004	0.001	0.004
6.160	60.426	0.002	0.005	0.002	0.005
6.625	64.989	0.002	0.005	0.002	0.006
7.101	69.661	0.002	0.006	0.002	0.006
7.814	76.656	0.003	0.007	0.003	0.007
8.290	81.328	0.003	0.008	0.003	0.008
8.828	86.598	0.004	0.009	0.003	0.009
9.304	91.269	0.004	0.010	0.003	0.009
9.791	96.050	0.004	0.010	0.004	0.010
10.267	100.721	0.004	0.010	0.004	0.010
10.804	105.991	0.004	0.011	0.004	0.011
11.281	110.663	0.005	0.011	0.004	0.011
11.746	115.226	0.005	0.012	0.004	0.011
12.222	119.898	0.005	0.012	0.004	0.011
12.759	125.168	0.005	0.012	0.005	0.011
13.235	129.839	0.006	0.012	0.005	0.011

The measurements and also the linear interpolations are showed in Figure 2.5.3, Figure 2.5.4, Figure 2.5.5 and Figure 2.5.6. As it is possible to see from the previous table, the two tests without the foam insert lead to the same values of deformation after a certain weight is applied. This is caused because without the insert the wheel become less stiff, so the tyre reach the maximum possible value of deformation. For this reason, these values are not considered for the evaluation of the stiffness of the tire.

Knowing the equation that best fit the measured data, it is possible to evaluate the stiffness with a derivate. In this case, using a linear interpolation, the derivate is a constant value. In Table 2.5.5 the stiffness values for all the configurations are shown.

Table 2.5.5 – Stiffness values for all the possible configurations.

Configuration	Stiffness [N/m]
Tire LOS 45023 with insert	18277
Tire LOSB 7240 with insert	18746
Tire LOS 45023 without insert	7368
Tire LOSB 7240 without insert	7078

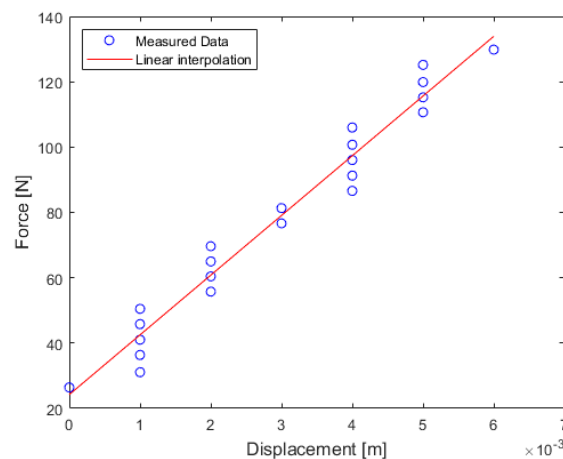


Figure 2.5.3 – Measured data and linear interpolation for tire LOS 45023 with insert.

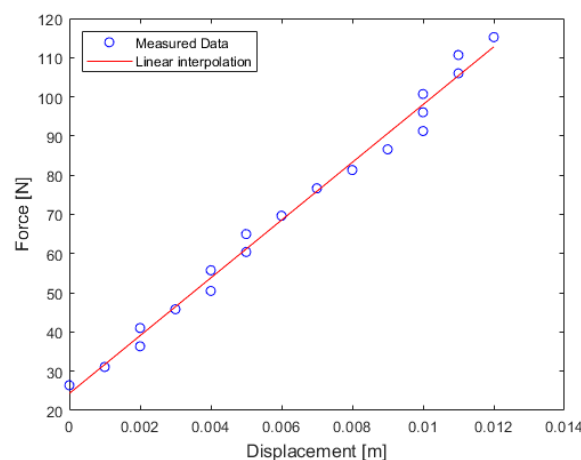


Figure 2.5.4 – Measured data and linear interpolation for tire LOS 45023 without insert.

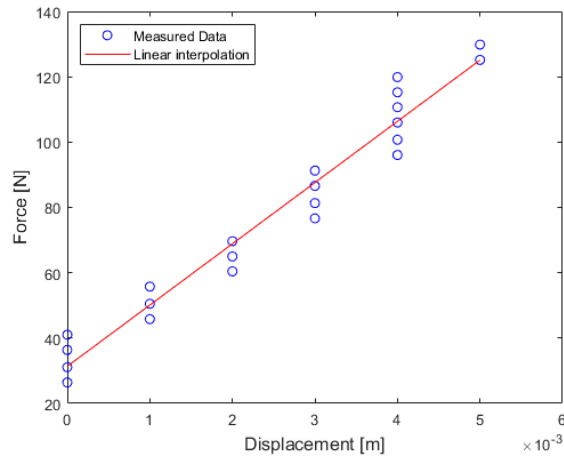


Figure 2.5.5 – Measured data and linear interpolation for tire LOSB 7240 with insert.

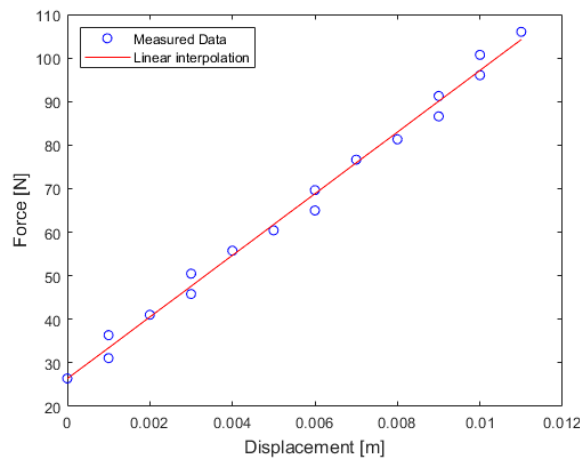


Figure 2.5.6 – Measured data and linear interpolation for tire LOSB 7240 without insert.

2.6 Wire study

Using the same technique also the wire stiffness can be estimated. The measured wire will be used for the dynamic tests to hold the weights. The procedure is simple: the wire is tied on a fixed structure on one end while at the other end a known weight is applied. Measuring the deformations, the stiffness can be estimated. Figure 2.6.1 shows the setup.



Figure 2.6.1– Experimental setup.

The tests have been done for three different length of the wire. For each length, the measured data have been interpolated and the results are showed in Figure 2.6.2, Figure 2.6.3 and Figure 2.6.4.

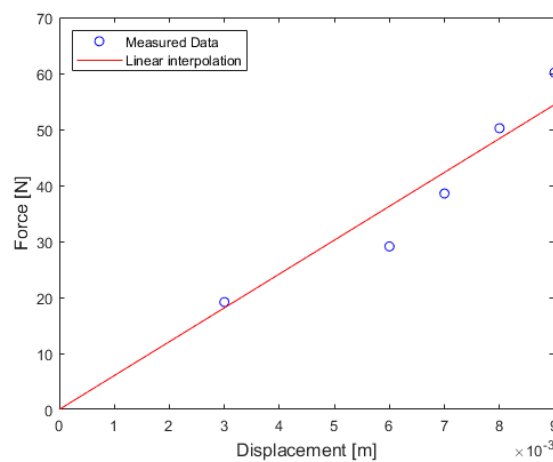


Figure 2.6.2– Measured data and linear interpolation for length $l=0.405\text{m}$.

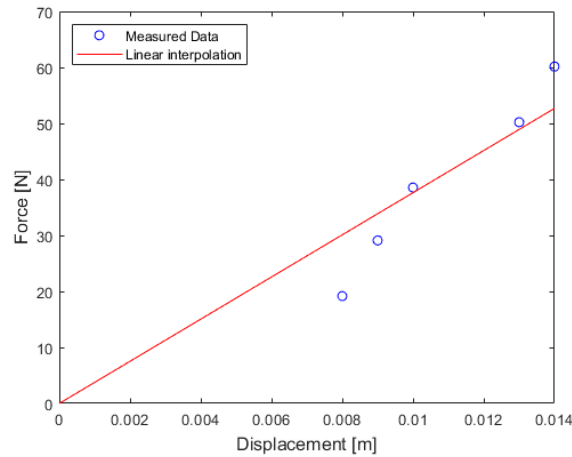


Figure 2.6.3– Measured data and linear interpolation for length $l=0.62\text{m}$.

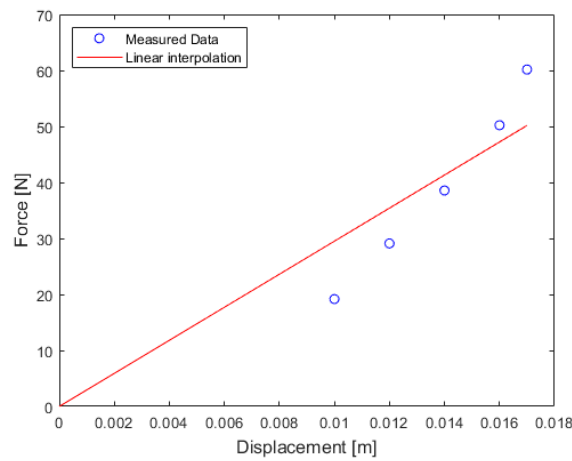


Figure 2.6.4– Measured data and linear interpolation for length $l=0.795\text{m}$.

Knowing the wire stiffness and the wire geometry, the wire Young modulus can be determined using the formula:

$$k = \frac{EA}{l} \quad (2.6.1)$$

And its reverse formula:

$$E = k \frac{l}{A} \quad (2.6.2)$$

Where k is the wire stiffness (estimated) while l and A are the wire length and the wire cross section area.

The results are shown in Table 2.6.1; the resultant average young modulus is $E=189.1 \text{ MPa}$.

Table 2.6.1 – Results of wire static tests.

l₀ [m]	m [kg]	F [N]	l [m]	Δx [mm]	k [N/m]	d[mm]	A [m²]	E [MPa]
0,405	1,955	19,169	0,408	0,003	6047	4	1,25664E-05	194,89
	2,968	29,106	0,411	0,006		4	1,25664E-05	
	3,932	38,554	0,412	0,007		4	1,25664E-05	
	5,121	50,217	0,413	0,008		4	1,25664E-05	
	6,134	60,154	0,414	0,009		4	1,25664E-05	
0,62	1,955	19,169	0,628	0,008	3764	4	1,25664E-05	185,71
	2,968	29,106	0,629	0,009		4	1,25664E-05	
	3,932	38,554	0,63	0,01		4	1,25664E-05	
	5,121	50,217	0,633	0,013		4	1,25664E-05	
	6,134	60,154	0,634	0,014		4	1,25664E-05	
0,795	1,955	19,169	0,805	0,01	2951	4	1,25664E-05	186,69
	2,968	29,106	0,807	0,012		4	1,25664E-05	
	3,932	38,554	0,809	0,014		4	1,25664E-05	
	5,121	50,217	0,811	0,016		4	1,25664E-05	
	6,134	60,154	0,812	0,017		4	1,25664E-05	

Another important information to determine is the wire density. For this purpose, the wire has been weighted. Knowing the wire mass and its geometry, it is possible to evaluate its density. The wire mass, length, diameter and the evaluated volume are reported in Table 2.6.2.

Table 2.6.2 – Results of wire density estimation.

L [m]	D [mm]	A [m²]	V [m³]	M [kg]	ρ [kg/m³]
1	4	1,26E-05	1,26E-05	0,012	954,9

3. Tyre test-rig

3.1 Test-rig project

In order to study the wheel dynamics, an appropriate test-rig is required. The starting point is the study of the old test-rig used in previous tests (Figure 3.1.1).

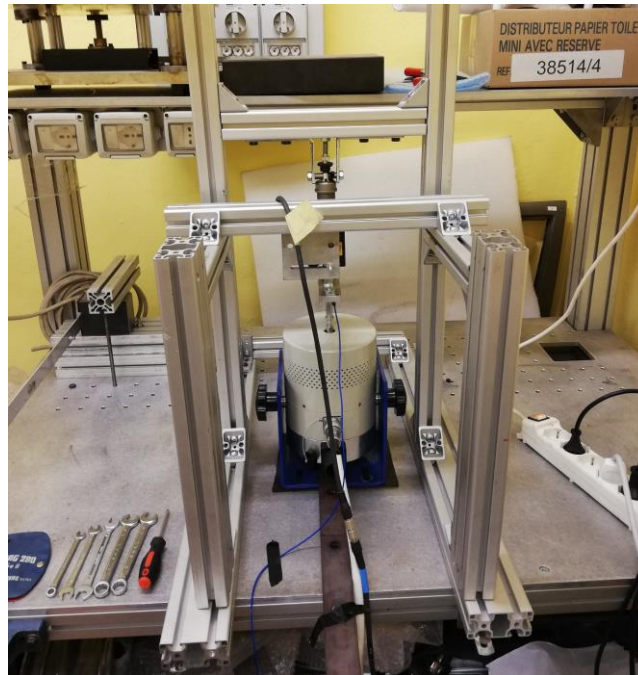


Figure 3.1.1 – Old test-rig configuration, used in other experiments

The main components are:

- Shaker (Figure 3.1.2) model ESD-045 by Dongling-Italy: this component is the core of the test-rig. The aim of the shaker is to apply a force with amplitude and frequency known. The available shaker can apply a force up to 450 N in the frequency range from 5 Hz to 3000 Hz [1].



Figure 3.1.2 – Shaker

- Piezoelectric load cell (Figure 3.1.3) model PCB 208c02 [2]: its aim is to measure the applied force. It must be mounted on the same axis of the shaker shaft thanks to two female thread. Also, two M6 adapter will be necessary because of the strange threads' standard of the load cell (10-32 of the Unified Thread Standard) [1]. This model of load cell can measure force up to 450 N circa and it convert it in an electrical signal with a sensitivity of ($\pm 15\%$) 50 mV/lb (11241 mV/kN). The frequencies range goes from 0.001 Hz to 36000 Hz.

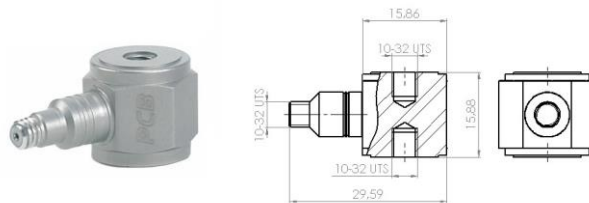


Figure 3.1.3 – Piezoelectric load cell.

- Laser meter (Figure 3.1.4) model LK-H050 by Keyence [3]: the laser meter is used to measure the displacement of the wheel. It works thanks to a laser beam (emitted by the laser meter) pointed to the object that must be measured. The laser beam is reflected by the object and the reflected beam impact to a measuring system. If the object moves, the reflected beam changes its path and the displacement can be measured. The laser meter has some standard holes so it can be mounted on a plate already present in the test-rig. Then the plate is fixed on the frame.



Figure 3.1.4 – Laser meter with a detailed view of the laser emitter (the dark blue square on the upper part) and the receiver (the light blue square on the lower part)

- Aluminium bars (Figure 3.1.5): all the instruments must be mounted on a frame. In this case an aluminium frame is used. These aluminium bars allow to create a simple, configurable and easy to build frame thanks to the use of angular brackets and screws for fixing all together with no needs of welding. Some modifies are needed to adapt the existing frame to this new experiment.

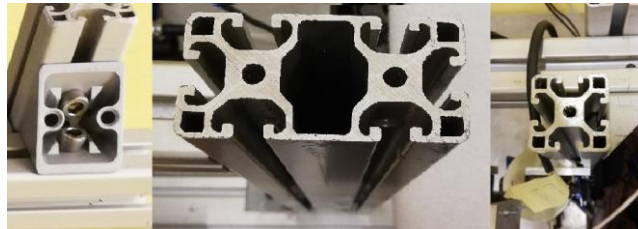


Figure 3.1.5 – Different type of aluminium bar and angular support

- Wheel support: a support is needed to place the item to be tested on the shaker. In the old test-rig dampers were tested, so a customized support was prepared to fit those dampers. In this experiment wheels will be tested so a completely new support must be built.

The wheel support is the component used to connect the shaker to the wheel. The basic idea is to maintain the general scheme like to the old one showed in [1]. The general scheme is showed in Figure 3.1.6 [1].

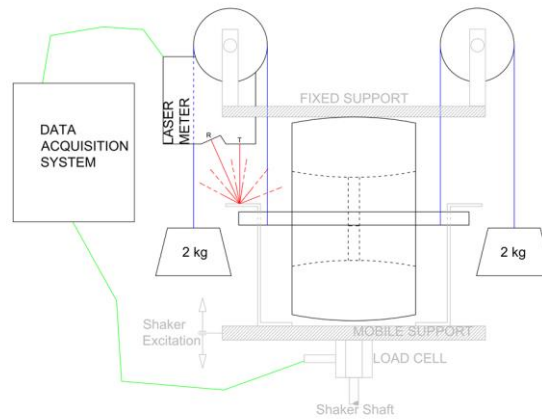


Figure 3.1.6 – Main scheme of the wheel support

On the lower side the shaker shaft is visible with the load cell mounted on top of it. Over the load cell the proper wheel support is shown.

The base of the support is a 10 mm thick steel plate already present in laboratory. On this plate two lateral bracket are mounted to sustain an 18 mm shaft on which the wheel is fitted.

On the upper side a fixed support (the fixed frame) is the contact plane of the wheel. The fixed frame is used also for mounting the laser meter that measures the distance of the mobile support.

There are furthermore two counterweight that have the purpose of simulate the real work conditions of the wheel. The car model studied in this experiment has a mass of about 16 kg so approximatively 4 kg load per wheel must be applied. This mass is divided in half (2 kg for each side) and applied to the wheel using pulleys.

Then a data acquisition system is required to collect all the data from the load cell and the laser meter.

The first step in this project is to define a 3D CAD model of the assembly in order to investigate the feasibility of the project and its weakness. The first 3D model of the wheel support is shown in Figure 3.1.7 and Figure 3.1.8.



Figure 3.1.7 – First scheme of the wheel support



Figure 3.1.8 – Exploded view of the wheel support

The features in the project were mainly:

- the wheel must be well fixed to the support;
- the support should not be too heavy because the wheel will be mounted and dismounted frequently;
- the time to mount/dismount the wheel should be as less as possible.

All these considerations take as the result the configuration shown in Figure 3.1.8.

In the lower part of the figure there is the steel plate mentioned before, it is also possible to see the central hole that is where the shaker shaft and the load cell are fixed. Mounted on this plate there are two lateral brackets that have two through hole for the M18 screw that hold the wheel. In order to maintain the wheel in its position, two spacers have been inserted to prevent any axial movement.

3.2 Wheel support building

Few components have to be added to the previous test-rig: the lateral brackets, the spacers and the M18 screw and nut.

Since that the lateral brackets have a very particular shape that is difficult to find it is been decided to use two different brackets (instead of one) fixed together with some screw. The two new brackets (shown in Figure 3.2.1, Figure 3.2.2 and Figure 3.2.3) are different, one is angular, and it is the one fixed on the main plate with screws; the other one is a plain plate fixed on the angular plate to obtain the desired measures of the project's bracket.

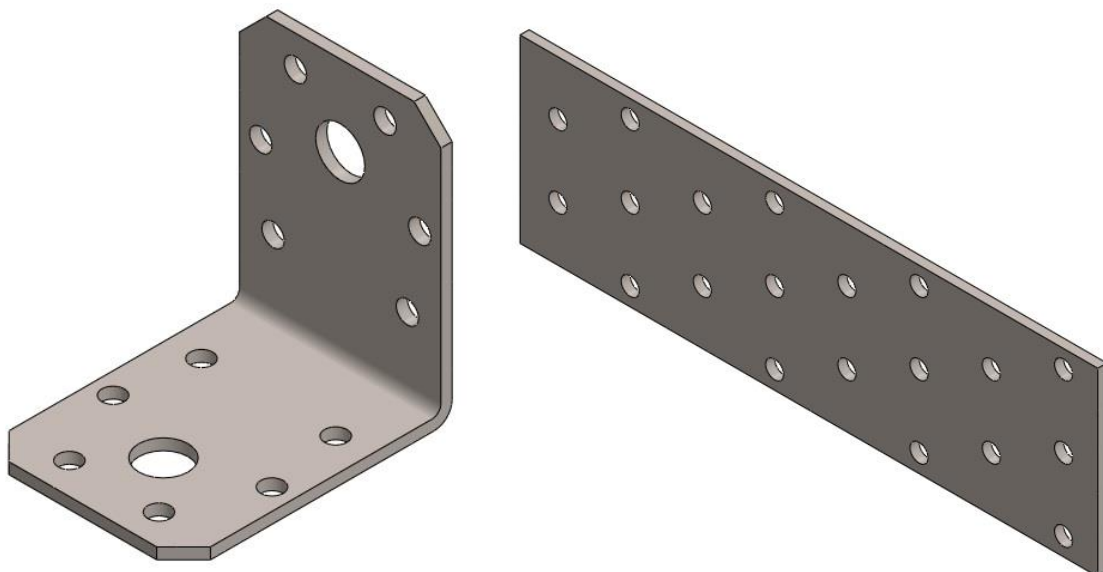


Figure 3.2.1 – Angular plate

Figure 3.2.2 – Plain plate

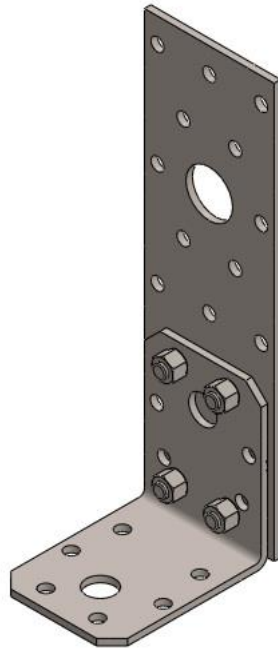


Figure 3.2.3 – Angular plate and plain plate fixed together

As you can see in Figure 3.2.3 the plain plate needs also a little modification. One of the holes in fact needs to be enlarged to allow the mounting of the M18 screw that holds the wheel. The new wheel support with all the modifies is shown in Figure 3.2.4.

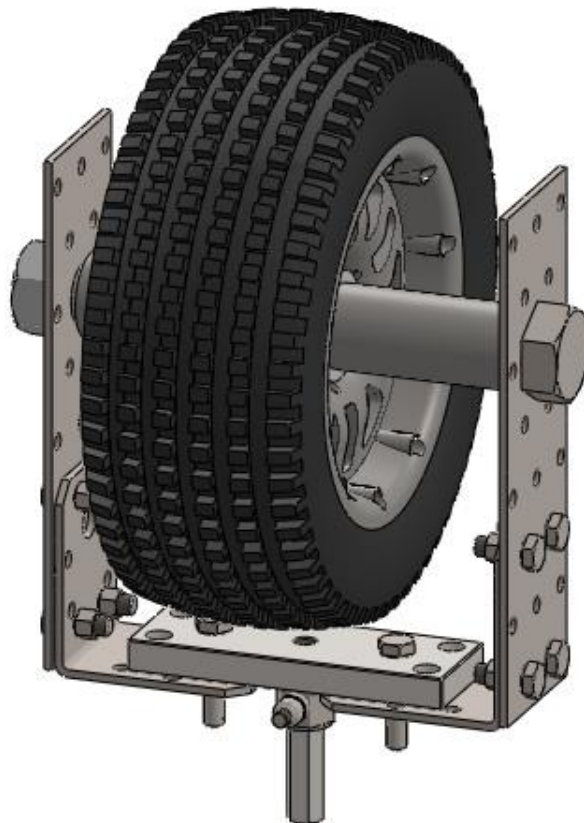


Figure 3.2.4 – Wheel support after the modification

3.3 Counterweight system

Besides the support wheel also the frame needs some changes because of the counterweights. In the project the wheel must lean on the upper side, so to use the counterweights some pulleys are needed. These pulleys are easy to buy but they still need some modifications. In Figure 3.3.1 the original pulley is shown, while in Figure 3.3.2 the modified one is shown. The changes are due to the fixing method. The original one has a hook on top of it, while in the modified one, the hook has been removed and a through hole is made, used to fix the pulley directly on the frame with a screw.

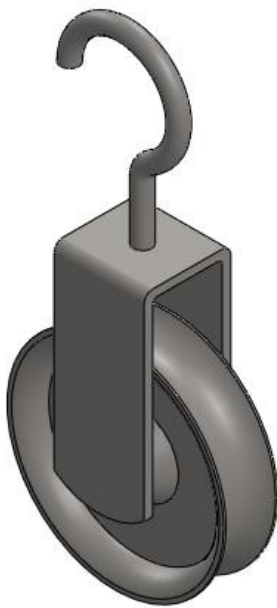


Figure 3.3.1 – Original pulley



Figure 3.3.2 – Pulley with modification

Putting together all the pieces the test rig should look like the CAD drawing showed in Figure 3.3.3.

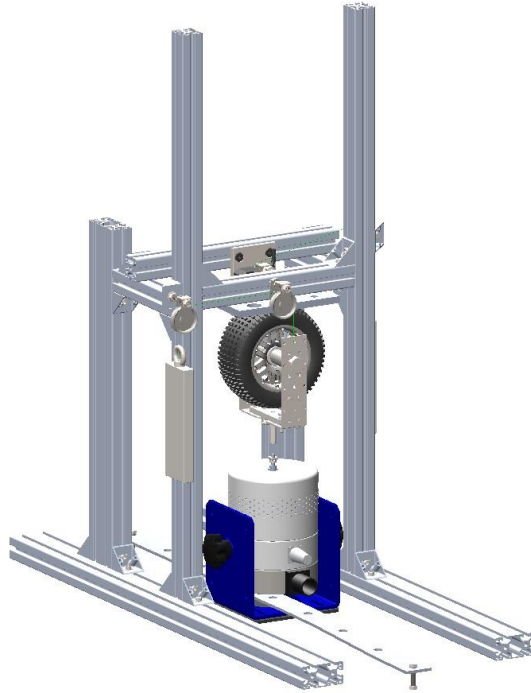


Figure 3.3.3 – CAD drawing of the entire test rig with all the changes

3.4 Feasibility study

After the definition of all the details of the test rig that will be used to test the wheels, some calculations are needed to try to understand if the project is good and if the results of the tests would be acceptable or not. The main problems analysed below concern the mass of the wheel support, the estimation of the tire stiffness and the fixing method between the angular plates and the main plate.

3.4.1 Wheel support mass

The wheel support mass is an important factor for the success of the experiment. The wheel support and the wheel itself are linked to the shaker and so they are in movement during the whole experiment. The heavier the wheel support is, the more important will be the inertial forces. If the mass is too high the results could be compromised, so all the component should be weighed in order to understand better the impact of this mass.

The weights value of all the components are indicated in Table 3.4.1.1 together with the relative weight.

Table 3.4.1.1 – Mass value of the wheel support component and relative weight.

Component	Weight [kg]	Weight %
Wheel	0.617	30.15
Screw M18	0.3492	17.06
Main Plate	0.2523	12.33
Plain plate 2	0.1548	7.56

Plain plate 1	0.1526	7.46
Spacer 1	0.1262	6.17
Spacer 2	0.1223	5.98
Angular plate 1	0.0878	4.29
Angular plate 2	0.0877	4.29
Nut M18	0.0416	2.03
Screws	0.027	1.32
Washer 1	0.0141	0.69
Washer 2	0.0139	0.68
Total	2.0465	

Looking at the table it is possible to see some important information. First, the total mass is about 2 kg and secondly, the wheel weight is only 30% of the total. The heaviest components (excluding the wheel) are the screw M18 and the main plate.

In conclusion, the wheel support has a total weight of about 2 kg that, added to the 4 kg of the counterweights, bring the total mass of the moving components to about 6 kg. Knowing the maximum force that the shaker can apply (450 N), using the reverse of:

$$F = m\ddot{x} \quad (3.4.1.1)$$

it is possible to estimate the maximum acceleration that can be applied. The result is a maximum acceleration of about 45 m/s².

3.4.2 Angular plate fixing

One of the most critical part of the wheel support is the angular plates fixing on the main plate. The first idea was the use of two screw per plate in order to increase the fixing strength. But when searching the components, it becomes clear that an angular plate with already two holes coincident to the ones on the main plate would be impossible. The only way to have the two holes coincident would be by the modification of the angular plate or the main plate. But the main plate cannot be modified, and so the angular plate because two more holes could decrease the material strength. These problems lead to the fixing configuration with only one screw as shown in Figure 3.4.2.1. The problem with this configuration is that at high frequencies the angular plates could be deformed under the high inertial forces. This deformation could introduce vibrations and could also bring to wrong results.

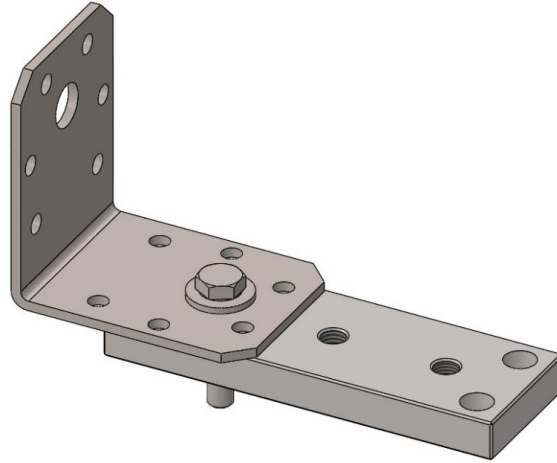


Figure 3.4.2.1 – Angular plate and main plate fixed with one screw

In order to investigate the deformations that could arise, the angular plate behaviour is studied. The plate is studied as a beam element, wedged on one side with a force F on the upper side (Figure 3.4.2.2).

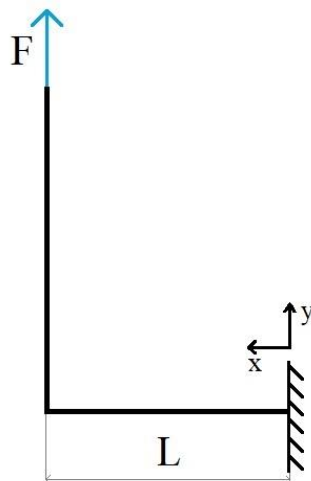


Figure 3.4.2.2 – Angular plate scheme

The deformation equation that result is:

$$y(x) = \frac{1}{EI_z} \left(\frac{FL}{2} x^2 - \frac{F}{6} x^3 \right) \quad (3.4.2.1)$$

The maximum deformation occurs in $x=L$, so it is:

$$y(L) = \frac{FL^3}{3EI_z} \quad (3.4.2.2)$$

Using as force value the maximum possible force the shaker is capable of ($F=450$ N), it results a maximum deformation of about 0,9 mm. This value could be excessive so a different configuration

should be found. The easier way to solve the problem is to mount the angular plate under the main plate (Figure 3.4.2.3). This solution decreases the deformations.

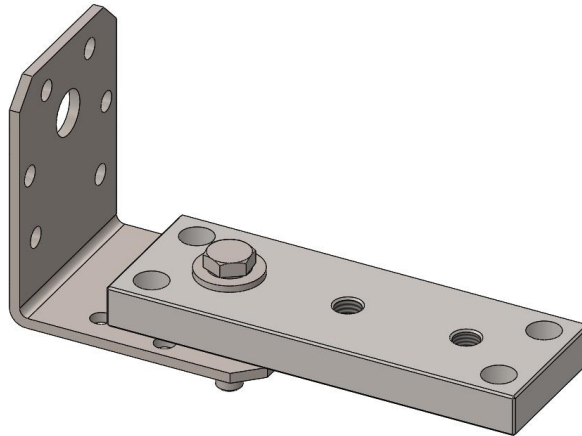


Figure 3.4.2.3 – Angular plate fixed under the main plate

3.5 Test-rig assembly

When the project is finished and all the components have been prepared, the test-rig can be assembled (during the dynamic tests the projected test-rig has been slightly modified so in the next images and description the definitive test-rig version is shown). Figure 3.5.1 and Figure 3.5.2 show two view of the entire test-rig.

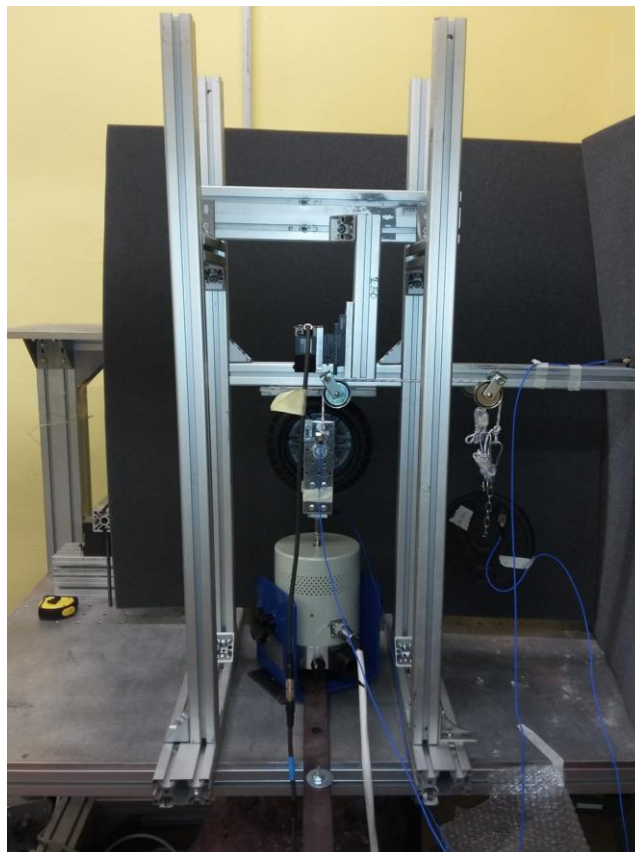


Figure 3.5.1 – Test-rig frontal view.

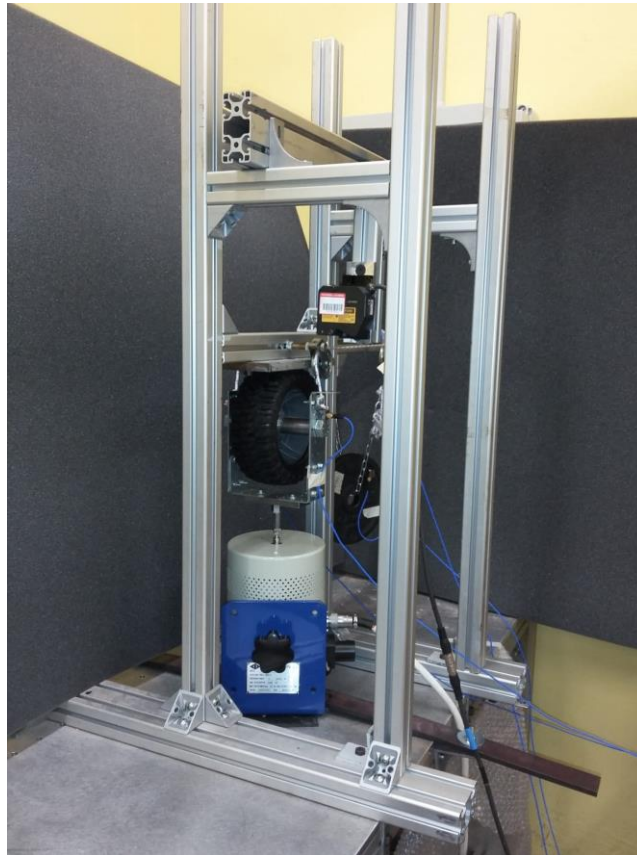


Figure 3.5.2 – Test-rig lateral view.

The first part to be assembled is the frame, composed by several aluminium bars fixed together with screws. The first bars have the purpose of merge the proper test-rig frame with the workbench used for the experiment. This connection must be as stiff and solid as possible, so two double profile bars have been used. These bars have been fixed on the workbench with four angular brackets (two for each bar) Figure 3.5.3.



Figure 3.5.3 – Angular brackets fixing the test-rig and the shaker on the workbench.

Up on these two bars four vertical bars have been fixed using two/three angular brackets each, in order to increase the frame stiffness (Figure 3.5.4). On the upper part of these vertical bars, three horizontal bars, with two brackets each, complete the main frame. One of these bars have the purpose of holding the plate where the wheel must be in contact. The other two have the purpose of increase the structure stiffness but also allow the mounting of the laser. In Figure 3.5.5 it is possible to see the upper part of the frame, with the horizontal bars, the wheel and the laser. On the left side of the frame, a single bar (fixed with two brackets) is mounted to hold two pulley that hold the weights (Figure 3.5.6).



Figure 3.5.4 –Frame lateral side.

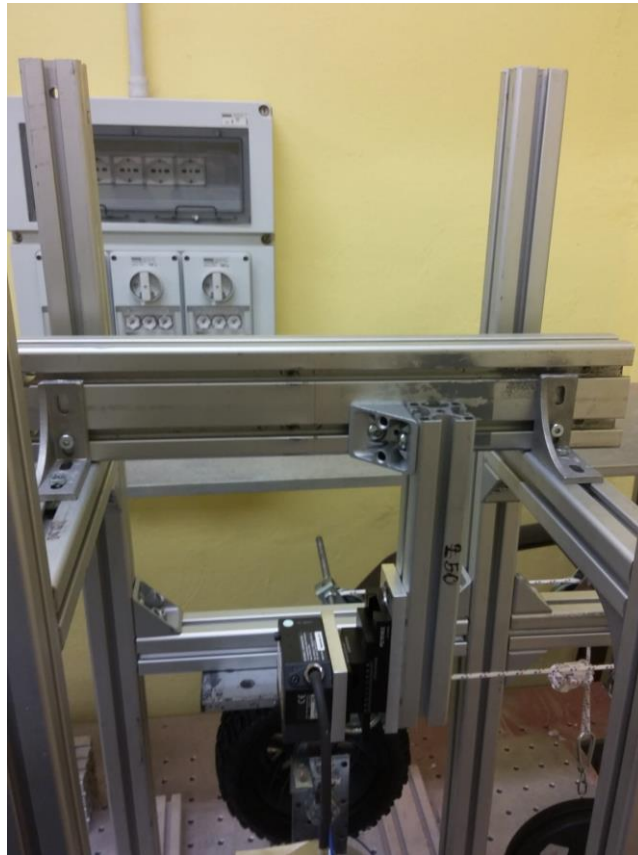


Figure 3.5.5 –Frame upper part.



Figure 3.5.6 –Test-rig counterweight system.

After the frame assembling the shaker, the laser, the wheel and all the sensors have been mounted. The shaker has been fixed using a metal band screwed directly on the workbench. A rubber mat has been put between the shaker and the workbench to reduce the vibrations (Figure 3.5.7).

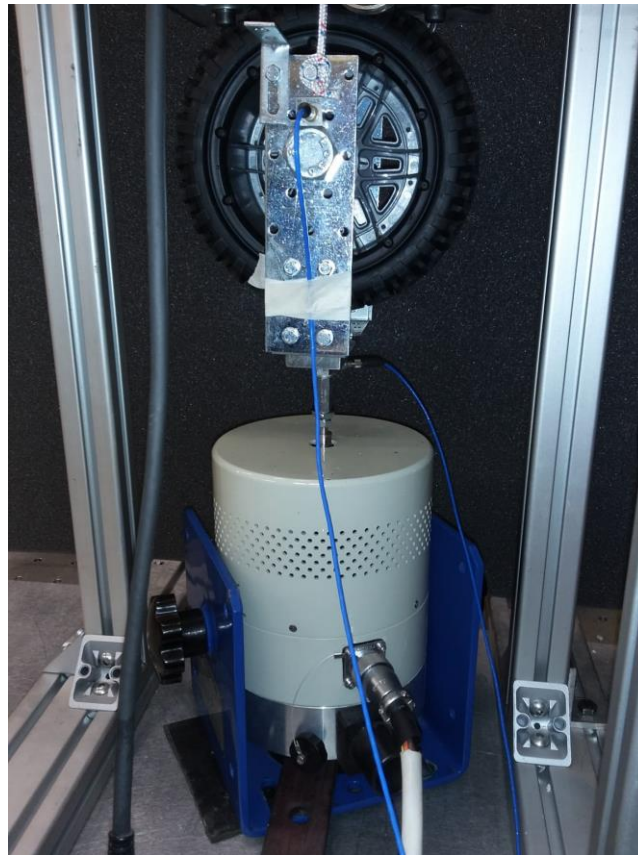


Figure 3.5.7 –Shaker mounting position.

On the shaker stem the piezoelectric load cell and the wheel support have been mounted, then the frame was adjusted to consent the contact of the wheel on the dedicated plate. Then two strings were tied to the wheel structure to consent the mounting of the weights. The laser was fixed on the upper part of the frame, using some aluminium bars to consent the mounting on the correct height. The used laser in fact must be mounted at the correct distance to the measuring point. In this case the measuring point is a plate fixed to the wheel support. In Figure 3.5.8 the laser and the measuring point are shown. It is also possible to see the red dot of the laser on the measuring plate. Figure 3.5.9 shows an overview of some components. In the lower part there is the shaker with the load cell and the wheel mounted on it. On the upper part the laser, some of the pulley and the weight are visible. The last components to be mounted are the accelerometers. A total of three three-axial accelerometers have been mounted; one on the wheel axis, one on the weight and the last one on the structure bar that holds the weight (Figure 3.5.10, Figure 3.5.11 and Figure 3.5.12).



Figure 3.5.8 –Laser.

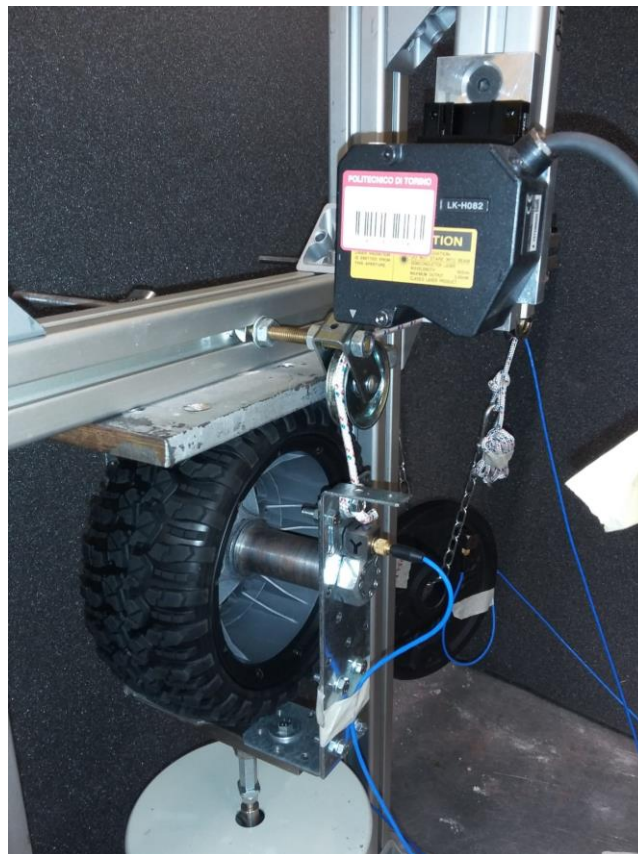


Figure 3.5.9 –Test-rig lateral detail.

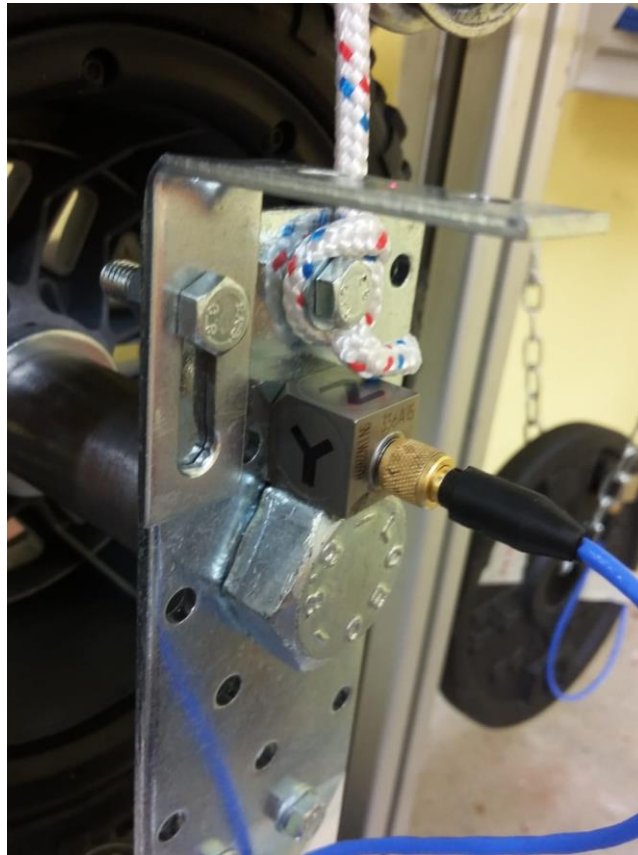


Figure 3.5.10 –Wheel axis accelerometer.



Figure 3.5.11 –Weight accelerometer.

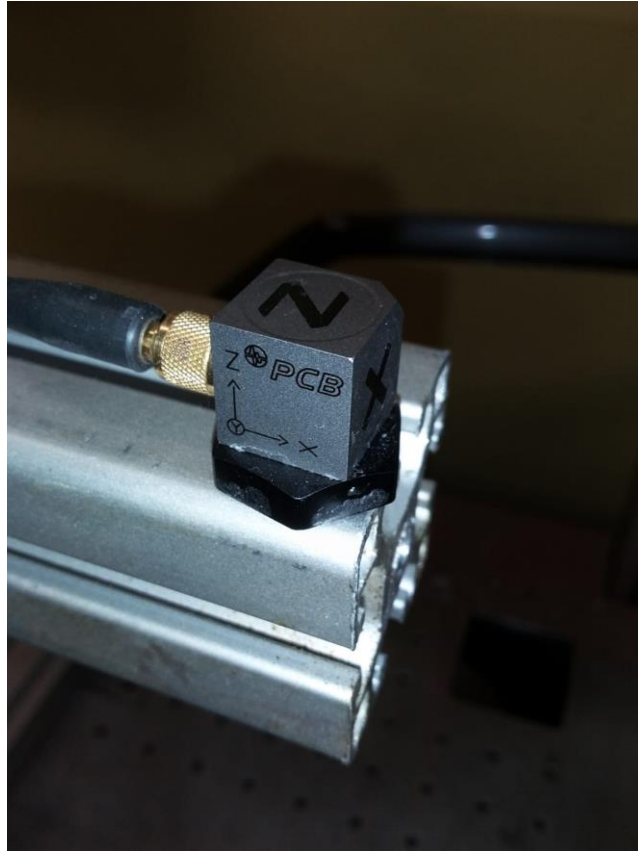


Figure 3.5.12 –Structure accelerometer.

4. Dynamic stiffness evaluation

The goal of this experiment is to define the dynamic behaviour of the tyre. The idea is to use the shaker to apply a known sinusoidal force to the wheel and use the sensors to measure the accelerations, the displacement and the actual applied force to understand the wheel behaviour in all the four configurations.

4.1 Setup

4.1.1 Hardware setup

After the test-rig building the shaker, laser and the other sensors still need to be connected to the data acquisition system. In this case the Siemens LMS SCADAS is used (Figure 4.1.1.1).



Figure 4.1.1.1 –Siemens LMS SCADAS.

All the sensors are connected to the SCADAS as input signal, while the shaker is connected as output signal. The accelerometers and the load cell are ICP sensors. This means that they are self-powered using the same low voltage wire used for the signals. For this reason, the accelerometers and the load cell are directly connected to the SCADAS, with just one wire for both signal and power transmission. The laser instead needs a proper alimentation. Therefore, the laser connections are slightly different from the previous one. The laser in fact is connected to a dedicated controller that have the purpose of power the laser, but it also converts the laser signal to generate a suitable signal for the SCADAS (the SCADAS in fact handles only $\pm 10V$ signal).

The shaker is connected to the SCADAS output. The SCADAS output are also $\pm 10V$ signal. This could be a problem because the shaker produces a force proportional to the input voltage signal. The 10V signal therefore could be too low for the test purpose. This is why an amplifier is needed. Hence the SCADAS output is connected to the amplifier that increase the signal voltage and send it to the shaker. In this way higher force values can be reached by the shaker. Figure 4.1.1.2 shows the laser controller and the shaker amplifier.

The SCADAS then is connected to a laptop that is used for the testing. The software used to communicate with the SCADAS is a Siemens software named LMS Test.Lab 17.



Figure 4.1.1.2 –Shaker amplifier with laser controller on it.

4.1.2 Software setup

After the hardware setup, it is time to launch the software to configure the last parameter. The first important thing to do is to configure the sensors. This can be done in the Channel Setup tab (Figure 4.1.2.1) of the software. First of all, the channel used by the sensors must be activated clicking on the respective box. Then, the measured quantity, the sensor type, the sensor sensitivity, the point and direction where the sensor is applied.

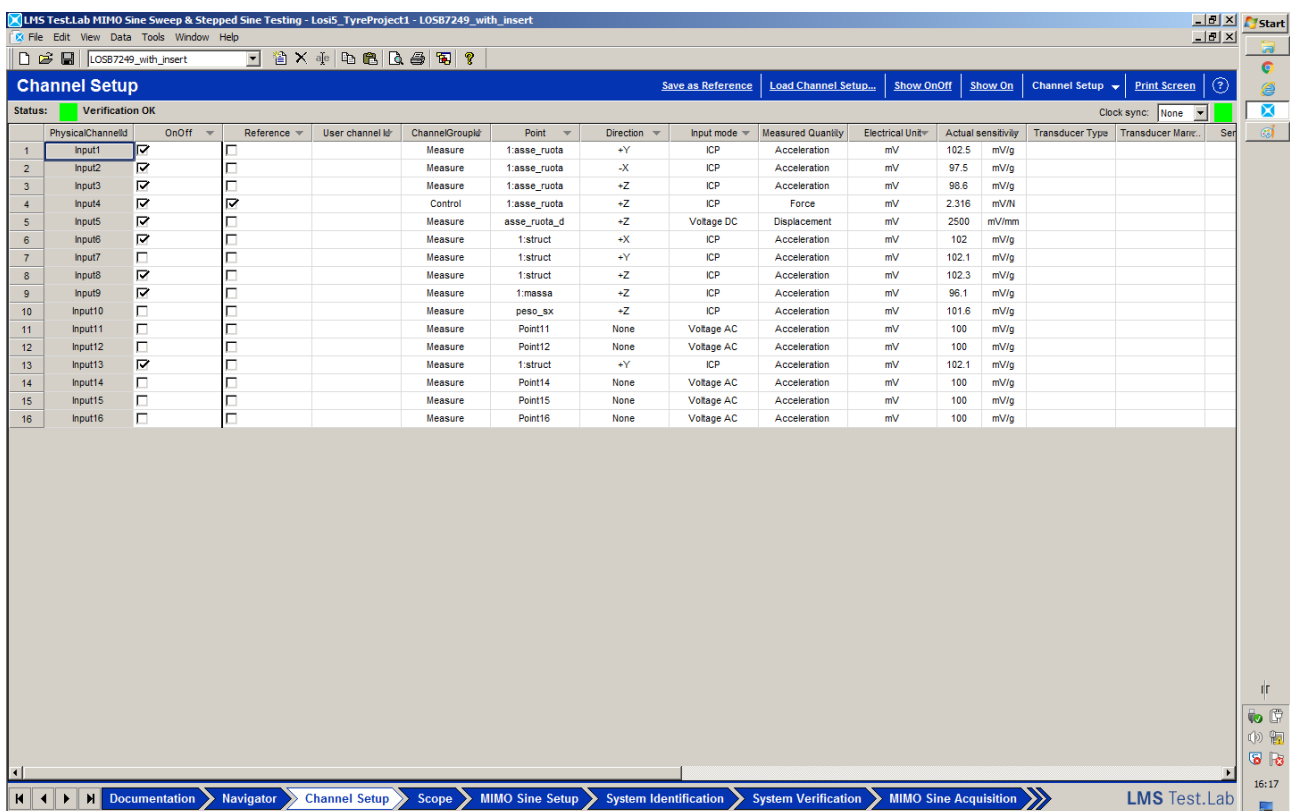


Figure 4.1.2.1 –Channel Setup tab.

As it is possible to see in Figure 4.1.2.1 the first three channel are used by the three-axial accelerometer mounted on the wheel axis. This is an ICP sensor that measure the wheel accelerations and the sensitivities are defined by the constructor.

The fourth channel is connected to the load cell. It measures the vertical forces applied to the wheel by the shaker. It is also an ICP sensor and the sensitivity is defined by the constructor. The load cell is important because the applied force is the quantity that will be controlled. This means that the applied force value is defined by the user, the software sends the signal to the shaker to obtain the desired force and the load cell closes the loop measuring the actual force applied by the shaker. In this way the software can adjust the signal to the shaker to minimize the difference between the desired and the actual applied force. To do this, the software must know that the load cell is used as reference and this is done by checking the second column box and by setting the channel as control channel instead of measuring channel.

The fifth channel is the laser. The laser is not an ICP sensor, it is DC powered. It measures the wheel axis vertical displacement and the sensitivity can be calculated knowing the voltage and the displacement range. The voltage as said before is $\pm 10V$ and the range is decided by the user. In this case the chosen range is $\pm 4mm$ so the sensitivity is $2500mV/mm$.

The sixth, eight and the thirteenth channel are connected to the accelerometer mounted on the frame structure; while the ninth channel is used by the accelerometer mounted on the weight (only one channel is used because for the weight only the vertical accelerations are measured). Again, these accelerometers are ICP sensors, they measure accelerations and the sensitivities are defined by the constructors.

After the channel setup, an initial test is done to determine the required voltage level signal to send to the shaker. This test can be done in the Scope tab. For this experiment a maximum of 0.5V turned out to be appropriate.

At this point all the initial setup and configurations are done; it is time to define the applied force profile and the test characteristic. This can be done in the MIMO Sine Setup tab (Figure 4.1.2.2).

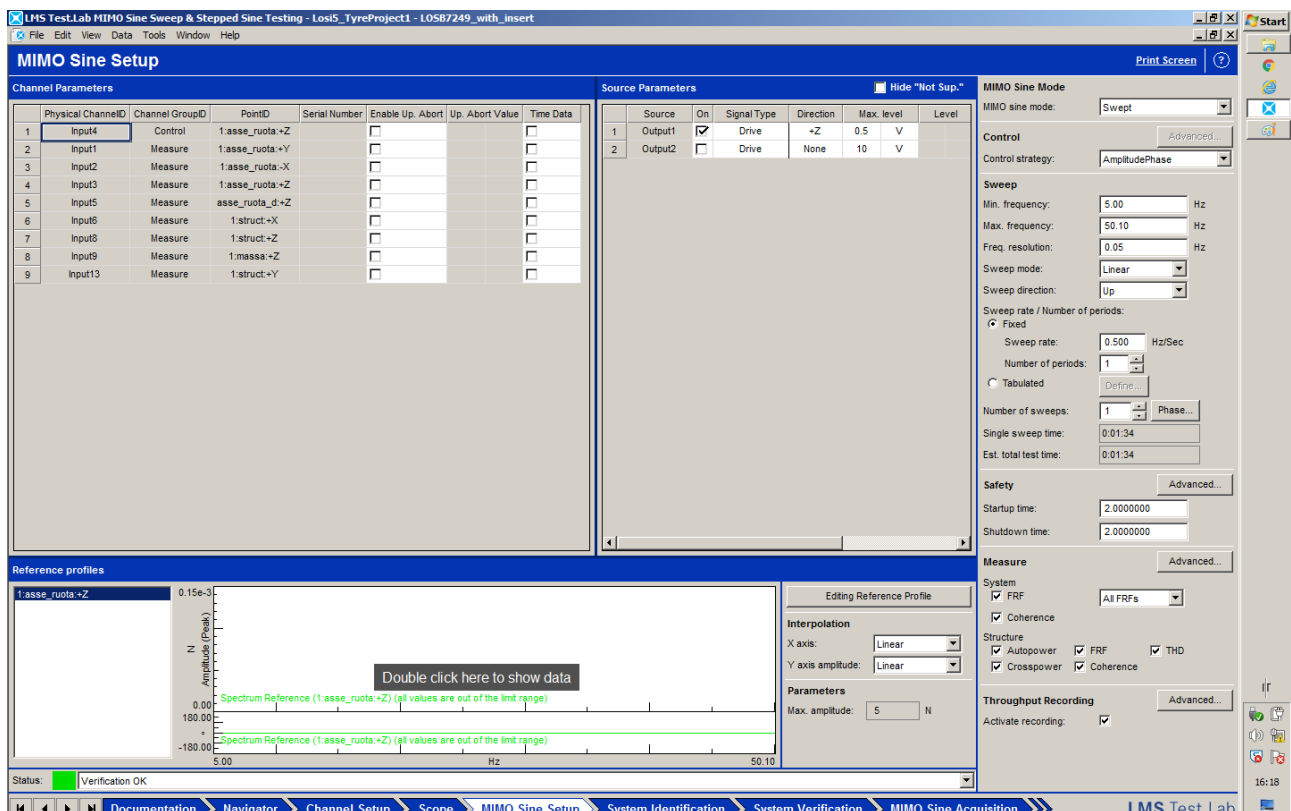


Figure 4.1.2.2 –MIMO Sine Setup tab.

The test is a sweep test; these types of tests are basically tests with varying frequency. The starting/finish points and the frequency rate are chosen by the user. In this case it is been decided that all the tests are done linearly from 5Hz to 50Hz with a frequency rate of 0.5Hz/s.

In the same tab, opening the “Editing Reference Profile” window it is possible to define the desired applied force. In this case the applied force profile is sinusoidal, with constant amplitude of 5N (Figure 4.1.2.3). With this final setup, the data acquisition can start.

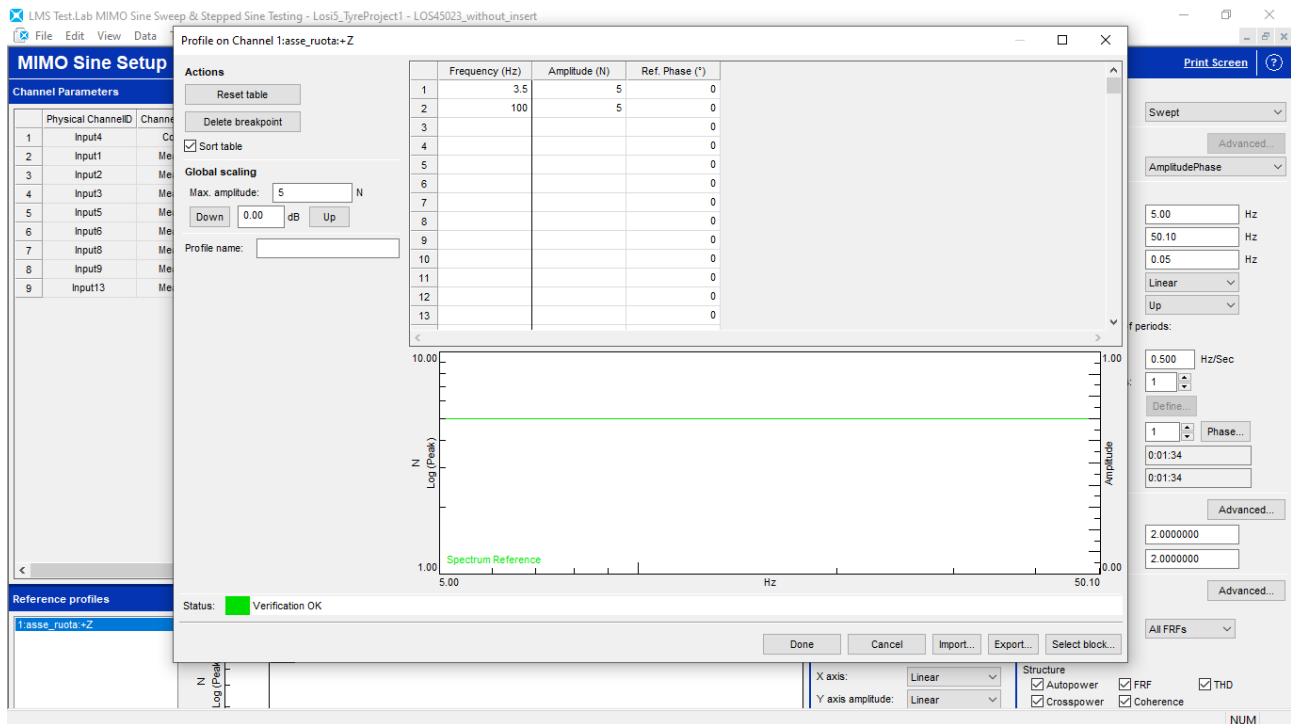


Figure 4.1.2.3 – Editing Reference Profile window.

4.2 Data acquisition

The first thing to do at the beginning of every test is the system identification. It can be done in the System Identification tab (Figure 4.2.1). The system identification is important because it is the way that the software use to try to correlate the tension signal sent to the shaker to the applied force. In this phase, the program sends to the shaker a random tension signal and read the sensors response.

After the identification there is the system verification. It can be done in the System Verification tab (Figure 4.2.2) and its purpose is to create the drive (the tension signal sent to the shaker during the entire test) starting from the system identification results. In the lower part of Figure 4.2.2 the drive is visible. Once the drive has been calculated, the proper test can start. The test can be performed in the MIMO Sine Acquisition tab (Figure 4.2.3). In the upper part of Figure 4.2.3 there is a graph showing the measured applied force (red line) and the desired applied force (green line). The closer the red line is to the green line, the better it is. In this case the red line has 4.73N as minimum value and 5.39 as maximum value, so it is a quite good test considered that the desired value is 5N. In case the actual force is not close to the desired one it is possible to do some iterations. It is in fact possible to use the results of an acquisition as the starting point of a new drive. This should improve the results in few iterations.

At the end of the acquisition the data are stored, and a new configuration can be studied.

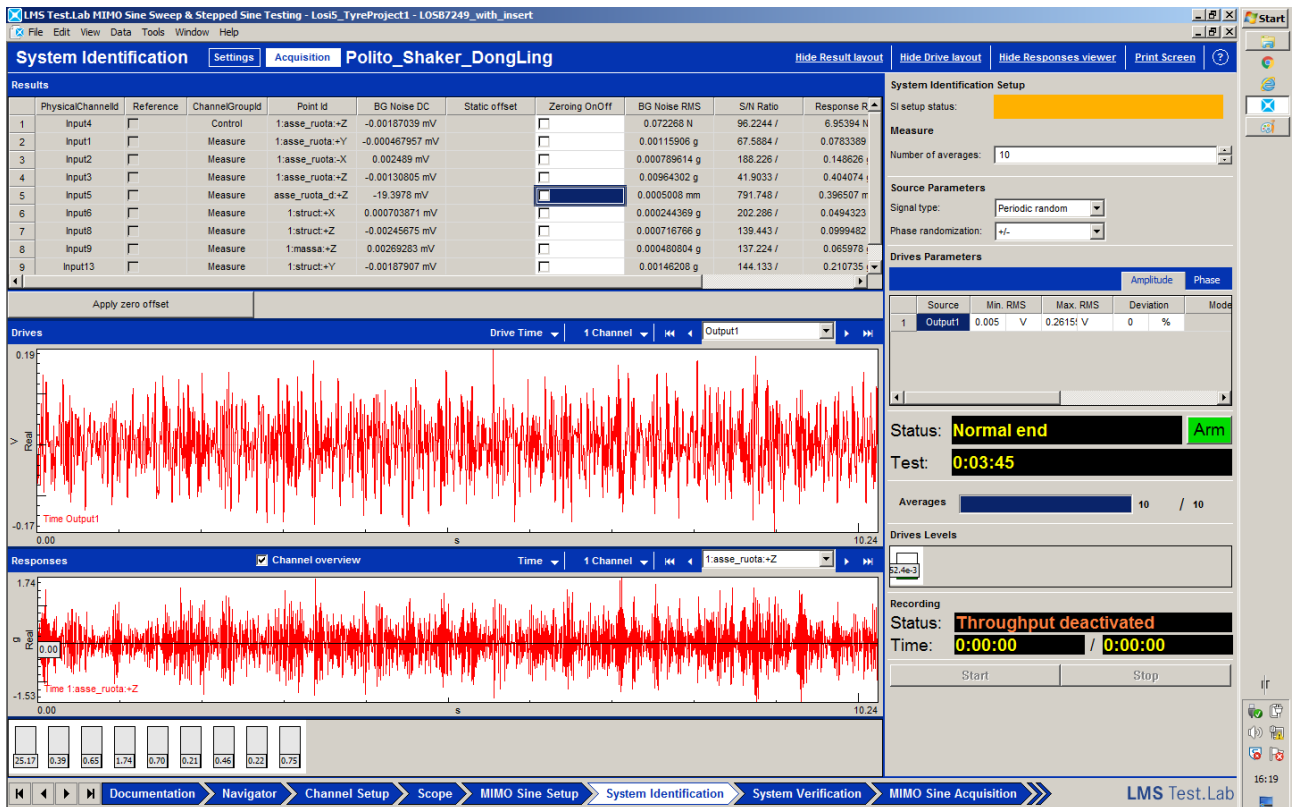


Figure 4.2.1 – System Identification tab.

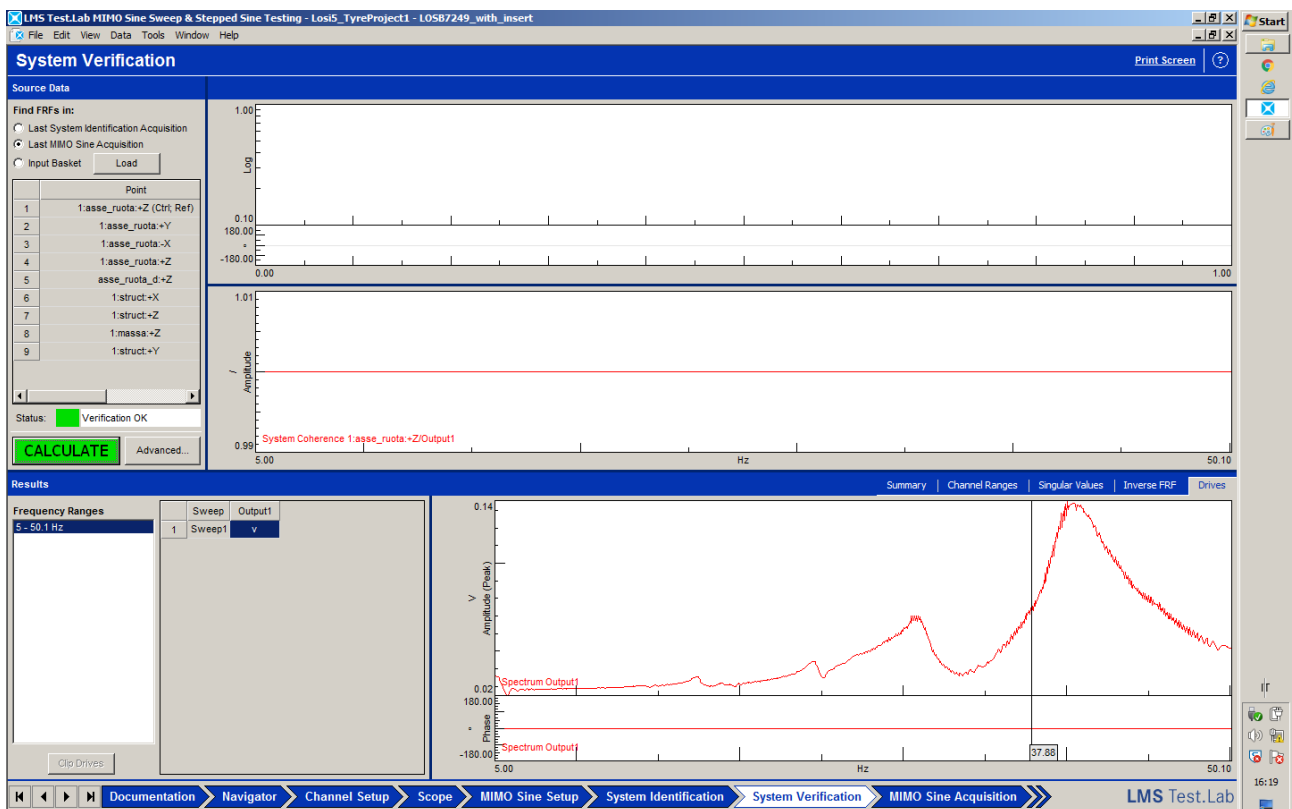


Figure 4.2.2 – System Verification tab.

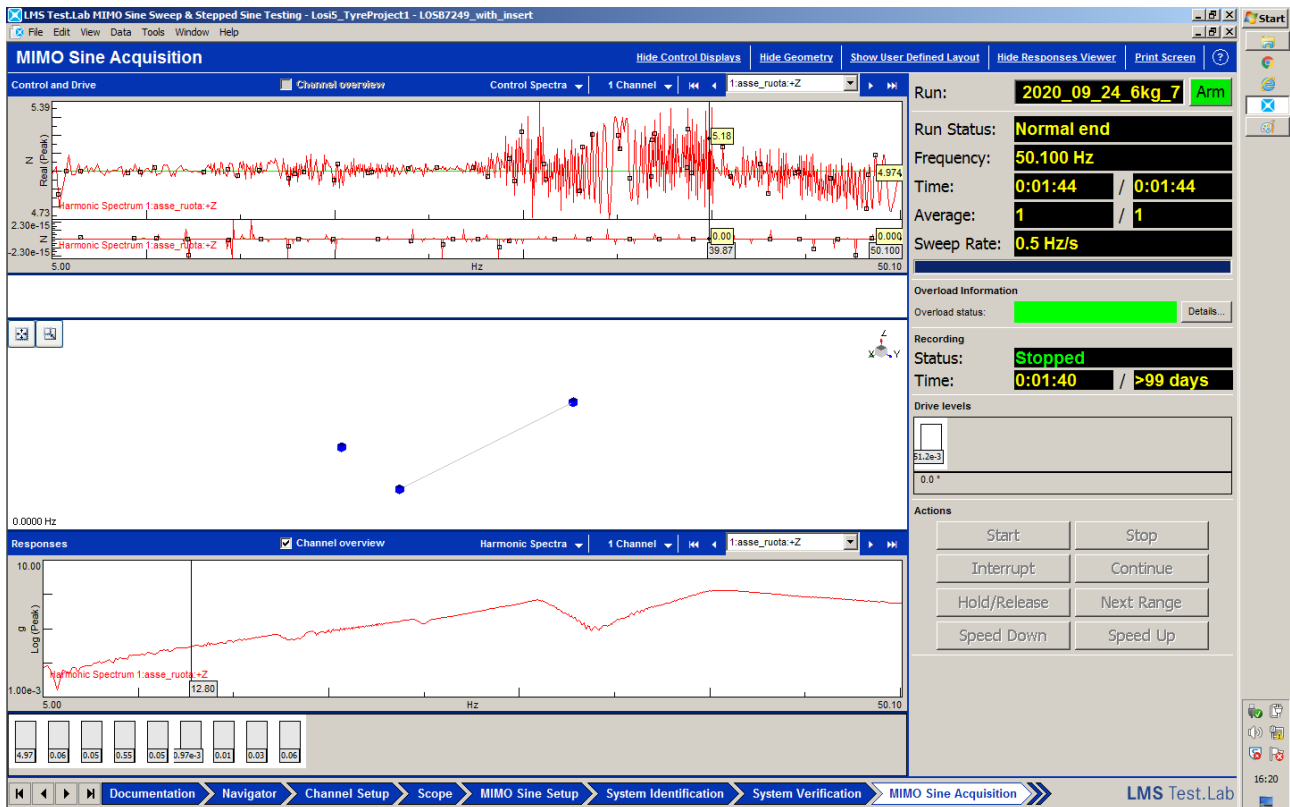


Figure 4.2.3 – MIMO Sine Acquisition tab.

4.3 Raw data

After finishing the acquisition, the raw data can be analysed inside the same software. In the Navigation tab (Figure 4.3.1) in fact, it is possible to plot the results but also to export the data to other software such as Matlab for example.

Figure 4.3.2, Figure 4.3.3, Figure 4.3.4 and Figure 4.3.5 show the four wheel configuration results after there are been exported in Matlab environment. The tyre configuration with insert have been tested with weight values from 2kg to 6kg with an increase of 1kg. The tyre configuration without insert instead, have the same weight range but with an increase of 0.5kg per test. This has been done to better study the behaviour of the tyres without insert due to the predicted lower stiffness.

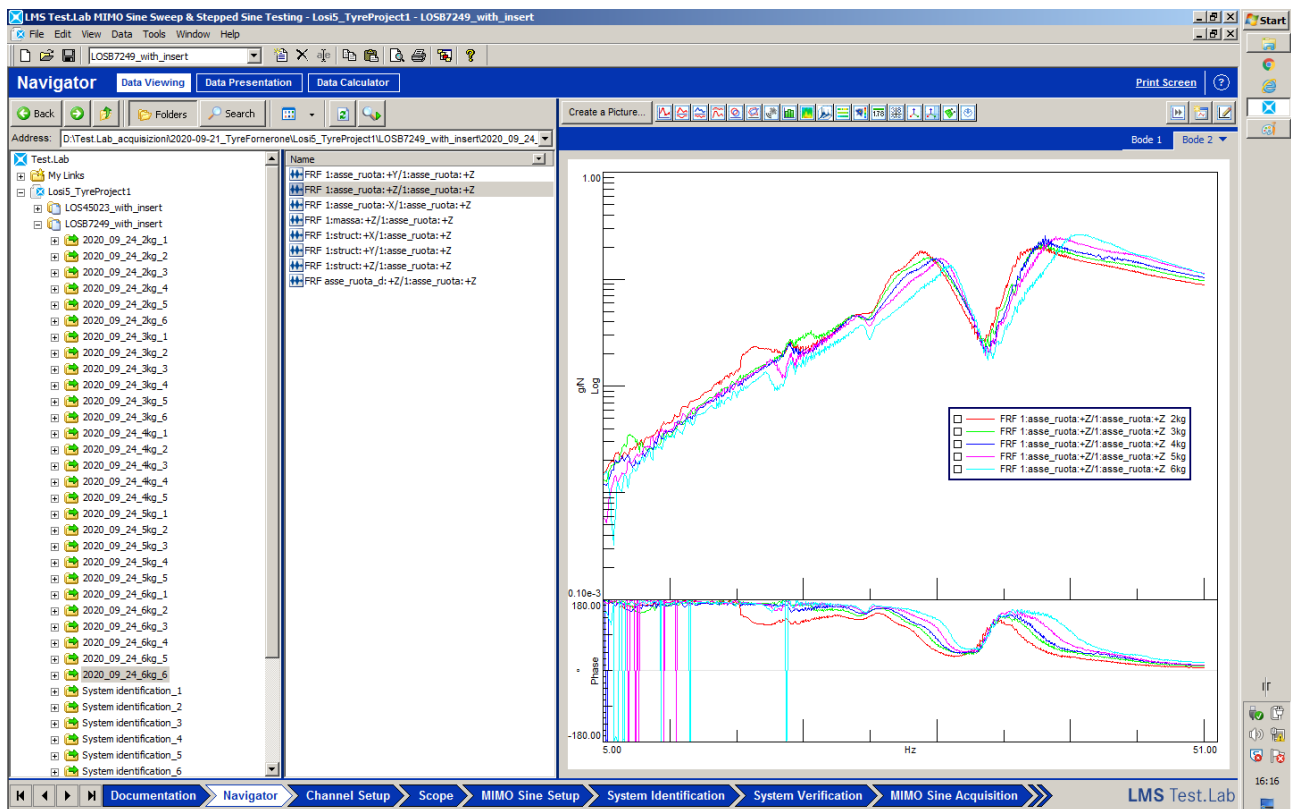


Figure 4.3.1 – Navigation tab.

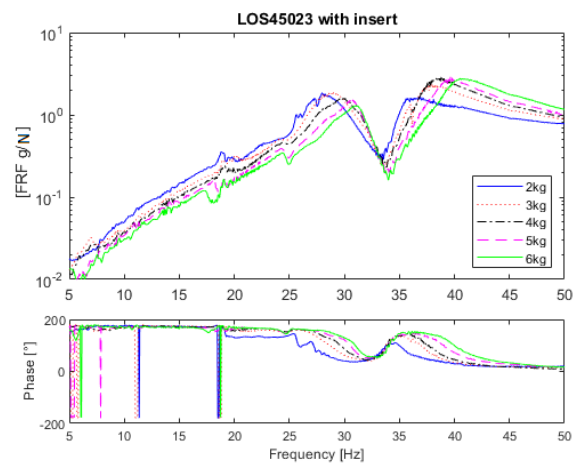


Figure 4.3.2 – LOS45023 with insert raw data.

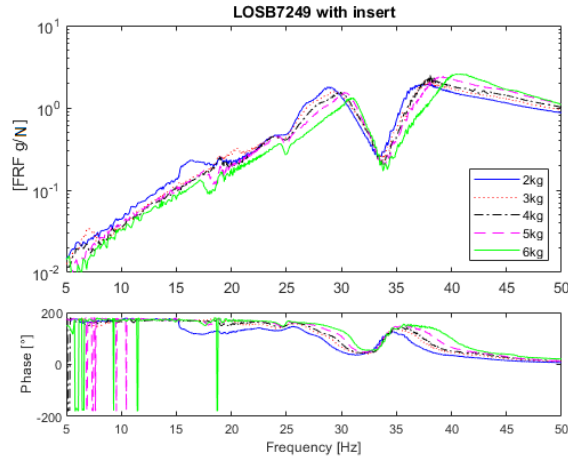


Figure 4.3.3 – LOSB7240 with insert raw data.

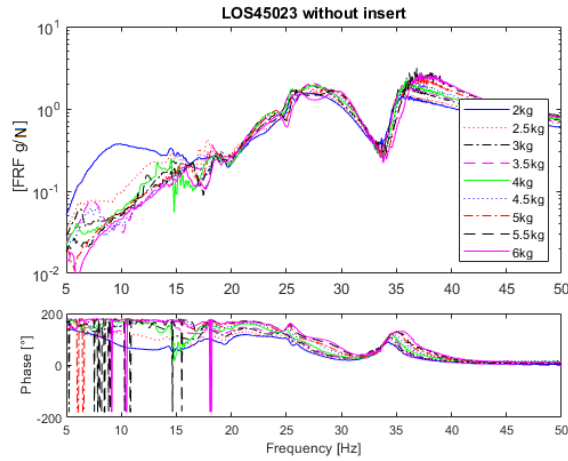


Figure 4.3.4 – LOS45023 without insert raw data.

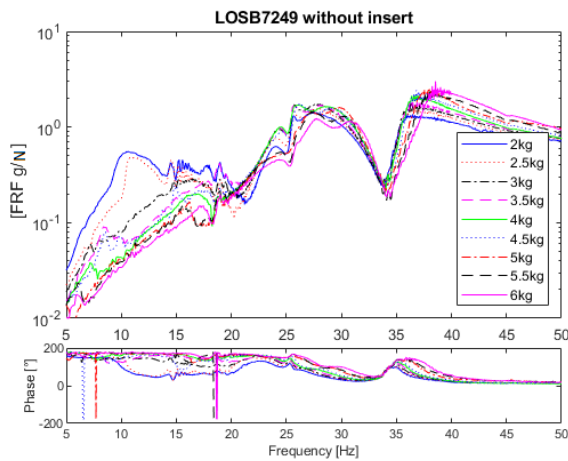


Figure 4.3.5 – LOSB7240 without insert raw data.

From the previous figures it is easy to determinate the two natural frequencies of the system. The two peaks are in fact very evident. It is also easy to notice that these two natural frequencies tend to slide at higher frequency values while increasing the weight. This is true for all the configurations.

Figure 4.3.6 and Figure 4.3.7 show a comparison between the configuration with insert and without insert while Figure 4.3.8 and Figure 4.3.9 show a comparison between the two different tyre type configurations. From Figure 4.3.6 and Figure 4.3.7 it is possible to understand the insert behaviour. Both configurations (LOS45023 and LOSB7240) in facts, show lower natural frequencies without the insert. This is due to the fact that the removal of the insert causes a reduction of the tyre stiffness. This behaviour is clear, especially at the higher weight values.

Figure 4.3.8 shows the comparison between LOS45023 and LOSB7240, both with insert. From this figure it is possible to see that the differences between the configurations is minimal. The curves in fact are almost the same, especially at higher weight values. Figure 4.3.9 instead show some differences. This figure shows the comparison between LOS45023 and LOSB7240, both without insert. In this case the lack of the insert causes a more evident difference between the two tyre type. The LOSB7240 has slightly higher values for the natural frequencies. This means that LOSB7240 is probably stiffer than LOS45023.

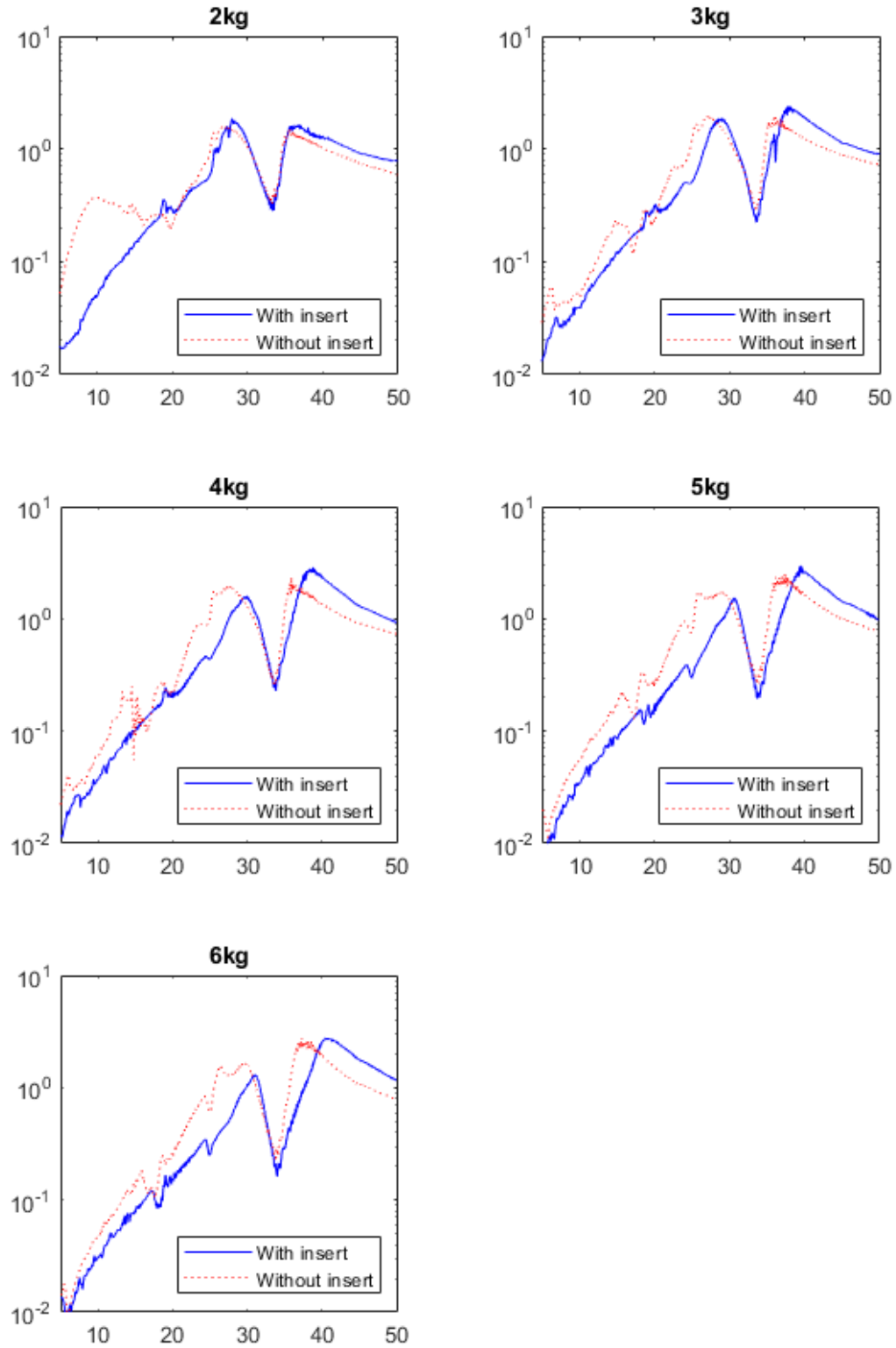


Figure 4.3.6 – LOS45023 with and without insert.

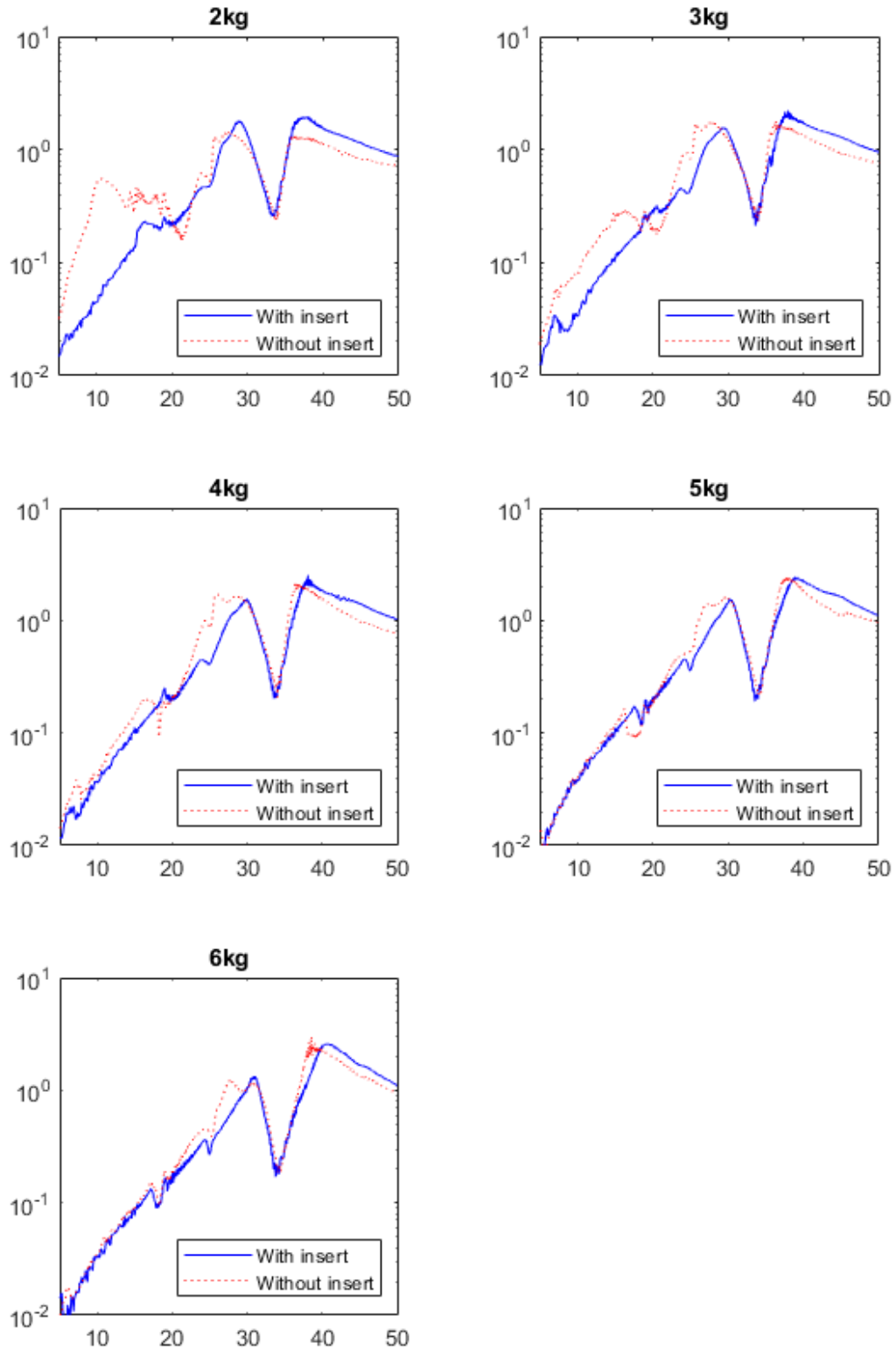


Figure 4.3.7 – LOSB7240 with and without insert.

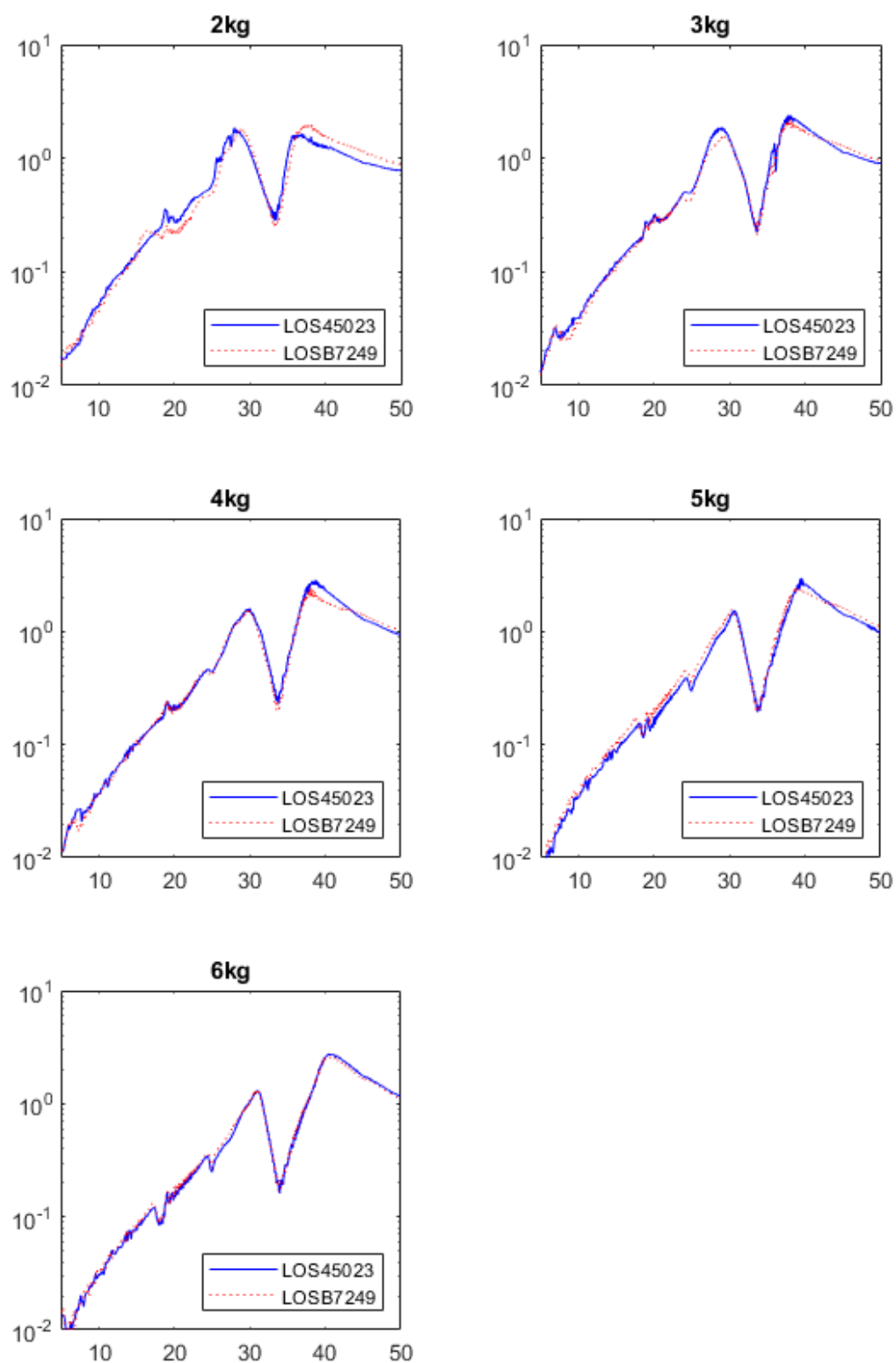


Figure 4.3.8 – LOS45023 and LOSB7240 with insert.

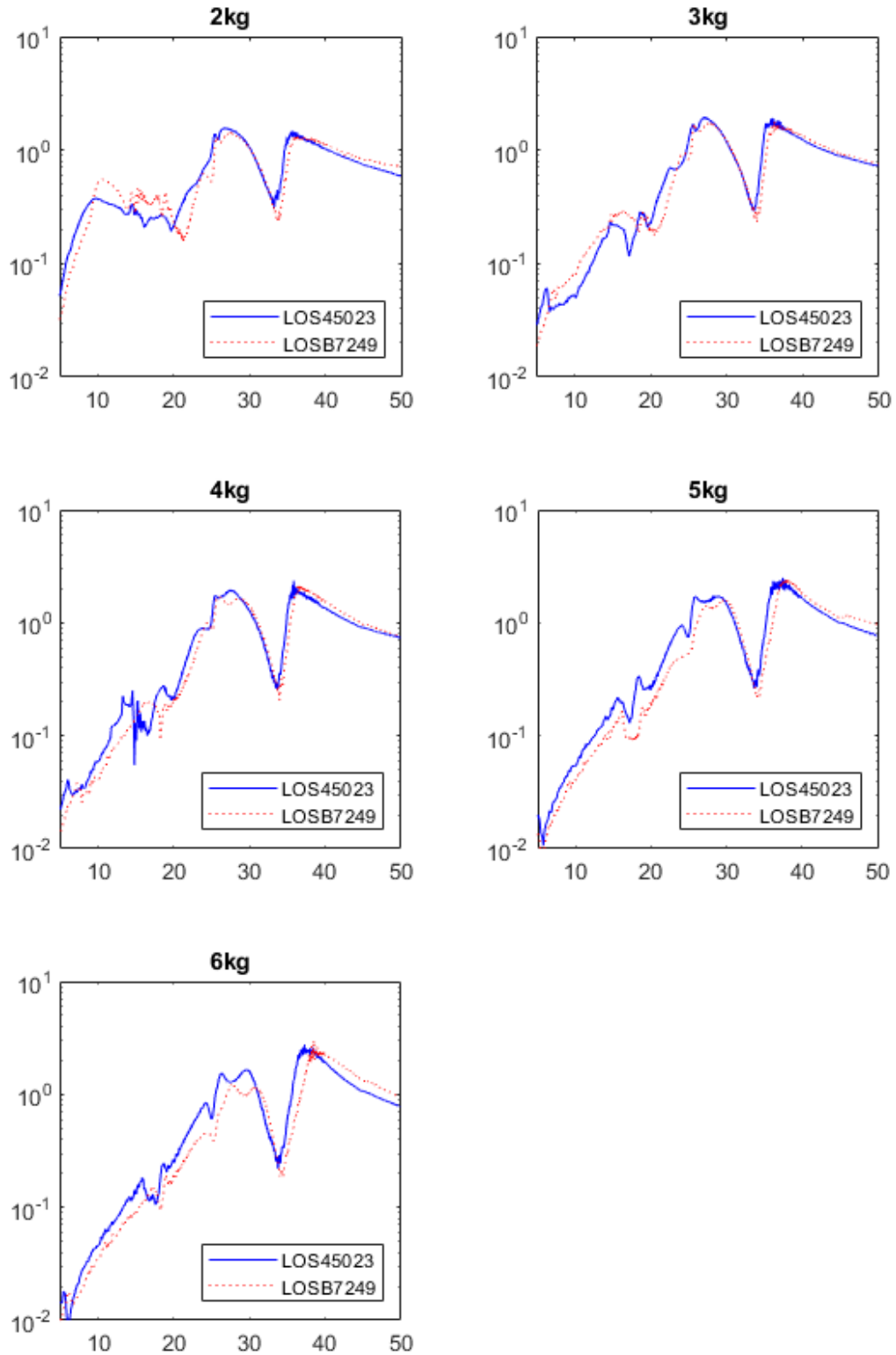


Figure 4.3.9 – LOS45023 and LOSB7240 without insert.

4.4 Post-processing

After a quick look at the raw data, a post-process is needed in order to obtain more useful information. The post-process can be done directly on the same software used for the tests (TestLab 17) using the PolyMAX tab and its own tab.

The first step is the data selection, this can be done in Band tab (Figure 4.4.1).

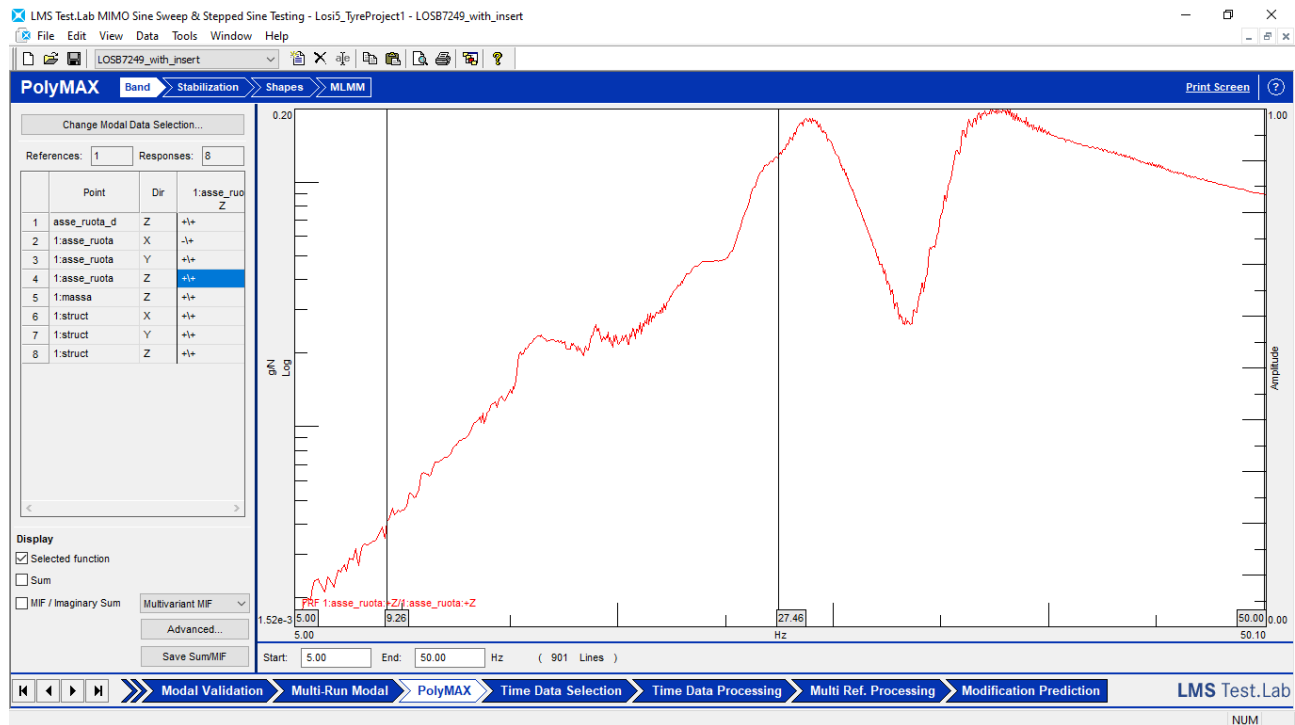


Figure 4.4.1 – PolyMax Band tab

The second step is the stabilization, done in the Stabilization tab (Figure 4.4.2). In this phase the software tries to fit the real curve using an iterative process increasing the number of poles each time. In this process, if a pole is identified in a large number of iterations it is a stable pole and probably a true mode of the system. In the Stabilization tab it is possible to see this study and the identified poles. In this case only the two poles that correspond to the two peaks are useful, so only that two are selected. In Figure 4.4.2 left side, the two selected modes are listed.

The next tab is the Shape tab (Figure 4.4.3). In this tab the mode shape is calculated using the two selected modes. In Figure 4.4.3 the selected modes are showed on the left, on the right a geometry sketch animation is showed. The last tab is the MLMM (Maximum Likelihood Modal Method) showed in Figure 4.4.4. This last step is an optimization procedure. The MLMM use as starting point the modes calculated by the previous passages and try to optimize them to better fit the experimental data.

After the calculations, the fitted curves can be analysed in the Modal Synthesis tab (Figure 4.4.5). In Figure 4.4.5 the selected modes are showed on the left, while on the right a graph shows both the original curve and the fitted curve. On the upper side it is possible to see the correlation and the error between the two curves.

After the post-process, all the useful data can be exported for further study.

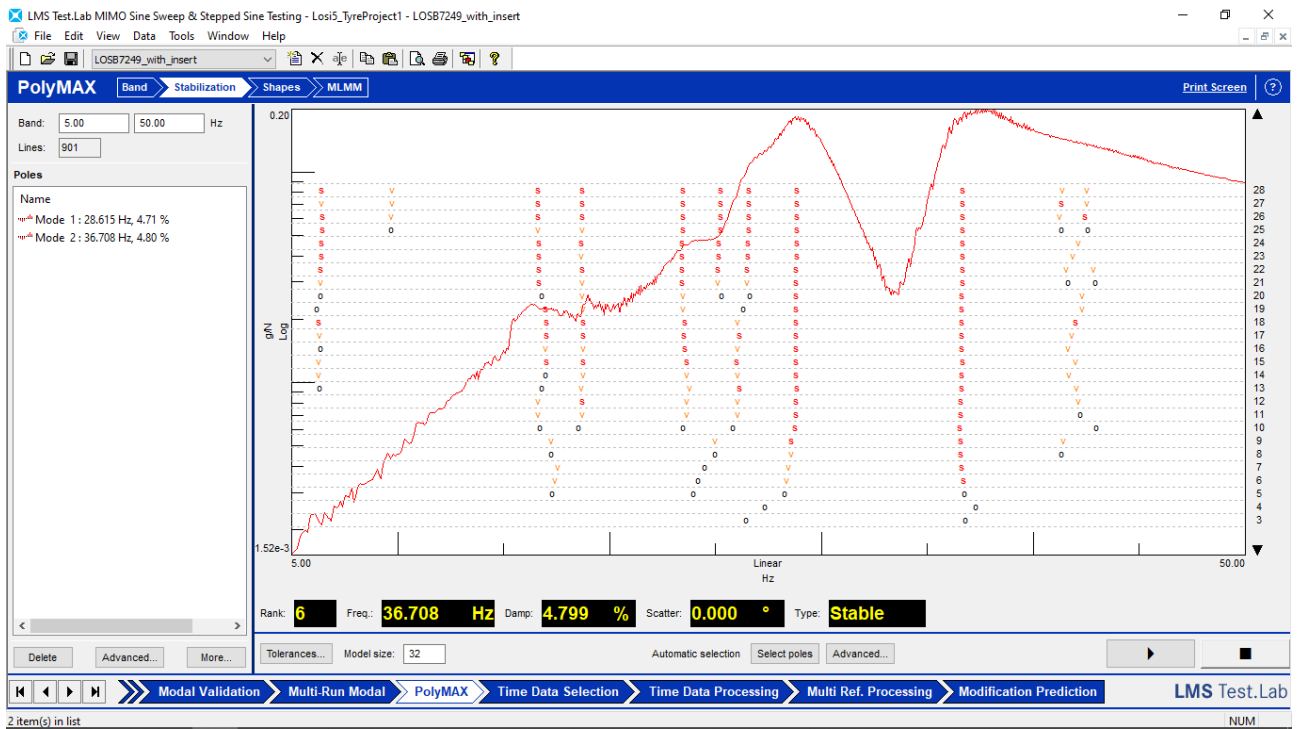


Figure 4.4.2 – PolyMax Stabilization tab

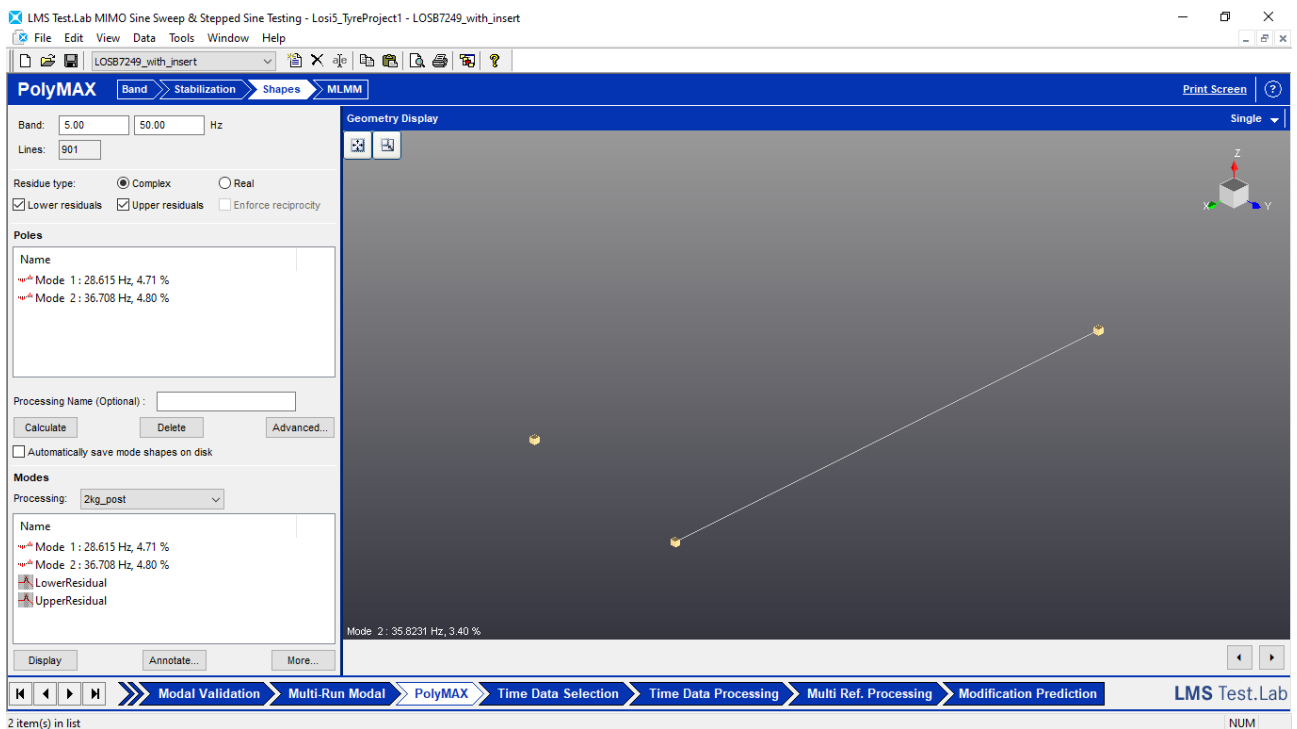


Figure 4.4.3 – PolyMax Shapes tab

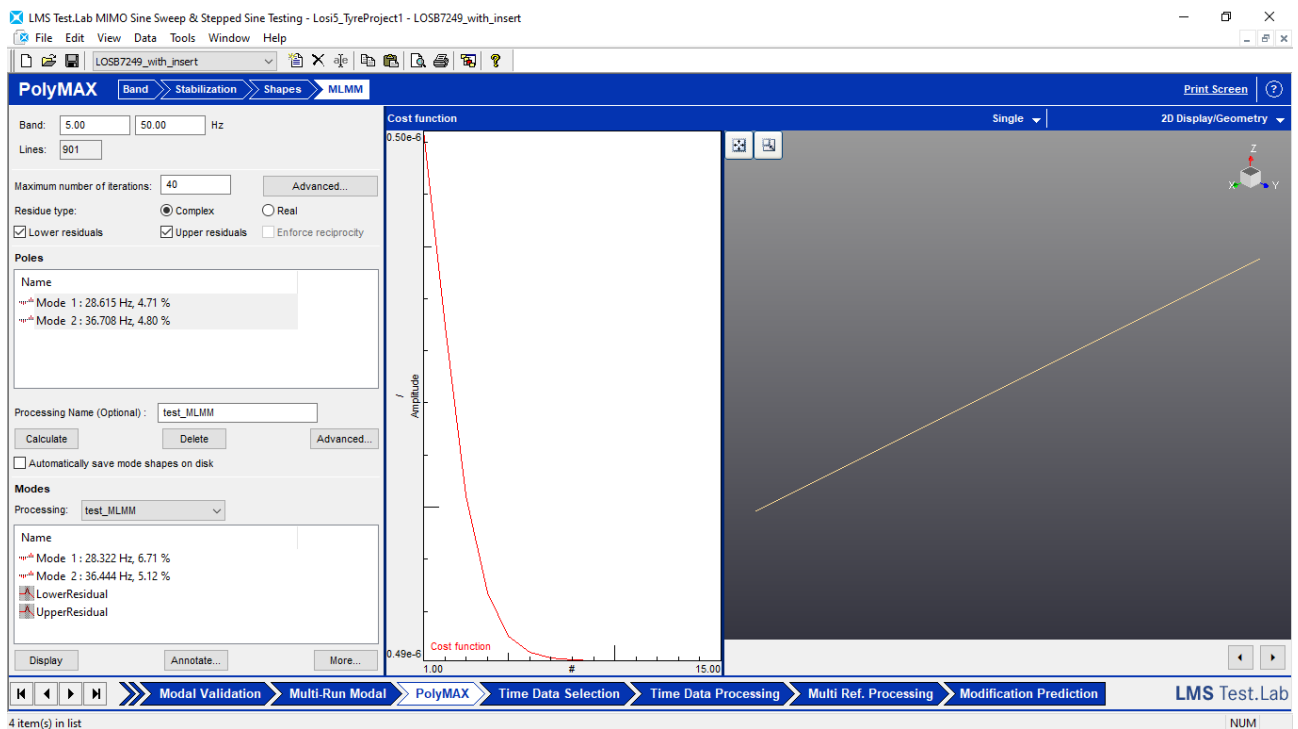


Figure 4.4.4 – PolyMax MLMM tab

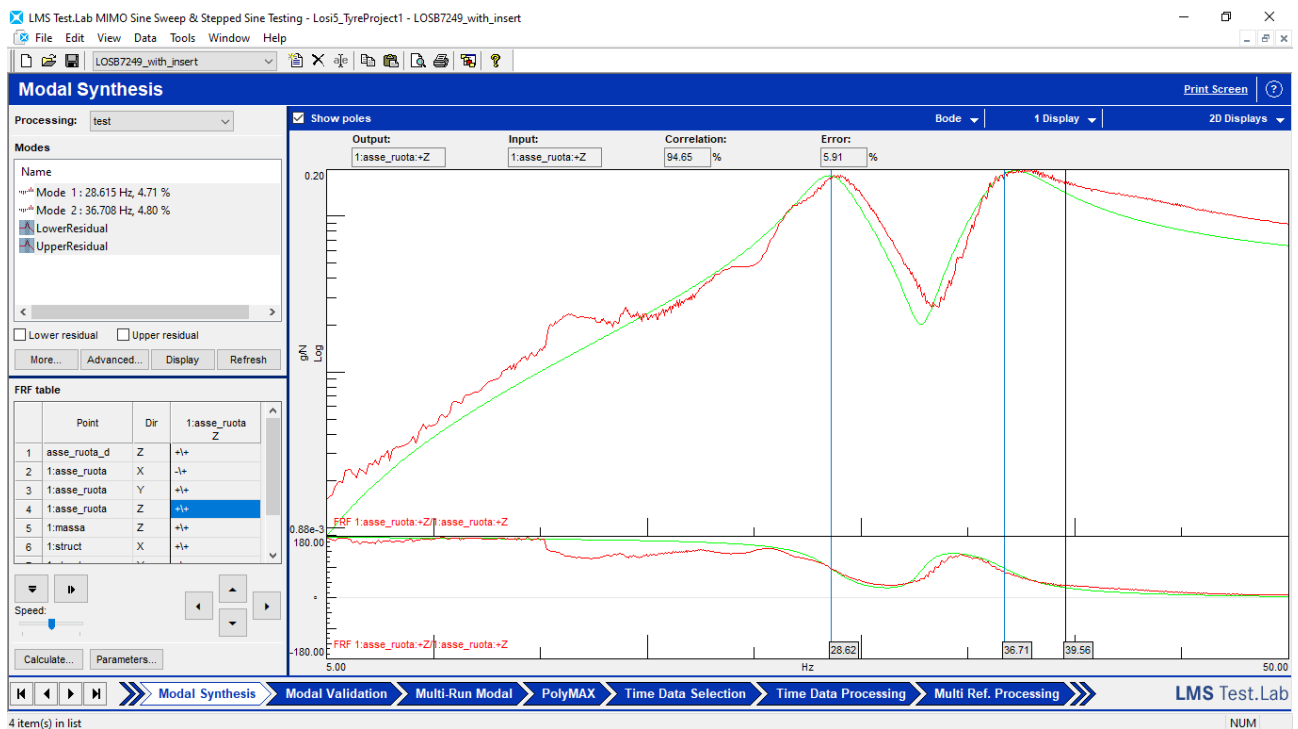


Figure 4.4.5 – Modal Synthesis tab

4.5 Natural frequencies (first attempt)

Once the post-process is done, the natural frequencies can be extracted. In Table 4.5.1 the natural frequencies values are showed for all the different configurations varying the weight.

Table 4.5.1 – Natural frequencies for all the configuration and weights.

	LOS45023 with insert		LOS45023 without insert		LOSB7240 with insert		LOSB7240 without insert	
m [kg]	ω_1 [Hz]	ω_2 [Hz]	ω_1 [Hz]	ω_2 [Hz]	ω_1 [Hz]	ω_2 [Hz]	ω_1 [Hz]	ω_2 [Hz]
2	27.979	35.904	26.890	35.282	28.647	36.750	27.714	35.739
2.5	-	-	27.076	35.063	-	-	28.122	35.932
3	29.185	37.660	27.042	35.171	29.149	37.344	28.124	36.036
3.5	-	-	27.271	35.615	-	-	28.478	36.240
4	30.084	38.222	27.617	35.824	29.494	37.730	28.894	36.497
4.5	-	-	28.564	35.784	-	-	29.374	36.758
5	30.548	39.533	29.138	37.315	30.265	38.891	29.733	37.390
5.5	-	-	29.511	37.554	-	-	30.248	37.857
6	31.059	40.498	29.536	36.660	30.861	40.179	31.177	38.612

Figure 4.5.1 and Figure 4.5.2 show the natural frequencies trend varying the weight for all the configuration.

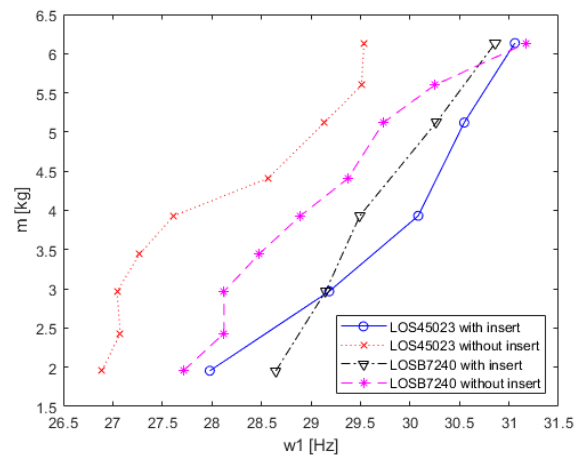


Figure 4.5.1 – ω_1 trend varying weight.

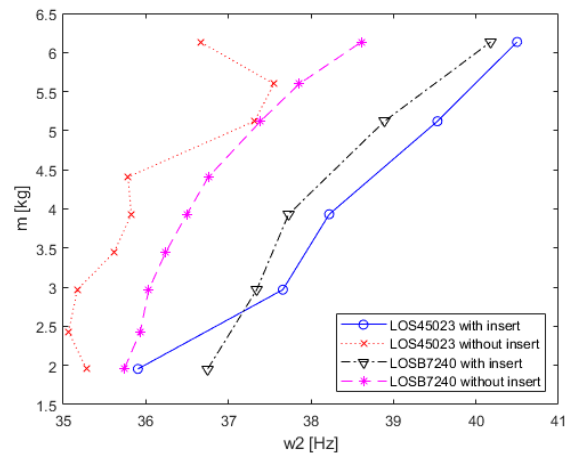


Figure 4.5.1 – ω_2 trend varying weight.

4.6 Dynamic stiffness calculation (first attempt)

Knowing the natural frequencies values, it is now possible to calculate the dynamic stiffness of the tyre. The configuration of wheel and weight used in the dynamic tests can be schematized as a two DOF problem like the one showed in Figure 4.6.1.

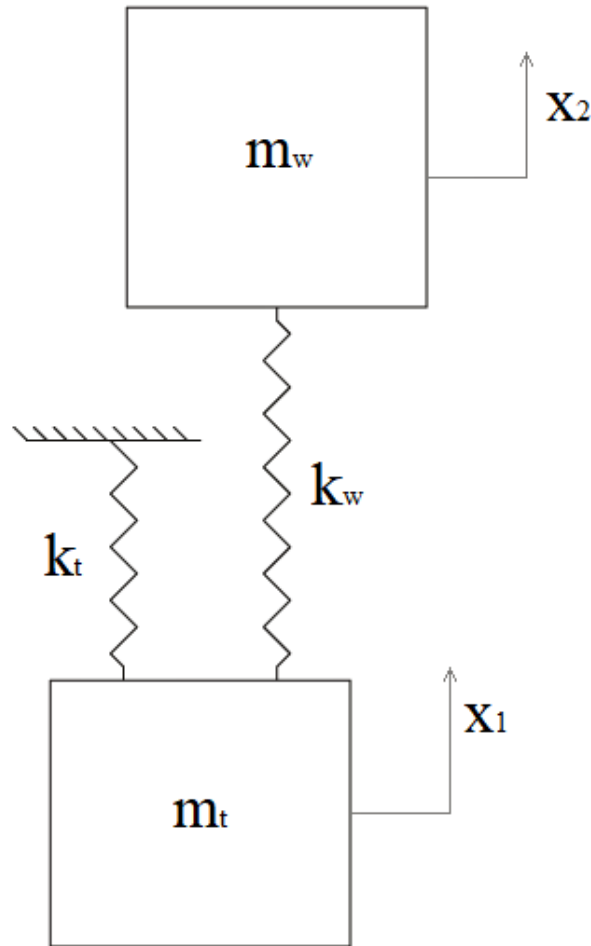


Figure 4.6.1 – Dynamic test scheme.

In Figure 4.6.1 m_t represent the mass of the wheel and its support, m_w the mass of the weight, k_t the tyre stiffness and k_w the wire stiffness.

For this problem the two differential equations can be written as:

$$\begin{cases} m_t \ddot{x}_1 + (k_t + k_w)x_1 - k_w x_2 = 0 \\ m_w \ddot{x}_2 + k_w x_2 - k_w x_1 = 0 \end{cases} \quad (4.6.1)$$

These equations can be converted in matrix form. It results:

$$\begin{bmatrix} m_t & 0 \\ 0 & m_w \end{bmatrix} \begin{Bmatrix} \ddot{x}_1 \\ \ddot{x}_2 \end{Bmatrix} + \begin{bmatrix} k_t + k_w & -k_w \\ -k_w & k_w \end{bmatrix} \begin{Bmatrix} x_1 \\ x_2 \end{Bmatrix} = \begin{Bmatrix} 0 \\ 0 \end{Bmatrix} \quad (4.6.2)$$

The natural frequencies can be calculated imposing:

$$\det([k] - \omega^2 [m]) = \det \begin{bmatrix} k_t + k_w - \omega^2 m_t & -k_w \\ -k_w & k_w - \omega^2 m_w \end{bmatrix} = 0 \quad (4.6.3)$$

It results

$$\omega^4 m_t m_w + \omega^2 (-k_t m_t - k_w (m_t + m_w)) + k_t k_w = 0 \quad (4.6.4)$$

That can be written also as:

$$a\omega^4 + b\omega^2 + c = 0 \quad (4.6.5)$$

It results that:

$$\begin{cases} a = m_t m_w \\ b = -k_t m_t - k_w (m_t + m_w) \\ c = k_t k_w \end{cases} \quad (4.6.6)$$

In this experiment the masses are known while the stiffnesses must be calculated so a is known while b and c are unknown.

Writing the resolutive formula for the 4.6.5 equation, it results:

$$\omega_{1,2}^2 = \frac{-b \pm \sqrt{b^2 - 4ac}}{2a} \quad (4.6.7)$$

$$\begin{cases} \omega_1^2 + \omega_2^2 = \frac{-b - \sqrt{b^2 - 4ac} - b + \sqrt{b^2 - 4ac}}{2a} \\ \omega_1^2 - \omega_2^2 = \frac{-b - \sqrt{b^2 - 4ac} + b - \sqrt{b^2 - 4ac}}{2a} \end{cases} = \begin{cases} \omega_1^2 + \omega_2^2 = \frac{-2b}{2a} \\ \omega_1^2 - \omega_2^2 = \frac{-2\sqrt{b^2 - 4ac}}{2a} \end{cases} \quad (4.6.8)$$

$$\begin{cases} b = -a(\omega_1^2 + \omega_2^2) \\ (\omega_1^2 - \omega_2^2)^2 a^2 = b^2 - 4ac \end{cases} = \begin{cases} b = -a(\omega_1^2 + \omega_2^2) \\ c = a\omega_1^2 \omega_2^2 \end{cases} \quad (4.6.9)$$

Knowing the value of a it results:

$$\begin{cases} b = -a(\omega_1^2 + \omega_2^2) \\ c = a\omega_1^2 \omega_2^2 \end{cases} = \begin{cases} b = -m_t m_w (\omega_1^2 + \omega_2^2) = -k_t m_t - k_w (m_t + m_w) \\ c = m_t m_w \omega_1^2 \omega_2^2 = k_t k_w \end{cases} \quad (4.6.10)$$

The result is a two equations system with only the stiffnesses as the unknown

$$\begin{cases} k_t = \frac{m_t m_w (\omega_1^2 + \omega_2^2) - k_w (m_t + m_w)}{m_t} \\ k_t = \frac{m_t m_w \omega_1^2 \omega_2^2}{k_w} \end{cases} \quad (4.6.11)$$

The result is a second-degree equation

$$k_w^2 (m_t + m_w) - k_w m_t m_w (\omega_1^2 + \omega_2^2) + m_t^2 m_w \omega_1^2 \omega_2^2 = 0 \quad (4.6.12)$$

The solutions are:

$$k_{w1,2} = \frac{m_t m_w (\omega_1^2 + \omega_2^2) \pm \sqrt{[m_t m_w (\omega_1^2 + \omega_2^2)]^2 - 4 m_t^2 m_w \omega_1^2 \omega_2^2 (m_t + m_w)}}{2(m_t + m_w)} \quad (4.6.13)$$

At this point the stiffness should be calculated for all the weights. But for the frequencies' values determined by the tests, the determinant of 4.6.13 is negative so the solution is impossible.

Another way to solve the problem and calculate the stiffnesses implies the imposition of a constant value for the wire stiffness. This choice is not completely true because the wire stiffness could change with the weight change. The key is to hypothesize that the wire stiffness change is way smaller than the tyre stiffness change. In this way all the stiffnesses can be calculated in a single step. The starting equation is the first of the 4.6.10 system.

$$k_t m_t + k_w (m_t + m_w) = m_t m_w (\omega_1^2 + \omega_2^2) \quad (4.6.14)$$

In this equation there are six unknowns: k_w and a value of k_t for each of the five weights. This equation can be written in matrix form as:

$$\begin{bmatrix} m_t + m_{w2kg} & m_t & 0 & 0 & 0 & 0 \\ m_t + m_{w3kg} & 0 & m_t & 0 & 0 & 0 \\ m_t + m_{w4kg} & 0 & 0 & m_t & 0 & 0 \\ m_t + m_{w5kg} & 0 & 0 & 0 & m_t & 0 \\ m_t + m_{w6kg} & 0 & 0 & 0 & 0 & m_t \end{bmatrix} \begin{Bmatrix} k_w \\ k_{t2kg} \\ k_{t3kg} \\ k_{t4kg} \\ k_{t5kg} \\ k_{t6kg} \end{Bmatrix} = \begin{Bmatrix} m_t m_{w2kg} (\omega_1^2 + \omega_2^2)_{2kg} \\ m_t m_{w3kg} (\omega_1^2 + \omega_2^2)_{3g} \\ m_t m_{w4kg} (\omega_1^2 + \omega_2^2)_{4kg} \\ m_t m_{w5kg} (\omega_1^2 + \omega_2^2)_{5kg} \\ m_t m_{w6kg} (\omega_1^2 + \omega_2^2)_{6kg} \end{Bmatrix} \quad (4.6.15)$$

That can be also written as:

$$[A]\{k\} = \{b\} \quad (4.6.16)$$

Using a pseudo-inverse, the stiffnesses can be calculated as:

$$\{k\} = [A]^{-1} \{b\} \quad (4.6.17)$$

The solution is still impossible because some of the stiffnesses are negative.

This led to the conclusion that the two main peaks identified in the raw curve probably are not the system natural frequencies. Hence the real frequencies values must be found.

4.7 Simulation

To overcome the problems arisen during the stiffnesses calculation, the whole test rig must be studied with a dedicated simulation. In this case, two different simulations have been done: the first one is done with Solidworks, using the whole three-dimensional model; the second one, is made using a Matlab based software called LUPOS (more information about this software can be found in the chapter five).

4.7.1 Solidworks simulation

This simulation is done using directly the 3D model of the system showed in Figure 4.7.1.1.

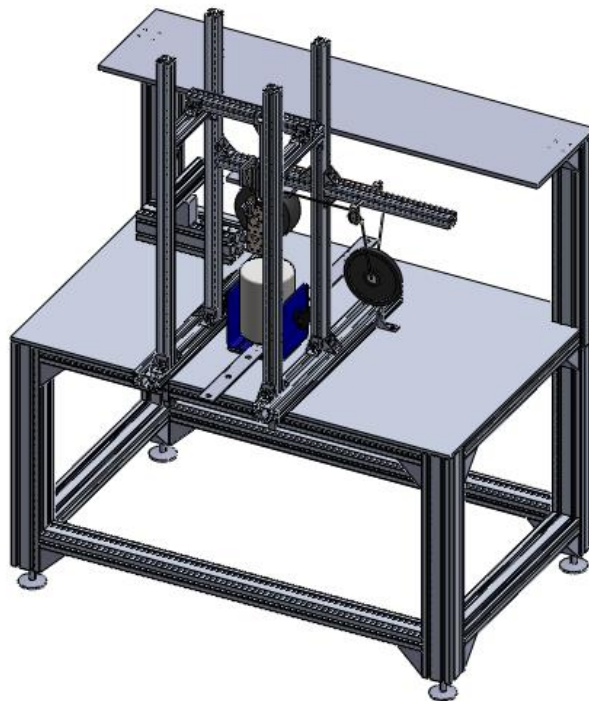


Figure 4.7.1.1 – Solidworks assembly model.

The first ten frequency results are showed in Table 4.7.1.1 with a brief description of the components involved.

Table 4.7.1.1 – Solidworks modes frequency values.

Mode	Frequency [Hz]	Description
1	0.702	Weight YX swing
2	2.846	Weight YZ swing
3	9.136	Wheel and Weight
4	19.57	Wheel and Weight
5	22.14	Weight

6	26.53	Weight
7	29.98	Workbench
8	31.45	Weight
9	32.01	Workbench
10	45.3	Wire

From this model the wheel-weight frequency seems to be the Mode 3 and Mode 4, and the resultant frequency: $\omega_1=9.136$ and $\omega_1=19.57$. These mode shapes are showed in Figure 4.7.1.2 and Figure 4.7.1.3.

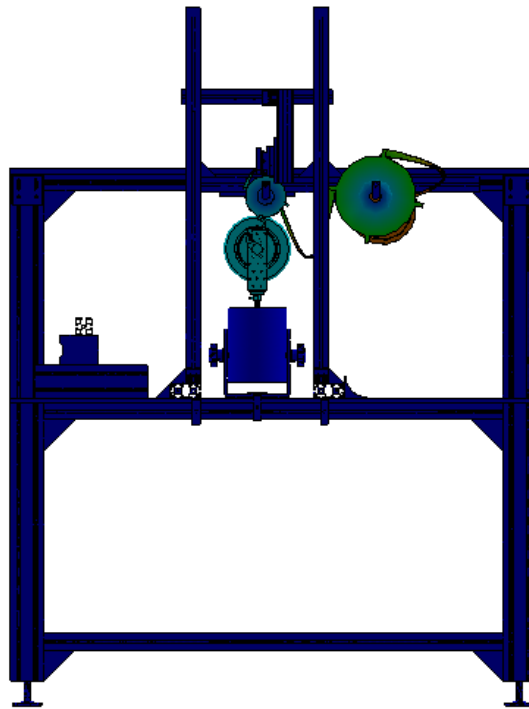


Figure 4.7.1.2 – Solidworks Mode 3.

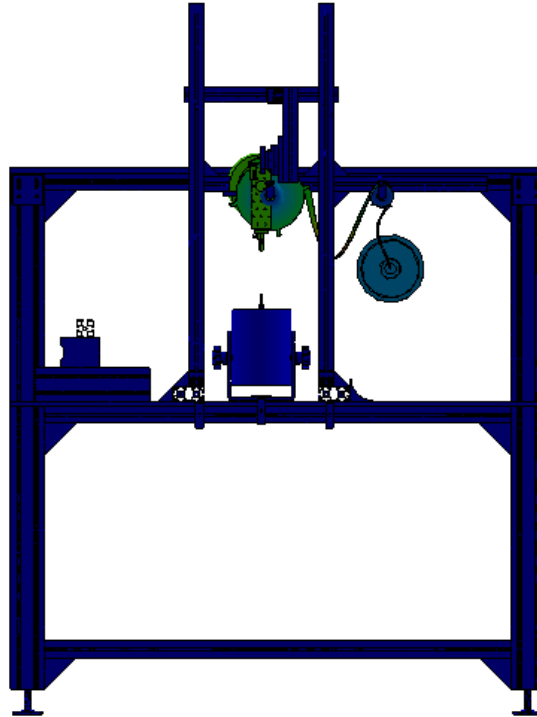


Figure 4.7.1.3 – Solidworks Mode 4.

4.7.2 LUPOS simulation

The first step into the LUPOS simulation is a schematization of an equivalent two degrees of freedom system, like the one shown in Figure 4.6.1. This model is shown in Figure 4.7.2.1.

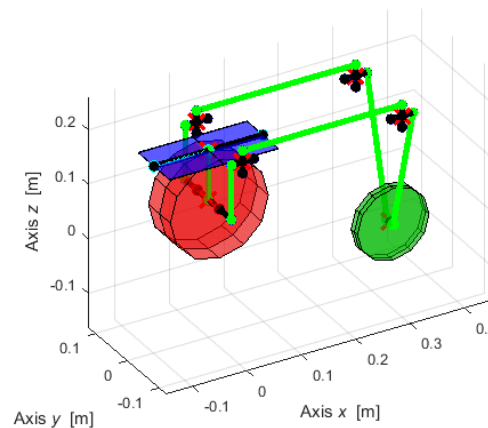


Figure 4.7.2.1 – LUPOS 2dof model.

This model uses the static stiffness values, estimated in the static tests, and the measured mass values of the wheel and the weight. in order to have an idea of the two natural frequencies of the system. The results for a single weight configuration are showed in Figure 4.7.2.2 and Figure 4.7.2.3 while the frequencies results of all the configurations are shown in Table 4.7.2.1.

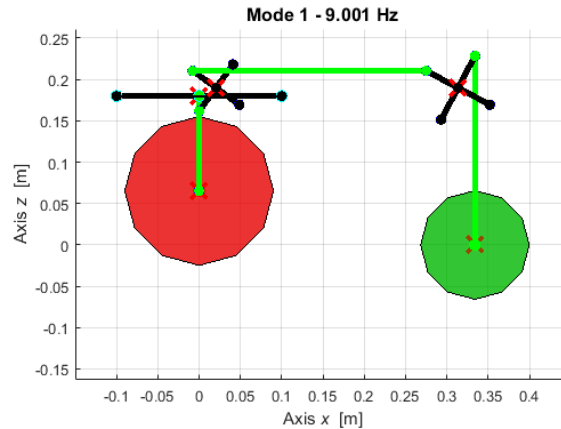


Figure 4.7.2.2 – LOS45023 with insert mode 1 with 2kg weight.

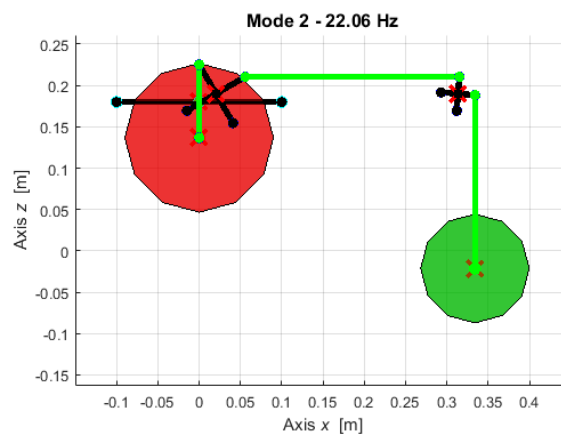


Figure 4.7.2.3 – LOS45023 with insert mode 2 with 2kg weight.

Table 4.7.2.1 – 2dof natural frequencies values for all the weight configurations.

	LOS45023 with insert		LOS45023 without insert		LOSB7240 with insert		LOSB7240 without insert	
m [kg]	w1 [Hz]	w2 [Hz]	w1 [Hz]	w2 [Hz]	w1 [Hz]	w2 [Hz]	w1 [Hz]	w2 [Hz]
2	9,001	22,06	6,462	20,18	9,077	22,20	6,357	20,14
3	7,584	21,25	5,585	18,95	7,641	21,41	5,499	18,90
4	6,704	20,89	5,005	18,37	6,750	21,05	4,931	18,31
5	5,944	20,64	4,486	17,96	5,983	20,81	4,421	17,90
6	5,466	20,51	4,151	17,73	5,500	20,68	4,091	17,67

The next step is a more detailed schematization, a model in between the Soliworks model and the previous 2dof model. This is possible increasing the model details such as the basic frame, the wheel support, the workbench, etc.

This second model is shown in Figure 4.7.2.4. The grey structure is the workbench, the blue one is the testrig frame. The orange part is the shaker, the green is the wheel support while the wheel itself is red and the weight is the black one.

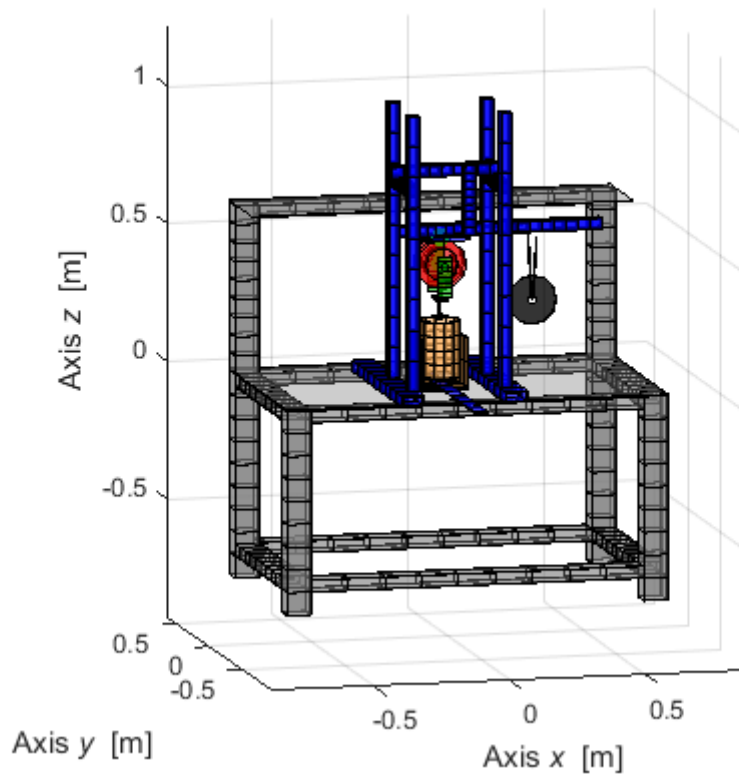


Figure 4.7.2.4 – LUPOS model.

Table 4.7.2.2 shows the first twenty resultant modes for the LOS45023 with insert-2kg configuration and the involved components.

Table 4.7.2.2 –Modes frequency values.

Mode	Frequency [Hz]	Description
1	0.105	Weight
2	0.353	Weight
3	0.523	Weight
4	0.723	Weight
5	2.911	Weight
6	8.146	Wheel and weight
7	18.2	Wire
8	18.4	Wire
9	18.4	Wire
10	18.44	Wire
11	18.44	Wire
12	19.19	Wheel and weight
13	19.75	Support wheel
14	26.3	Wire
15	26.34	Wire
16	26.37	Wire

17	26.37	Wire
18	26.52	Wire
19	29.28	Workbench and support wheel
20	35.49	Workbench and frame

From this model the two wheel-weight frequencies seem to be the Mode 6 and Mode 12 and the resultant frequencies: $\omega_1=8.146$ Hz and $\omega_2=19.19$ Hz. These two modes shapes are showed in Figure 4.7.2.5 and Figure 4.7.2.6.

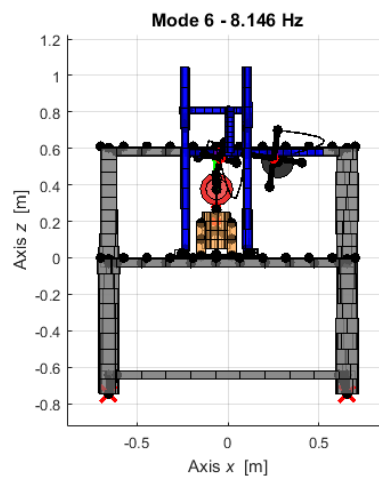


Figure 4.7.2.5 – LUPOS mode 6.

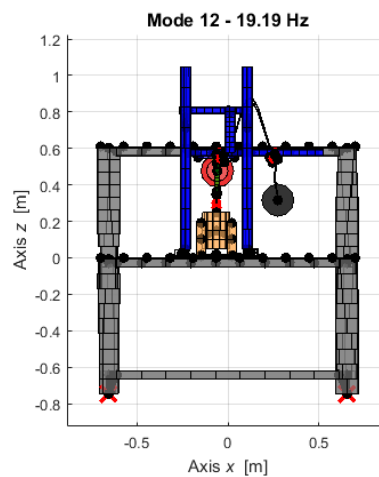


Figure 4.7.2.6 – LUPOS mode 12.

Table 4.7.2.3 shows the two natural frequencies of the system for all the possible combination of wheel configuration and applied weight.

Table 4.7.2.3 – LUPOS natural frequencies for all the configuration and weights.

	LOS45023 with insert	LOS45023 without insert	LOSB7240 with insert	LOSB7240 without insert
--	----------------------	-------------------------	----------------------	-------------------------

m [kg]	ω_1 [Hz]	ω_2 [Hz]	ω_1 [Hz]	ω_2 [Hz]	ω_1 [Hz]	ω_2 [Hz]	ω_1 [Hz]	ω_2 [Hz]
2	8,146	19,190	6,505	16,220	8,188	19,320	6,430	16,160
2.5	-	-	5,986	15,830	-	-	5,921	15,760
3	6,742	18,910	5,521	15,540	6,772	19,040	5,464	15,470
3.5	-	-	5,186	15,370	-	-	5,134	15,290
4	5,909	18,810	4,898	15,240	5,933	18,930	4,850	15,160
4.5	-	-	4,658	15,140	-	-	4,613	15,050
5	5,208	18,750	4,355	15,020	5,229	18,860	4,314	14,940
5.5	-	-	4,183	14,960	-	-	4,144	14,880
6	4,774	18,720	4,011	14,910	4,729	18,820	3,974	14,820

4.7.3 Frequencies comparison

Table 4.7.3.1 show a comparison between Solidworks and LUPOS frequencies results for the LOS45023-with-insert configuration.

Table 4.7.3.1 – Solidworks and LUPOS frequencies comparison.

Mode	Solidworks Frequency [Hz]	LUPOS Frequency [Hz]
1	0.702	0.105
2	2.846	0.353
3	9.136	0.523
4	19.57	0.723
5	22.14	2.911
6	26.53	8.146
7	29.98	18.2
8	31.45	18.4
9	32.01	18.4
10	45.3	18.44

As it is possible to see, in the LUPOS simulation the first ten frequencies have all a smaller value. This is due to the different wire behaviour between the two software.

4.8 Natural frequencies

Looking at the results of both the simulations, it is clear that the previous natural frequency obtained from the experimental test are the wrong one. The two big peaks in the FRF curve are probably due to the structure modes. For this reason, a new analysis in Polymax is needed.

This time the analysis is restricted in a specific frequency range to find values as close as the simulation results. During the Polymax process, in fact the selected poles are the closest to the one obtained by the simulations. In this way a new set of frequencies values are found.

Table 4.8.1 shows the natural frequencies values for all the different configurations varying the weight.

Table 4.8.1 – Polymax natural frequencies for all the configuration and weights.

	LOS45023 with insert		LOS45023 without insert		LOSB7240 with insert		LOSB7240 without insert	
m [kg]	ω_1 [Hz]	ω_2 [Hz]	ω_1 [Hz]	ω_2 [Hz]	ω_1 [Hz]	ω_2 [Hz]	ω_1 [Hz]	ω_2 [Hz]
2	9,821	19,286	6,759	16,255	8,640	19,130	6,283	16,214
2.5	-	-	6,279	15,799	-	-	6,028	16,099
3	7,304	19,087	5,314	15,567	6,480	18,951	5,333	15,539
3.5	-	-	6,302	15,453	-	-	5,678	15,223
4	6,500	18,709	5,341	15,146	5,933	18,913	5,376	15,159
4.5	-	-	5,311	14,887	-	-	5,391	14,991
5	5,698	18,476	5,314	15,262	6,039	18,931	5,308	14,767
5.5	-	-	5,473	14,798	-	-	5,456	14,639
6	5,441	18,703	5,381	14,728	5,490	18,727	5,747	14,616

4.9 Dynamic stiffness estimation

Now that the correct frequencies values have been found, the dynamic stiffness values must be estimated. For this purpose, the LUPOS simulation is used. The process consists in a parametric study in which the stiffness value (used in the simulation) change. The first value used is the static stiffness, then this value is adjusted to obtain the natural frequencies values of the simulation as close as possible to the one obtained from the experimental tests. To do so the least square method is used.

The first phase is the determination of the frequencies trend varying the stiffness value for each configuration. Figure 4.9.1 and Figure 4.9.2 show an example of the natural frequencies' variation of the LOS45023_with_insert configuration with a weight of 2kg in the range of stiffness of 10000-200000 N/m.

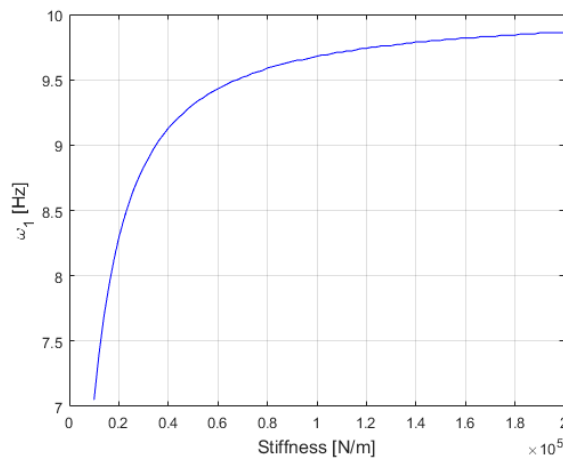


Figure 4.9.1 – LOS45023_with_insert_2kg ω_1 trend varying the stiffness value.

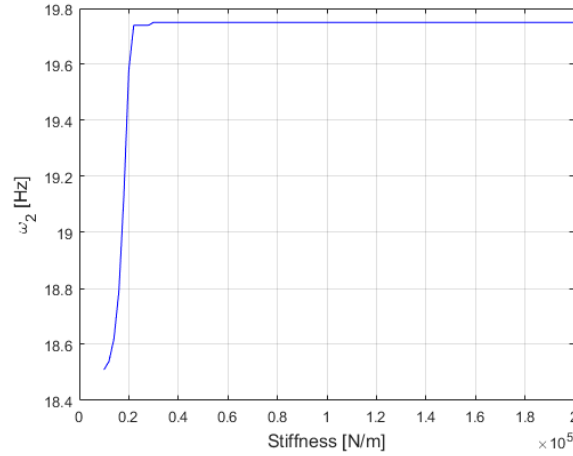


Figure 4.9.2 – LOS45023_with_insert_2kg ω₂ trend varying the stiffness value.

Once that all these curves have been determined for all the weights, the dynamic stiffness value can be estimated. For each wheel configuration, the least square method is used. The basic formula used is:

$$S = \sum_{i=1}^n (y - f(x_i))^2 \quad (4.9.1)$$

Where y is the frequency value obtained experimentally, while $f(x_i)$ is the simulation frequency value (that changes with the stiffness variation) for each applied weight.

At this point, the stiffness value that minimize the S function is the correct one.

Figure 4.9.3 shows the S function for the LOS45023_with_insert configuration with the same stiffness range used for the previous figures. Figure 4.9.4, Figure 4.9.5, Figure 4.9.6 and Figure 4.9.7 show a detailed view of the S function respectively for the LOS45023_with_insert, the LOS45023_without_insert, the LOSB7249_with_insert and the LOSB7249_without_insert. The red cross indicates the minimum point of every curve.

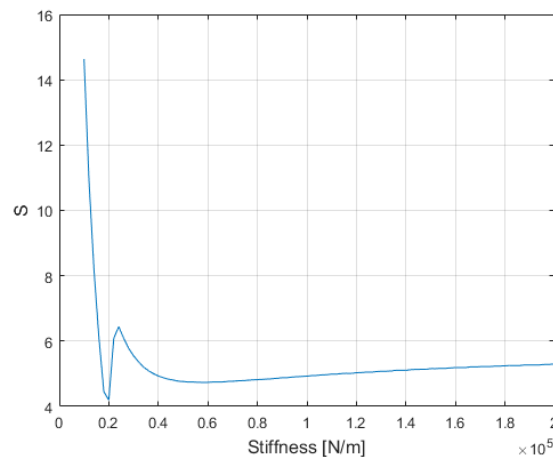


Figure 4.9.3 – S function trend varying the stiffness.

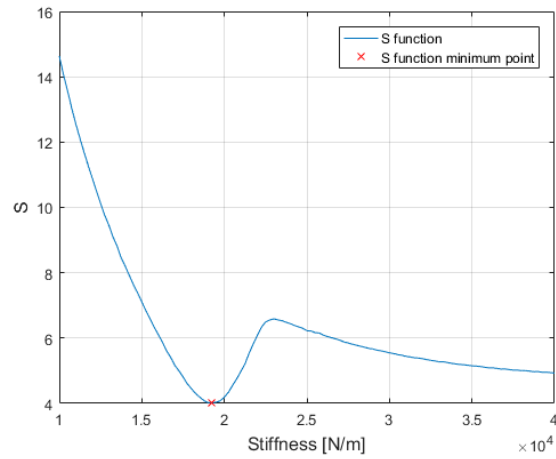


Figure 4.9.4 – Detail of S function trend varying the stiffness for LOS45023_with_insert.

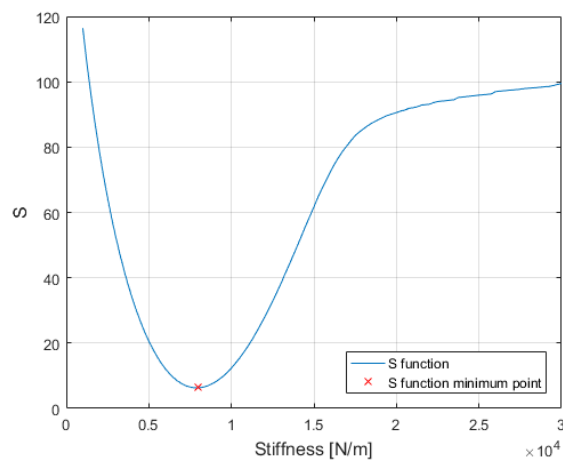


Figure 4.9.5 – Detail of S function trend varying the stiffness for LOS45023_without_insert.

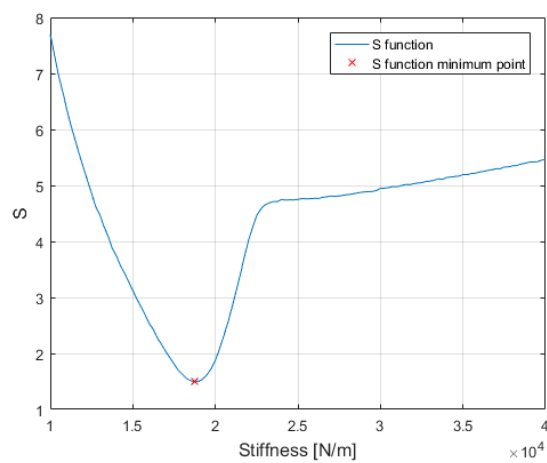


Figure 4.9.6 – Detail of S function trend varying the stiffness for LOSB7249_with_insert.

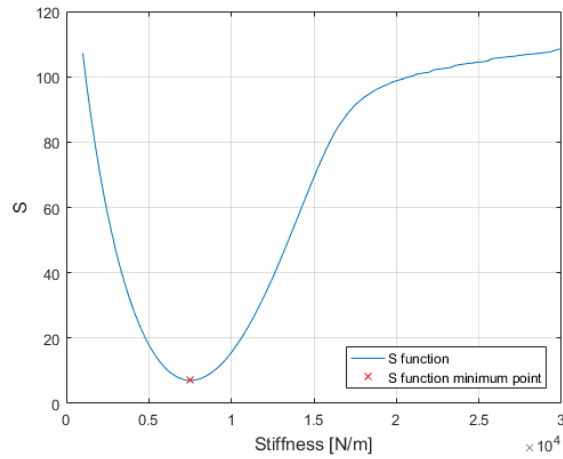


Figure 4.9.7 – Detail of S function trend varying the stiffness for LOSB7294_without_insert.

The minimum points of the previous images define the stiffness values for all the wheel configurations. Table 4.9.1 shows both the static and dynamic stiffness values for all the wheel configurations.

Table 4.9.1 – Stiffness values for all the possible wheel configuration.

Configuration	Static Stiffness [N/m]	Dynamic Stiffness [N/m]
Tire LOS45023 with insert	18277	19250
Tire LOSB7240 with insert	18746	18750
Tire LOS45023 without insert	7368	8000
Tire LOSB7240 without insert	7078	7500

5. Wheel simulation

Another step in the studying of the Losi 5ive wheel is a simulation study. The simulation is important to have a comparison for the experimental test.

In this case the simulation is done with the software LUPOS (LUMped Parameters Open Source FEM code), then some Solidworks comparisons are done. LUPOS is a parametric FEM code developed in Matlab environment at Politecnico di Torino mainly by the professor Elvio Bonisoli. The main user interface is shown in Figure 5.1.

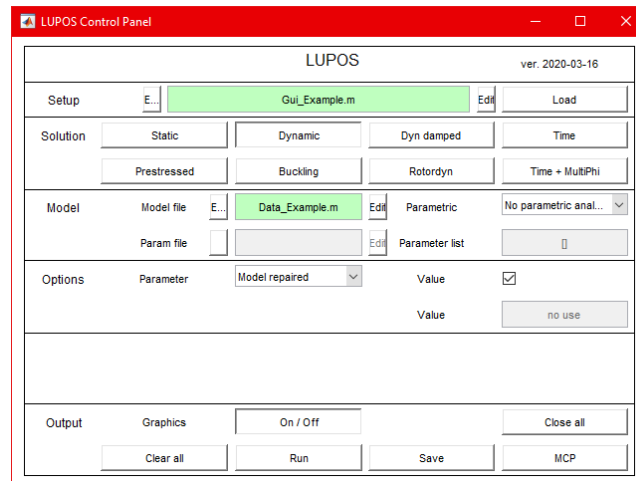


Figure 5.1 – LUPOS control panel.

5.1 Model structure

The first step in the simulation is the definition of the model structure. In this case the wheel is decomposed in pieces for a better study. The main parts are the disc, the rim and the tire.

To define the parts structures the best way is to define some characteristic points; than the proper structure is build using shell elements between the points.

In Figure 5.1.4, Figure 5.1.5, Figure 5.1.6, Figure 5.1.7 and Figure 5.1.8 the wheel component models are shown.



Figure 5.1.4 – Rim model.



Figure 5.1.5 – Insert model.



Figure 5.1.6 – Tire model.



Figure 5.1.7 – Lateral support large

Figure 5.1.8 – Lateral support

For future testing all the wheels components have been weighted. Knowing the weight of each component and also the volume (thanks to the model) it is possible to estimate the components density in order to understand of which material the components are composed by. After the choose of the material a comparison between the real mass and the estimated mass is shown in Table 5.1.1.

In Table 5.1.2 the presumed materials [5],[6] and their characteristics are shown. In Figure 1.1.9 the 3D wheel model is shown.

Table 5.1.1 – Mass comparison between the measured one and the estimated one.

Component	Material	Measured Mass [kg]	Estimated Mass [kg]	Error %
Rim	Nylon 101	0,1394	0,1442	3,42
Tyre	Epichlorohydrin rubber	0,3022	0,2969	-1,77
Insert	Rigid Polymer Foam	0,1305	0,1372	5,12
Lateral support large	Nylon 101	0,016	0,0155	-2,98
Lateral support small	Nylon 101	0,0145	0,0147	1,39
Screws	-	0,0144	0,0144	0,00
Wheel	-	0,617	0,6228	0,95

As it is possible to see from the previous table, the last line shows a comparison between the entire wheel weight in both cases, the measured one and the estimated one. The result is that there is only a difference of 0.95% between the two wheels masses, so the estimation is quite good.

Table 5.1.2 – Presumed materials and their characteristics.

Component	Material	Density [kg/m ³]	E [Mpa]	v
Rim	Nylon 101	1150	1000	0,3
Tyre	Epichlorohydrin rubber	1500	7,5	0,49
Insert	Rigid Polymer Foam	245	270	0,3
Lateral support large	Nylon 101	1150	1000	0,3
Lateral support small	Nylon 101	1150	1000	0,3



Figure 5.1.9 – Wheel model.

5.1.1 Structure points

The wheel and also its main parts have all an axial symmetry. Thanks to this characteristic just a few points of the cross section have to be defined; than these points are revolutionized around the wheel axis. For this purpose, there is a dedicated part of the code that have the structure points as input; then thanks to the revolution the profiles becomes surfaces and the surfaces become solids. After the revolution of all the single components, the code assembles the whole model using appropriate links and joints. The Figure 5.1.9 shows the 3D wheel model from which the points have been measured. The cross section of the rim, disc and tire and the respective points are shown in Figure 5.1.1.1, Figure 5.1.1.2 and Figure 5.1.1.3, Figure 5.1.1.4 and Figure 5.1.1.5.

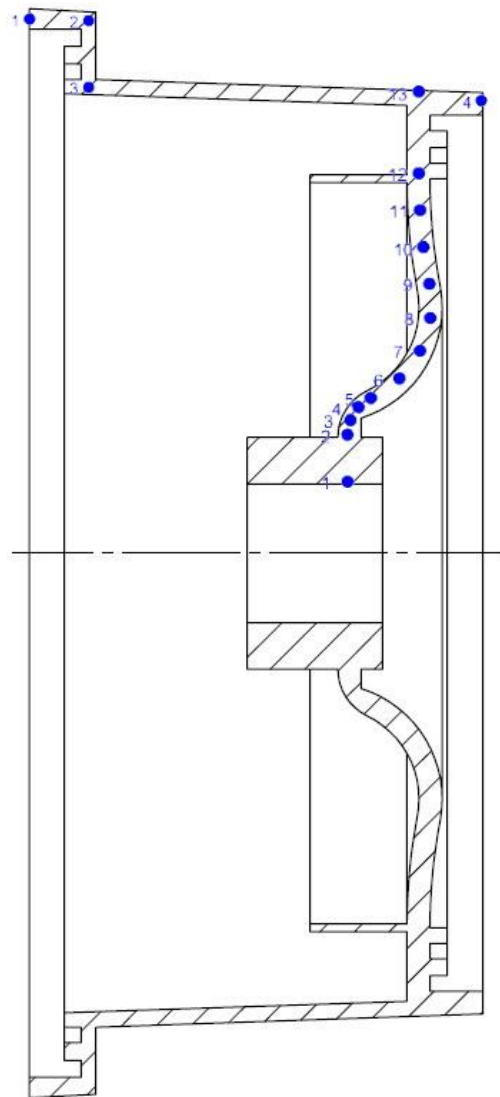


Figure 5.1.1.1 – Disc and rim cross section and section points (first version).

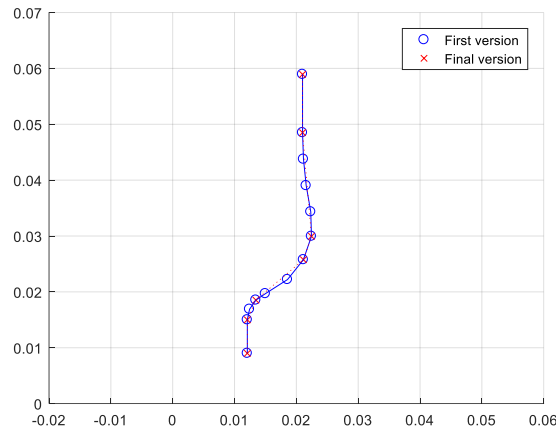


Figure 5.1.1.2 – Disc section points first version (blue) and final version (red).

Figure 5.1.1.2 shows the disc section points in their first and final version. The final version has some modifies; in particular the number of nodes has been decreased reducing the nodes used for the curved parts. Through the program then it will be possible to thicken the mesh.

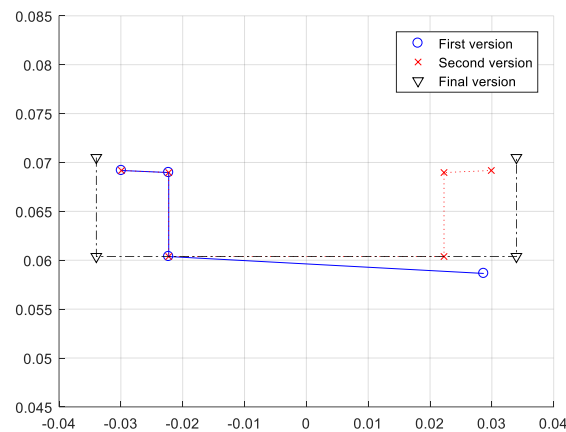


Figure 5.1.1.3 – Rim section points first version (blue), second version (red) and final version (black).

Figure 5.1.1.3 shows the rim section points in their three versions. The second version is different respect to the first one mainly because of the deleting of the fourth node and the mirroring of nodes one, two and three. This has been done in order to obtain a symmetrical model, easier to study with the used program. The program in fact is used for real car tyres that present a rim symmetry. The final version has been created to adapt the previous version to the real car rims. With this modify the tyre border will be located inside the rim (like the real cars) and not on the outside.

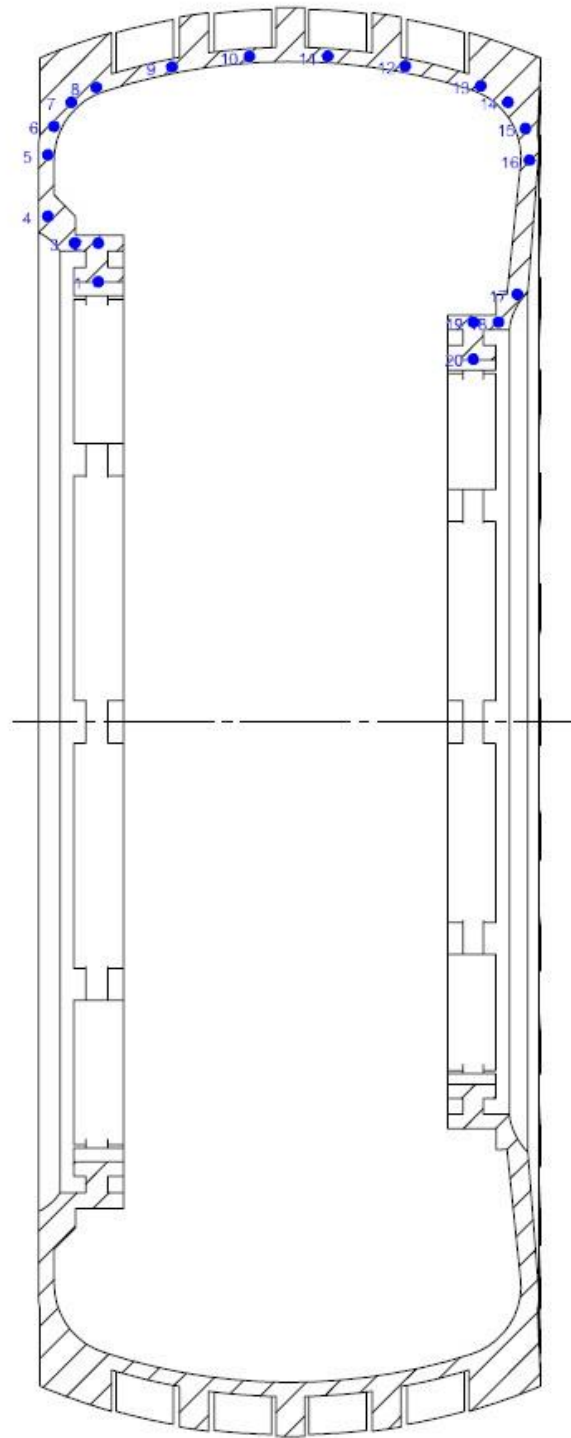


Figure 5.1.1.4 – Tire cross section and section points (first version).

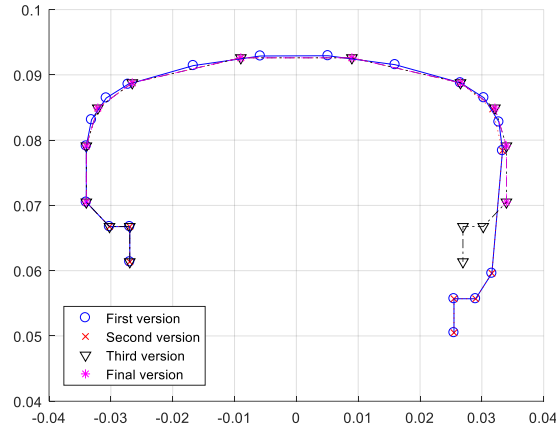


Figure 5.1.1.5 – Tire section points first version (blue), second version (red), third version (black) and final version (magenta).

Figure 5.1.1.5 shows the tire section points in their versions. The second version is different respect to the first one mainly because of the reduction of the nodes in the curved parts of the section. The third version is a modify done in order to obtain a symmetrical model, easier to study. The final version has been created to adapt the previous version to the real car rims. With this modify the tyre border will be located inside the rim (like the real cars) and not on the outside.

Figure 5.1.1.6 shows a section of the entire wheel and the section points of both disc, rim and tyre in their first version.

At this point, some other minor issues are fixed in order to obtain a model suitable for a script already used in other simulations. The main modify is the union of the disc and rim in a single file that is easier to integrate in the existing script. Another modify is the change of the numeration of the points to obtain a better nodes order. Also, some node has been slightly modified to better resemble a real car wheel. Figure 5.1.1.7 and Figure 5.1.1.8 shows the definitive points of both disc, rim and tyre.

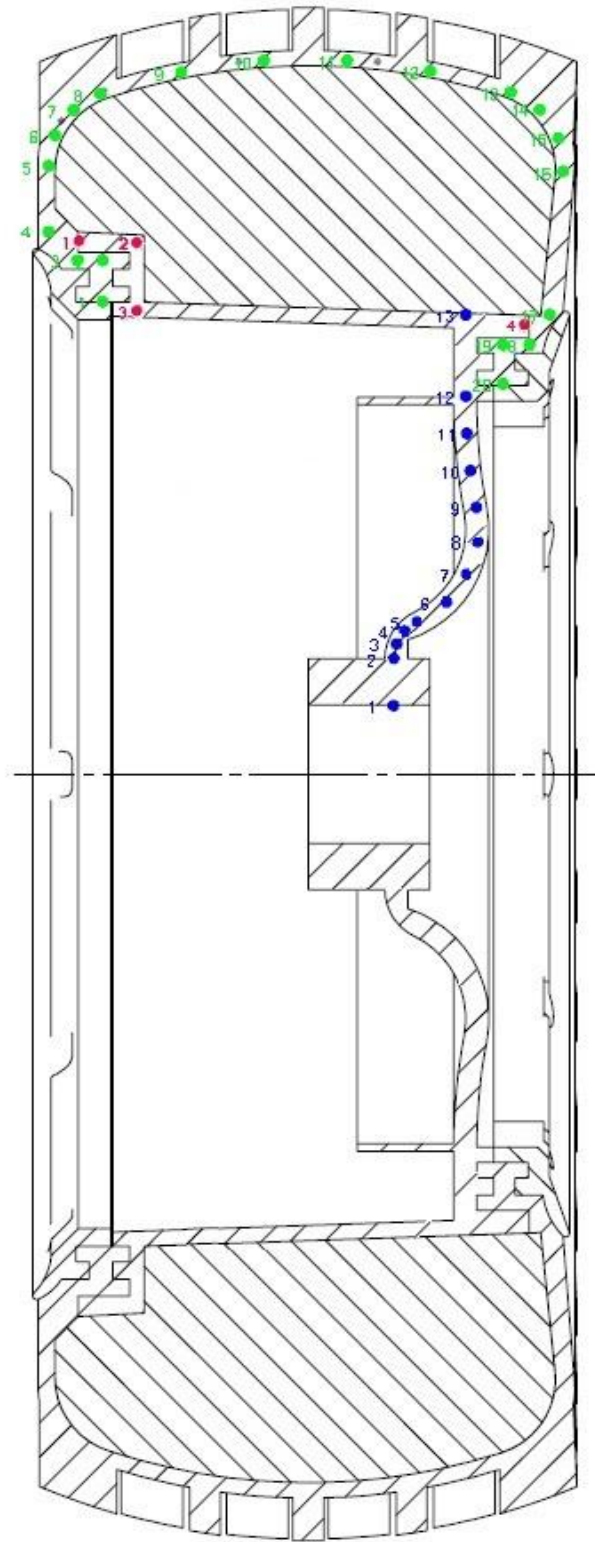


Figure 5.1.1.6 – Wheel cross section and model points (first version) of disc (blue) rim (red) and tire (green).

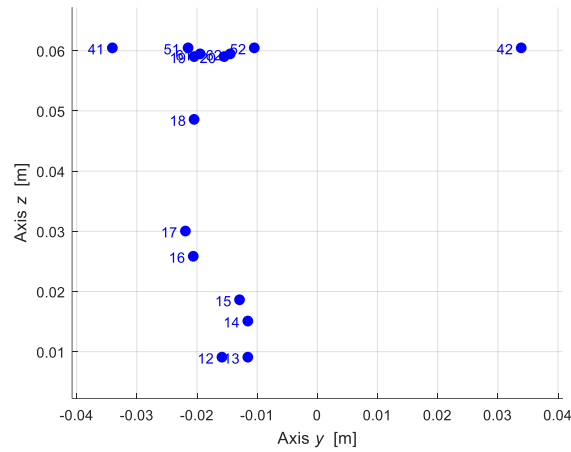


Figure 5.1.1.7 – Rim and disc definitive version with nodes number.

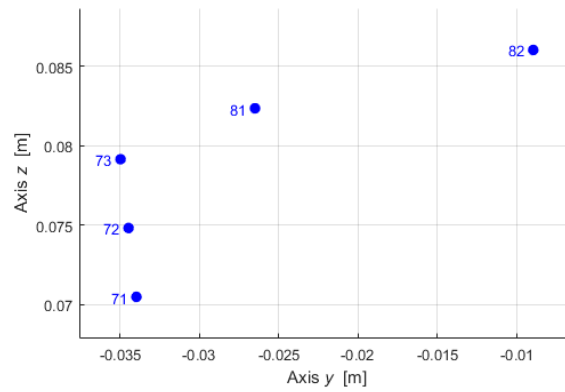


Figure 5.1.1.8 – Tyre definitive version with nodes number.

Once the model points are ready the above-mentioned script is used to create the complete model of the wheel, using LUPOS feature. Figure 5.1.1.9 shows the revolution of the model points while Figure 5.1.1.10 shows the complete wheel model. Table 5.1.1.1 shows some model geometric element, such as nodes, rod, rigid joints, lumped springs, shell elements and hexa element.

Table 5.1.1.1 –Model geometric element.

Element	Number
Geo	2844
Rod	36
Rjs	756
Els	324
Sh4	1008
Hex	1368

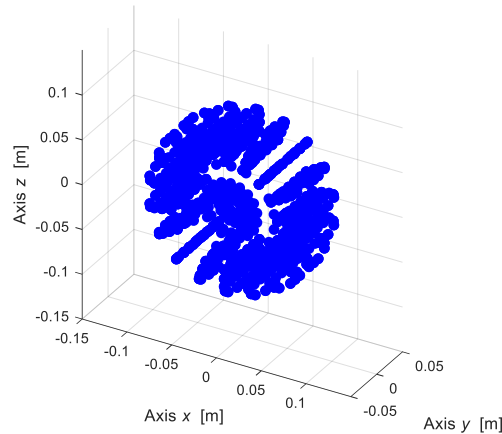


Figure 5.1.1.9 – Model nodes.

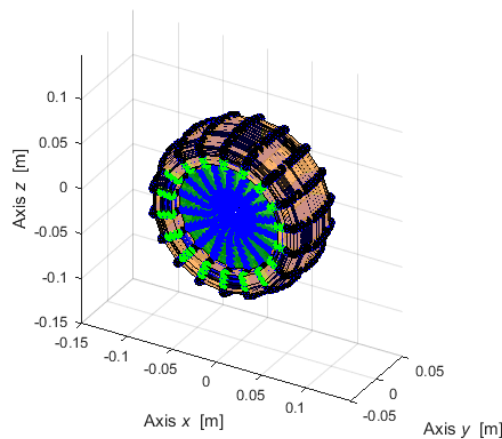


Figure 5.1.1.10 – LUPOS wheel model.

5.2 Parametric analysis

After the assembling of the model, some parameters have been investigated to understand how the model construction can influence the frequencies results. The goal of this parametric analysis is the determination of a model that produce reliable results without being too much complex. In the following tests, the parameters have been changed and the resultant frequencies and the node number (that are directly related to the model complexity) have been analysed.

This model is built starting with the definition of the nodes of a single cross-section. Then the cross section is duplicated using a revolution around the central axis to create the three-dimensional model. For this reason, the studied parameters are:

- the shell and hexa elements dimensions: these parameters modify the spacing between the nodes of the cross-section;
- the angular sector number: this parameter modifies the number of the angular cross-section.

The first parameter studied is the angular sectors number. This parameter modifies the numbers of angular sector that the model has. Figure 5.2.1 show the modes frequencies trends changing this parameter in the range 8-24.

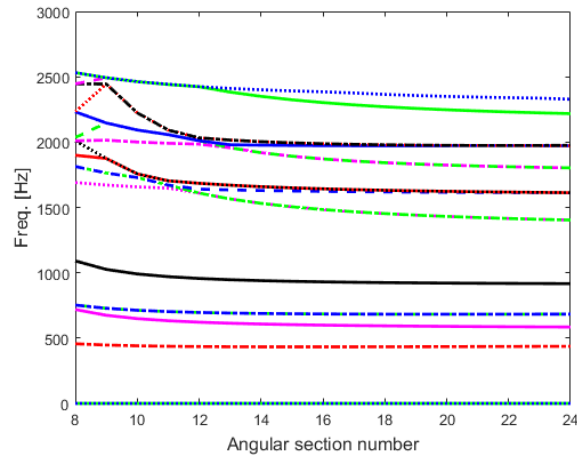


Figure 5.2.1 – Frequencies trend changing angular sectors number.

As it is possible to see the frequencies values are quite constant over 16 angular sectors. Below this value the frequencies values changes a lot. This is due to the fact that with too few angular sectors the wheel is not round anymore and that influence a lot the frequencies values. A value of 18 is enough to provide quite reliable results without increasing the nodes number too much.

The second study involve both the shell and hexa elements dimension. The shell element Figure 5.2.2 is a LUPOS characteristic element [7] defined by four nodes. It is used for surface meshing.

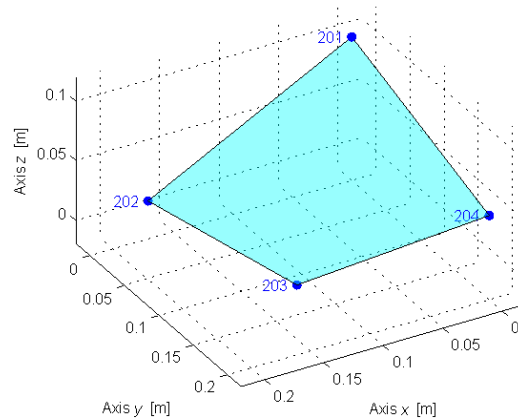


Figure 5.2.2 – Shell element example.

The hexa element Figure 5.2.3 is a LUPOS characteristic element [7] defined by eight nodes. It is used for volume meshing.

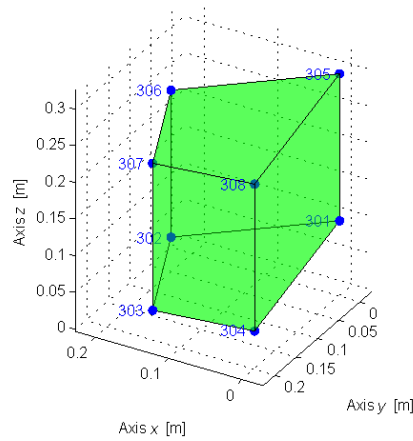


Figure 5.2.3 – Hexa element example.

In this study the elements dimension is varied between two and ten millimetres. Figure 5.2.4 shows the frequencies trend varying the elements dimension. Figure 5.2.5 and Figure 5.2.6 show the nodes number trend varying the element dimensions for the entire range and for a detailed smaller range.

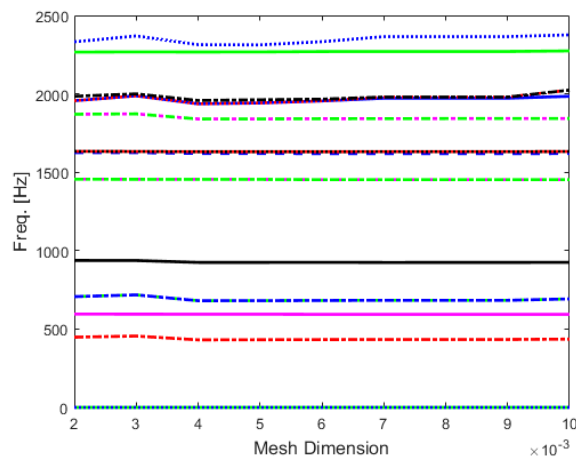


Figure 5.2.4 – Frequencies trend changing shell and hexa elements dimension.

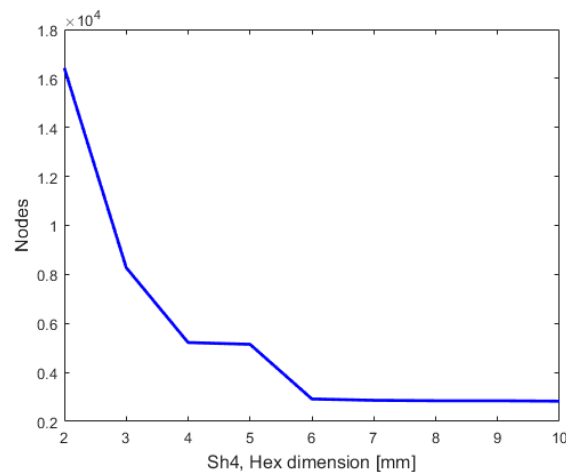


Figure 5.2.5 – Nodes number trend changing shell and hexa elements dimension.

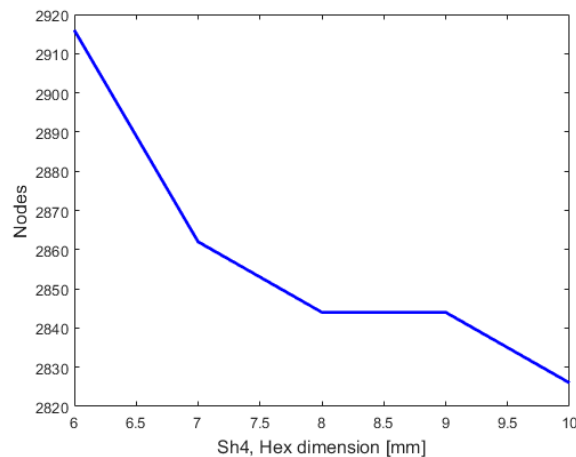


Figure 5.2.6 – Detailed nodes number trend changing shell and hexa elements dimension.

As it is possible to see from the previous figures, the frequencies values have only little variations varying the shell and hexa mesh dimensions. From Figure 5.2.5 it is possible too to see how the nodes number increase exponentially for elements dimension under six millimetres up to more than sixteen thousand. For this reason, it is preferable to choose as elements dimension a value over six millimetres. Figure 5.2.6 shows a detail of the Figure 5.2.5 excluding elements dimension values under six millimetres. This graph shows that a good value for the elements dimension could be around eight millimetres because the number of nodes is relatively small (2844) while the frequencies values are still reliable.

For this reason, for the next studies the angular sectors will be 18 while as the elements dimension a value of 8 mm will be used.

5.3 Free real modal analysis

After the completing of the wheel model the analysis starts. In this case a free real modal analysis is done using LUPOS code. Figure 5.3.1 shows LUPOS Control Panel with the used configurations.

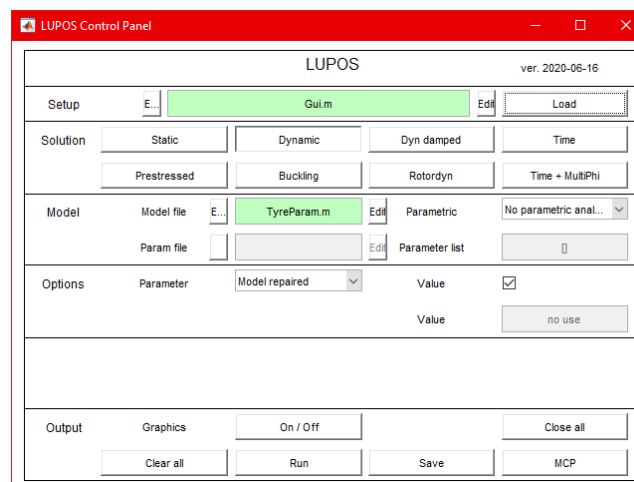


Figure 5.3.1 – LUPOS Control Panel

Table 5.3.1 shows the first twenty flexible mode frequency compared to the one obtained from Solidworks. From Figure 5.3.2 to Figure 5.3.21 the modes deformations (for both LUPOS and Solidworks) are shown. The first flexible mode is the number seven due to the free-free analysis, in this case in fact the first six modes are rigid body motion.

Table 5.3.1 –Modes frequency.

Mode	LUPOS Frequency [Hz]	Description	Solidworks frequency [Hz]
7	433.5	1 st Axial	479
8	593.6	1 st Flexural	487
9	593.6	2 nd Flexural	487
10	683.1	3 rd Flexural	735
11	683.1	4 th Flexural	748
12	924.7	5 th Flexural	954
13	924.7	6 th Flexural	955
14	1453	7 th Flexural	1096
15	1453	8 th Flexural	1098
16	1619	2 nd Axial	1346
17	1631	9 th Flexural	1349
18	1631	10 th Flexural	1373
19	1842	11 th Flexural	1647
20	1842	12 th Flexural	1652
21	1972	3 rd Axial	1678
22	1979	13 th Flexural	1679
23	1979	14 th Flexural	1745
24	2270	15 th Flexural	1748
25	2270	16 th Flexural	1790
26	2365	17 th Flexural	1922

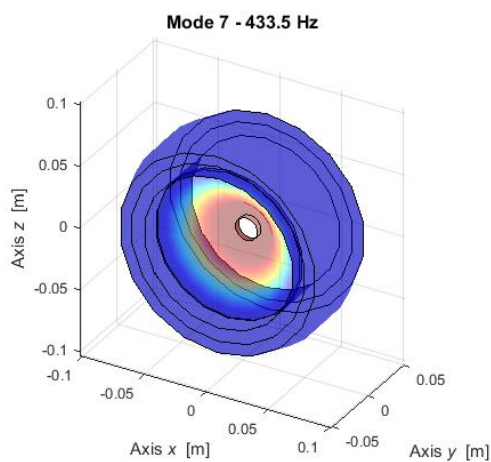


Figure 5.3.2 – LUPOS Mode 7.

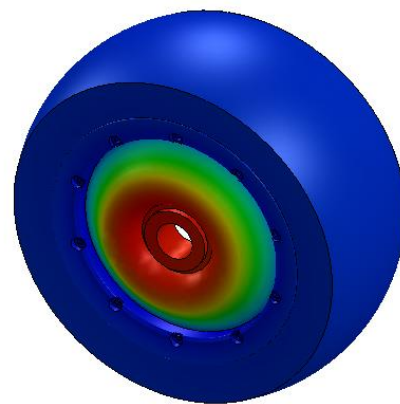


Figure 5.3.3 – Solidworks Mode 7.

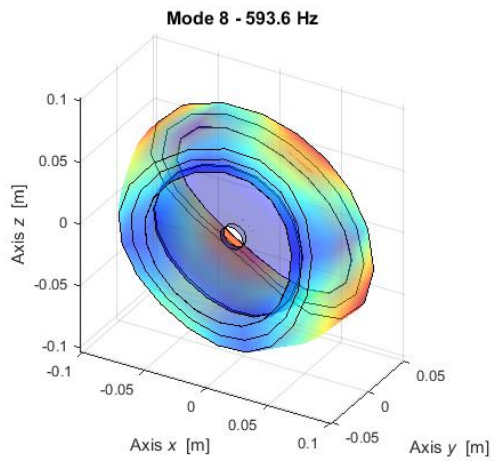


Figure 5.3.4 – LUPOS Mode 8.

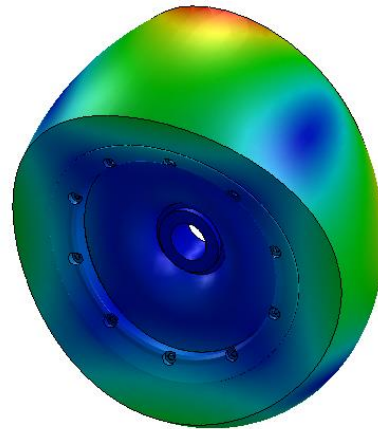


Figure 5.3.5 – Solidworks Mode 8.

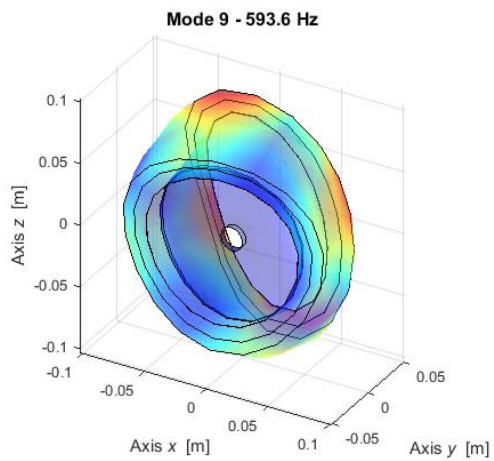


Figure 5.3.6 – LUPOS Mode 9.

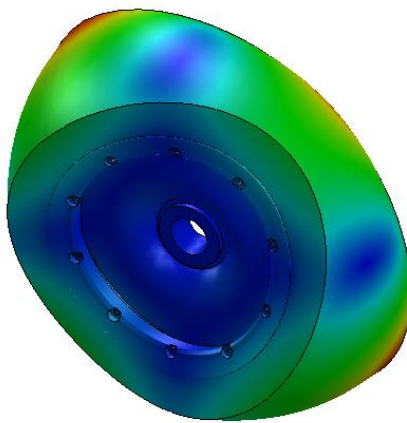


Figure 5.3.7 – Solidworks Mode 9.

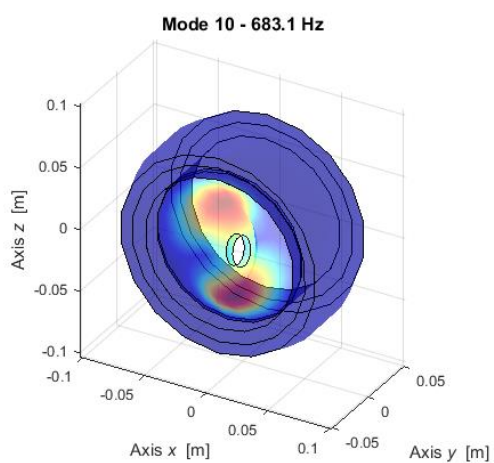


Figure 5.3.8 – LUPOS Mode 10.

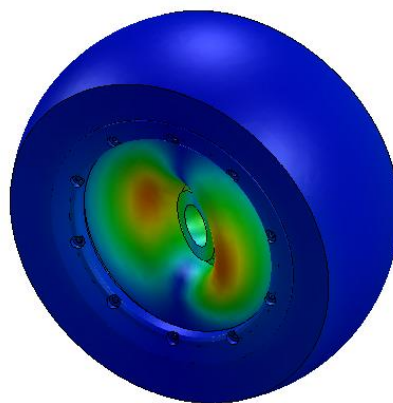


Figure 5.3.9 – Solidworks Mode 10.

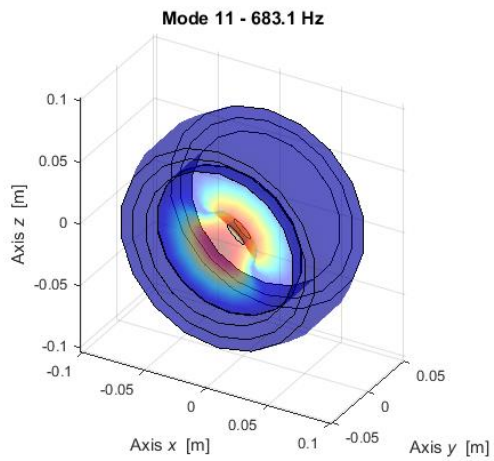


Figure 5.3.10 – LUPOS Mode 11.

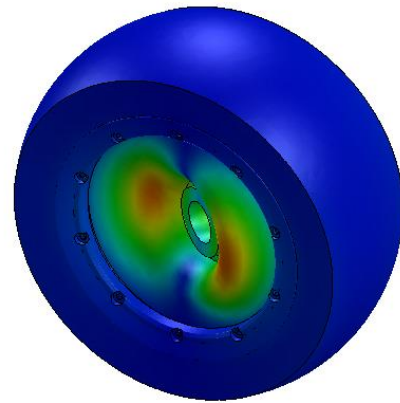


Figure 5.3.11 – Solidworks Mode 11.

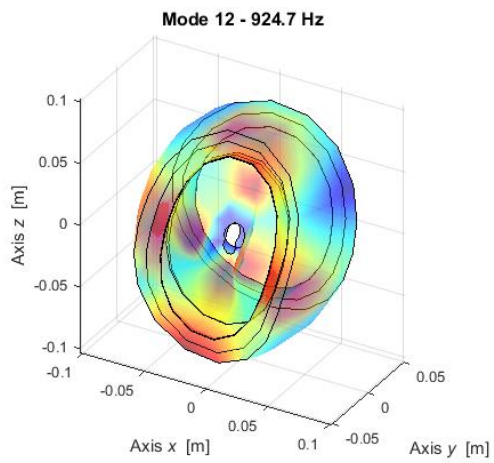


Figure 5.3.12 – LUPOS Mode 12.

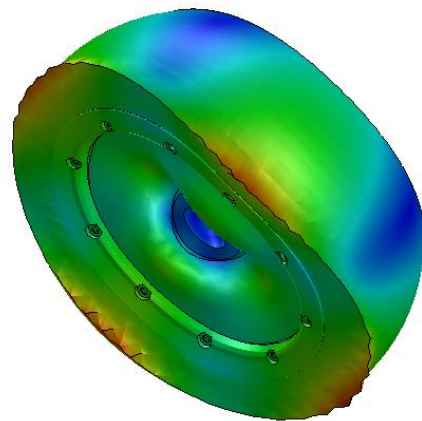


Figure 5.3.13 – Solidworks Mode 12.

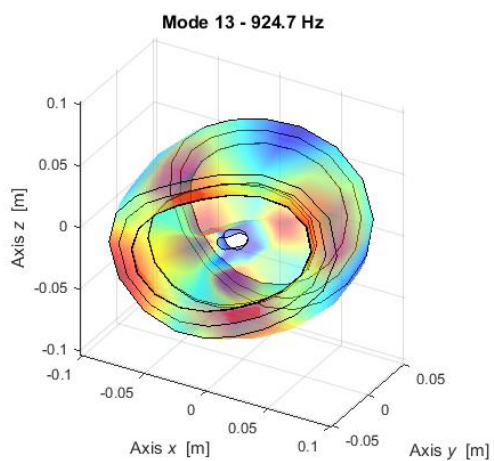


Figure 5.3.14 – LUPOS Mode 13.

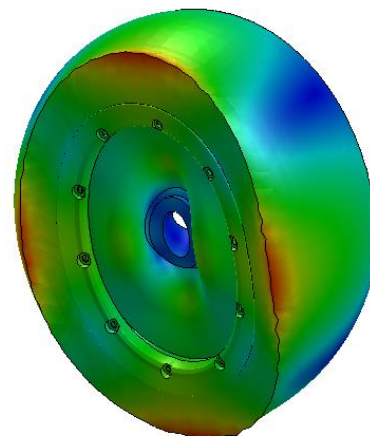


Figure 5.3.15 – Solidworks Mode 13

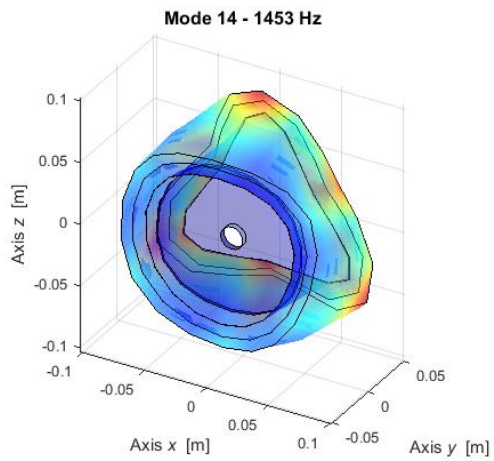


Figure 5.3.16 – LUPOS Mode 14.

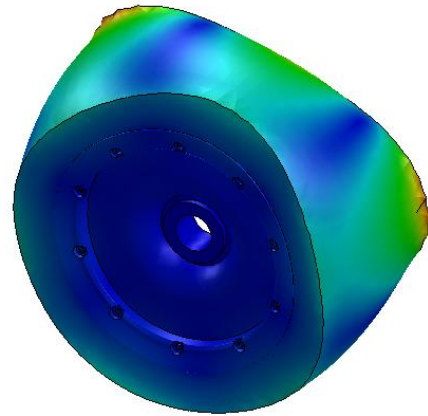


Figure 5.3.17 – Solidworks Mode 14.

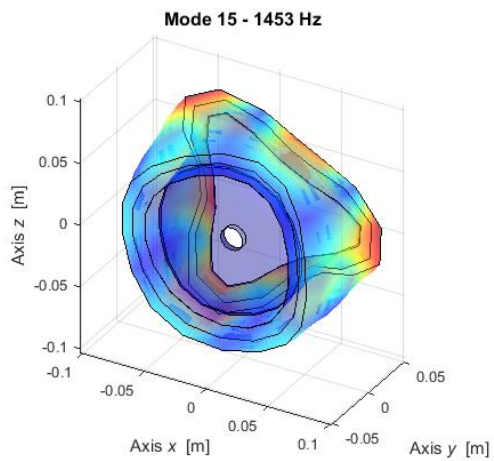


Figure 5.3.18 – LUPOS Mode 15.

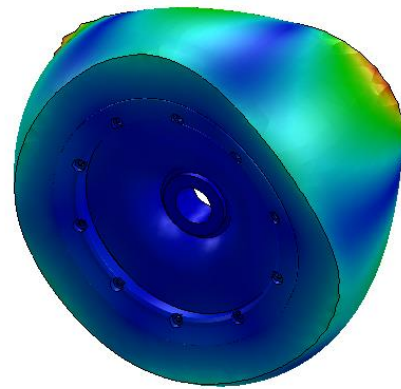


Figure 5.3.19 – Solidworks Mode 15.

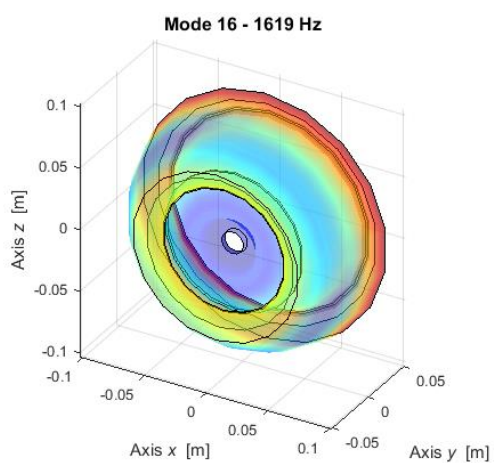


Figure 5.3.20 – LUPOS Mode 16.

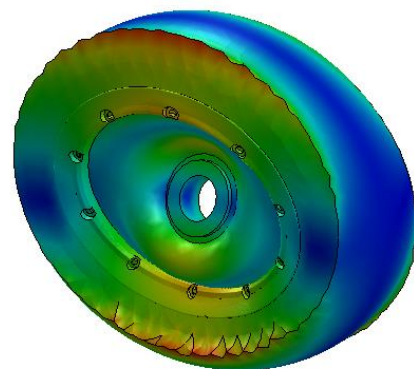


Figure 5.3.21 – Solidworks Mode 16.

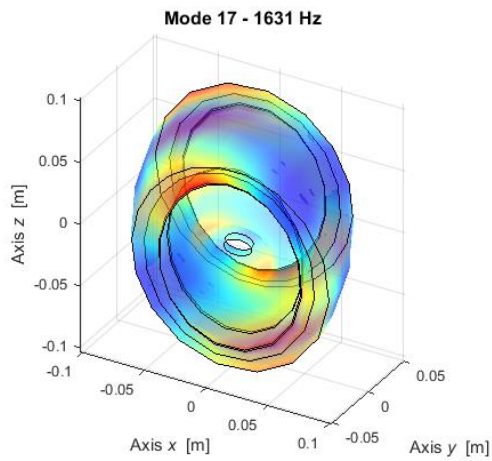


Figure 5.3.22 – LUPOS Mode 17.

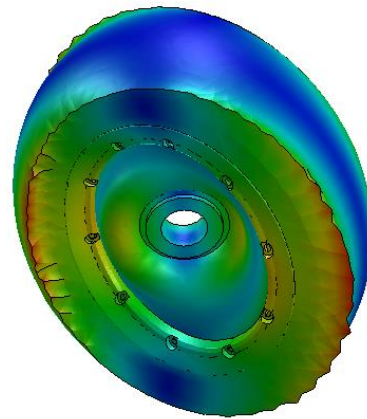


Figure 5.3.23 – Solidworks Mode 17.

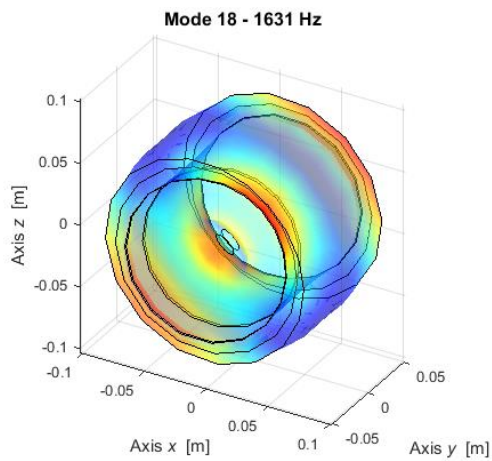


Figure 5.3.24 – LUPOS Mode 18.

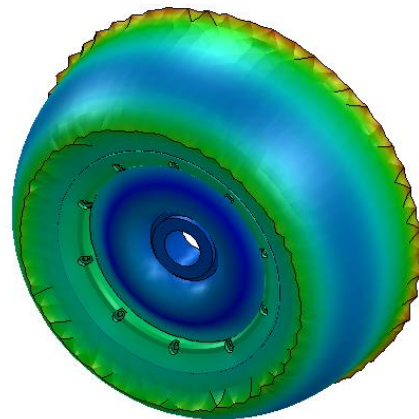


Figure 5.3.25 – Solidworks Mode 18.

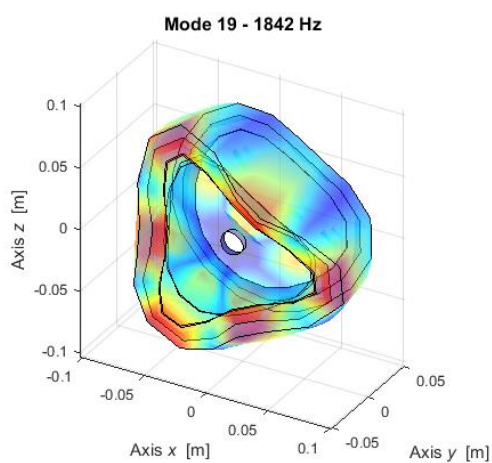


Figure 5.3.26 – LUPOS Mode 19.

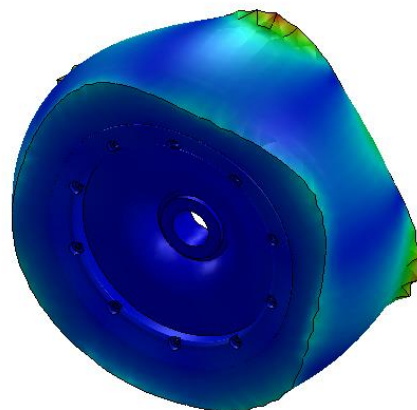


Figure 5.3.27 – Solidworks Mode 19.

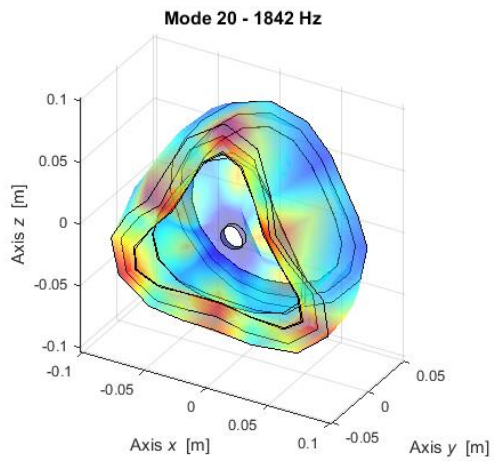


Figure 5.3.28 – LUPOS Mode 20.

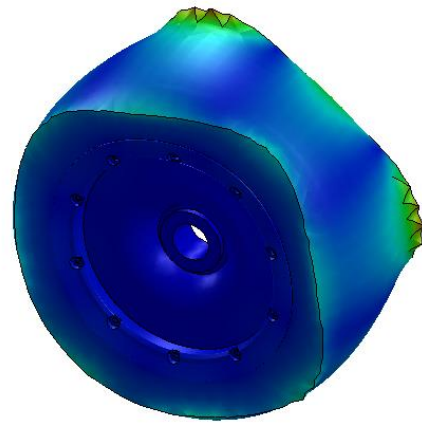


Figure 5.3.29 – Solidworks Mode 20.

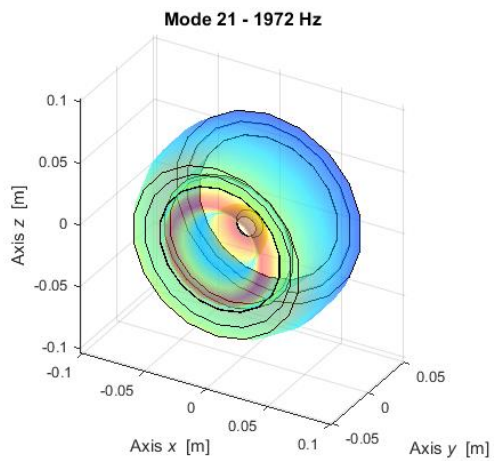


Figure 5.3.30 – LUPOS Mode 21.

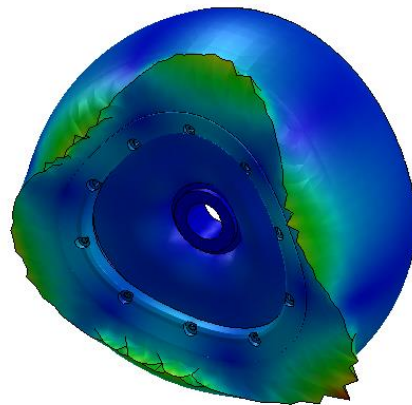


Figure 5.3.31 – Solidworks Mode 21.

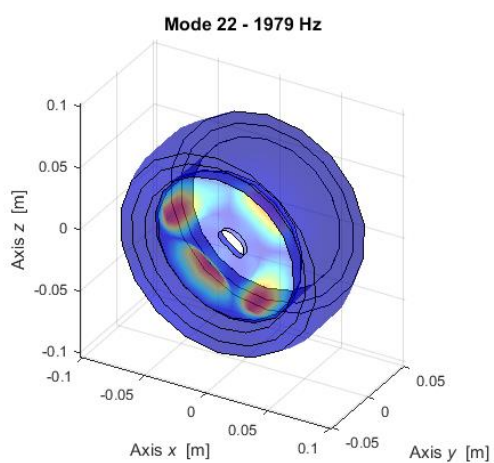


Figure 5.3.32 – LUPOS Mode 22.

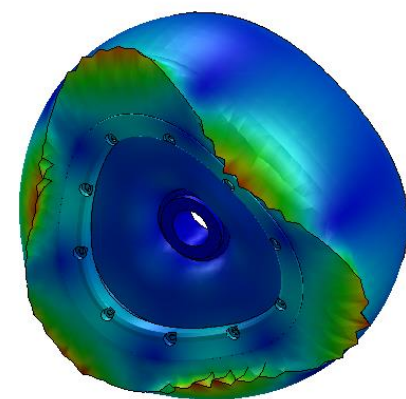


Figure 5.3.33 – Solidworks Mode 22.

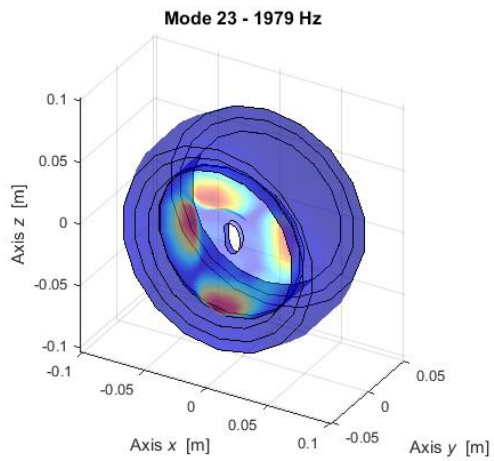


Figure 5.3.34 – LUPUS Mode 23.

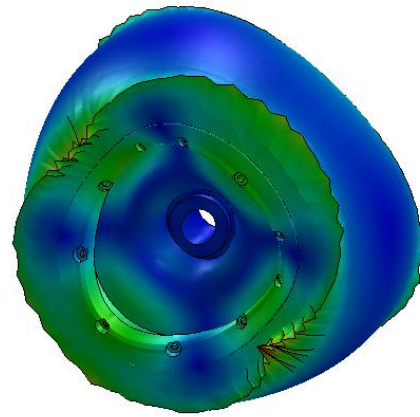


Figure 5.3.35 – Solidworks Mode 23.

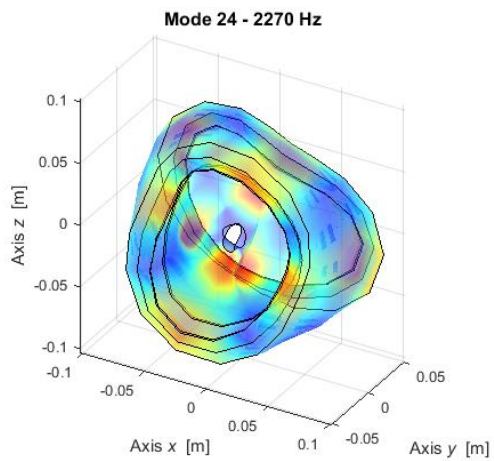


Figure 5.3.36 – LUPUS Mode 24.

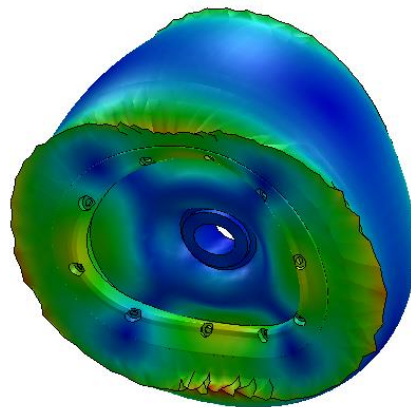


Figure 5.3.37 – Solidworks Mode 24.

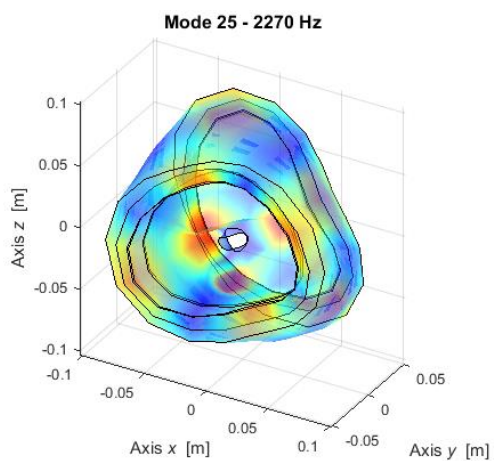


Figure 5.3.38 – LUPUS Mode 25.

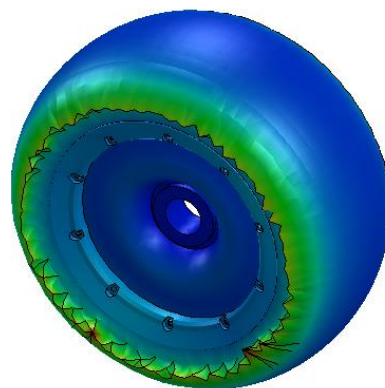


Figure 5.3.39 – Solidworks Mode 25.

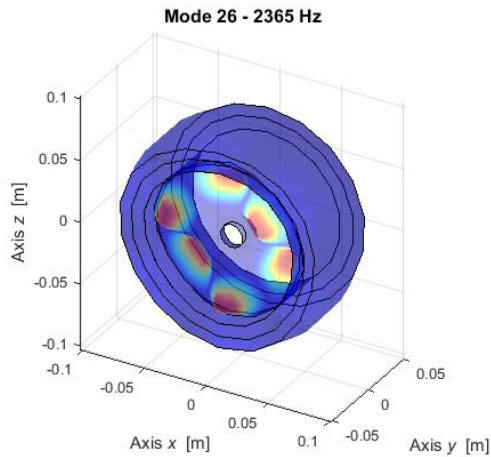


Figure 5.3.40 – LUPOS Mode 26.

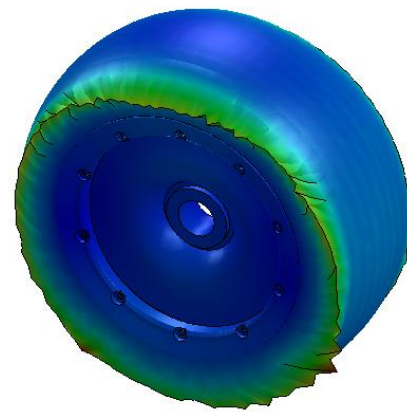


Figure 5.3.41 – Solidworks Mode 26.

After the modal analysis of the complete wheel, some real modal analyses of the single wheel components are done.

5.3.1 Rim and disc real modal analysis

In this case the model is composed only by the rim and disc. In the following analysis only the model geometry is changed. All the simulation parameters are the exact same of the one used for the entire wheel analysis. In Figure 5.3.1.1 the wheel model is shown. Table 5.3.1.1 shows some model geometric element, such as nodes, rod and shell elements. Table 5.3.1.2 shows the first twenty flexible modes frequencies of LUPOS and Solidworks analysis. From Figure 5.3.1.2 to Figure 5.3.1.41 the modes are shown.

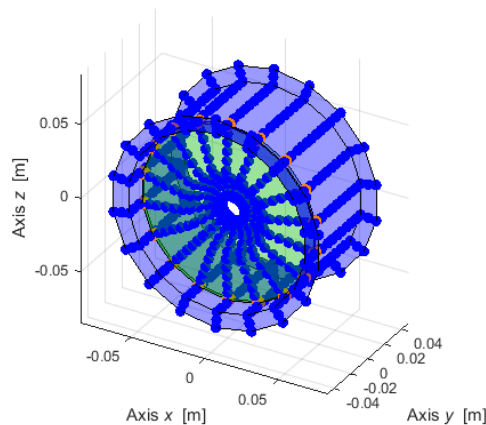


Figure 5.3.1.1 – Wheel model with rim and disc only.

Table 5.3.1.1 –Model geometric element.

Element	Number
Geo	612
Rod	36
Sh4	576

Table 5.3.1.2 –Modes frequency.

Mode	LUPOS Frequency [Hz]	Description	Solidworks Frequency [Hz]
7	222.2	1 st Flexural	257.8
8	222.2	2 nd Flexural	257.8
9	432.6	1 st Axial	448.3
10	622.4	3 rd Flexural	664.4
11	622.4	4 th Flexural	664.8
12	669.3	5 th Flexural	705
13	669.3	6 th Flexural	705.2
14	1077	7 th Flexural	1186
15	1077	8 th Flexural	1186
16	1193	9 th Flexural	1277
17	1193	10 th Flexural	1282
18	1473	11 th Flexural	1301
19	1473	12 th Flexural	1302
20	1604	13 th Flexural	1400
21	1604	14 th Flexural	1400
22	1619	15 th Flexural	1588
23	1619	16 th Flexural	1589
24	1630	17 th Flexural	1612
25	1630	18 th Flexural	1617
26	1647	2 nd Axial	1641

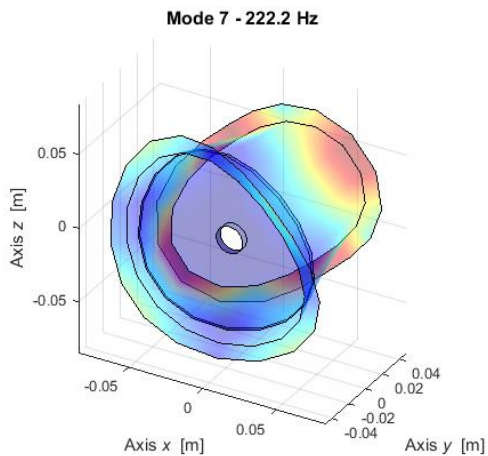


Figure 5.3.1.2 – LUPOS Mode 7.

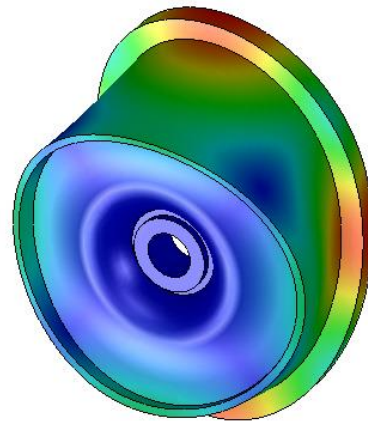


Figure 5.3.1.3 – Solidworks Mode 7.

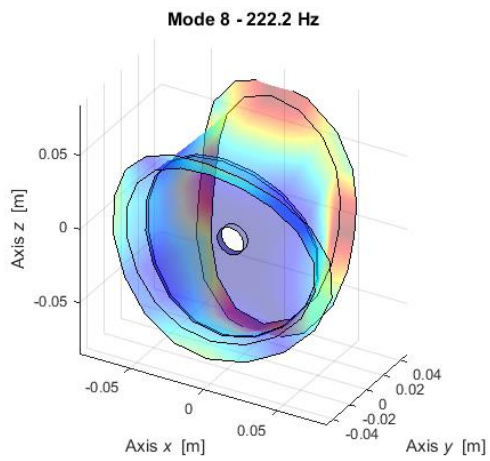


Figure 5.3.1.4 – LUPOS Mode 8.

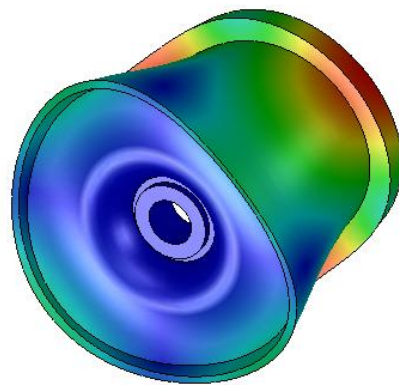


Figure 5.3.1.5 – Solidworks Mode 8.

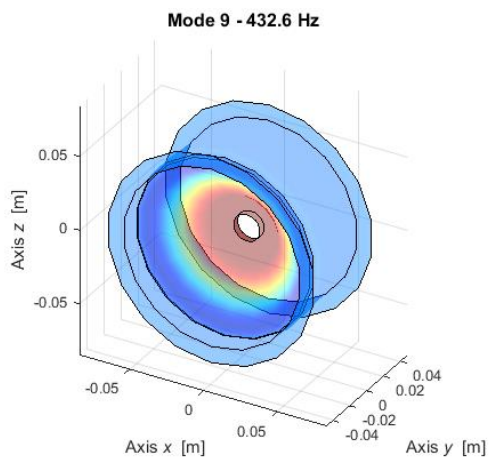


Figure 5.3.1.6 – LUPOS Mode 9.

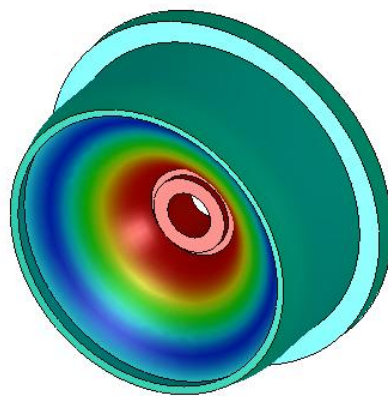


Figure 5.3.1.7 – Solidworks Mode 9.

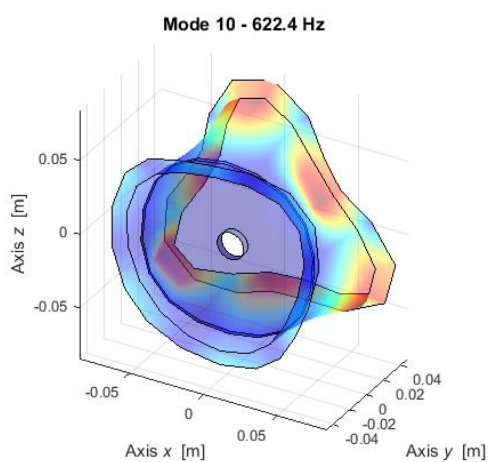


Figure 5.3.1.8 – LUPOS Mode 10.

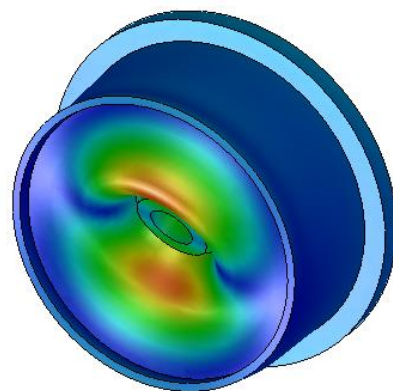


Figure 5.3.1.9 – Solidworks Mode 10.

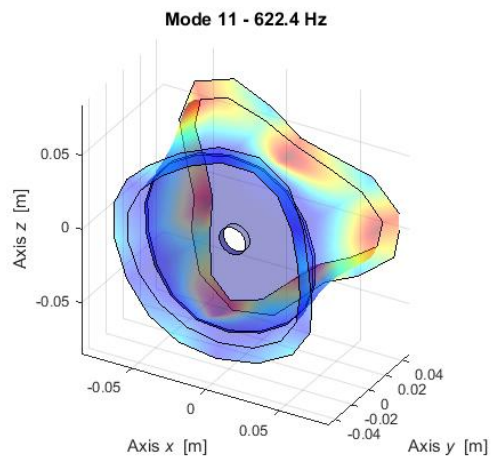


Figure 5.3.1.10 – LUPOS Mode 11.

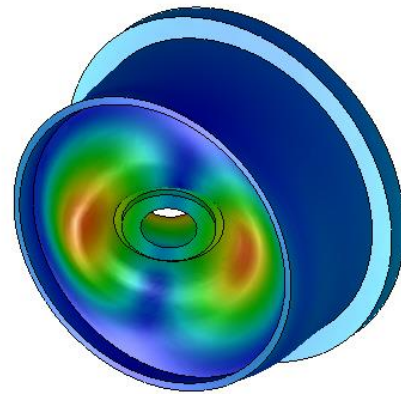


Figure 5.3.1.11 – Solidworks Mode 11.

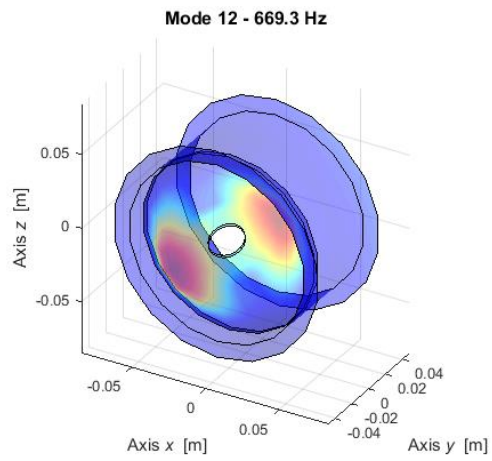


Figure 5.3.1.12 – LUPOS Mode 12.

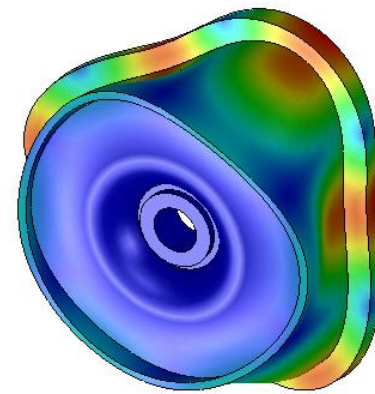


Figure 5.3.1.13 – Solidworks Mode 12.

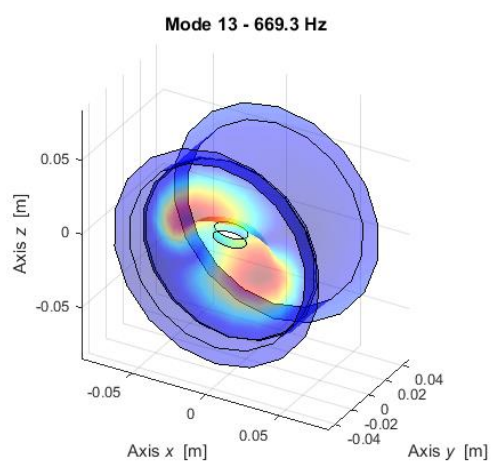


Figure 5.3.1.14 – LUPOS Mode 13.

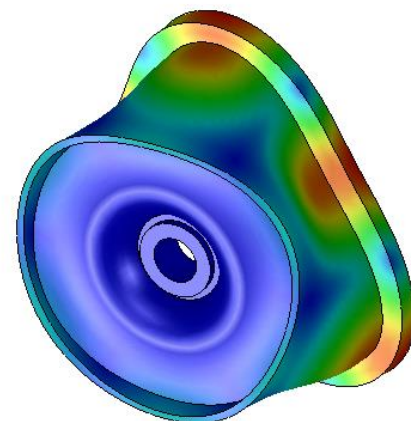


Figure 5.3.1.15 – Solidworks Mode 13

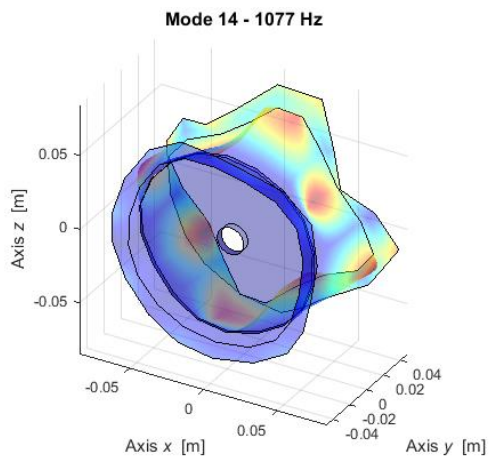


Figure 5.3.1.16 – LUPUS Mode 14.

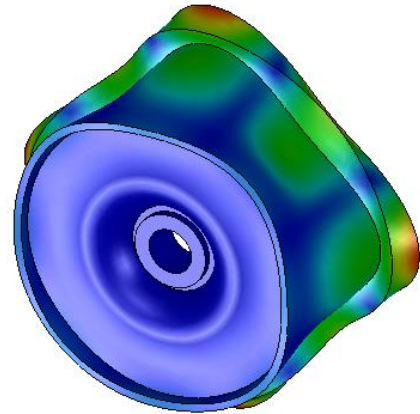


Figure 5.3.1.17 – Solidworks Mode 14.

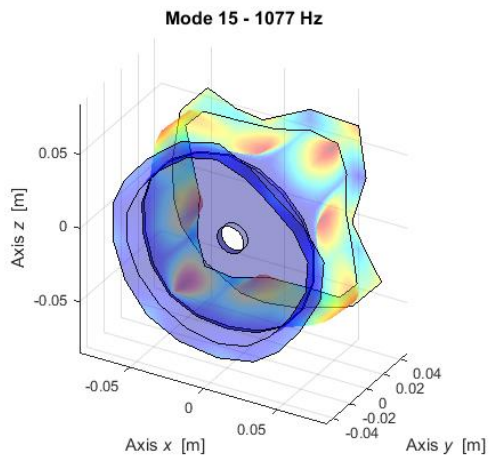


Figure 5.3.1.18 – LUPUS Mode 15.

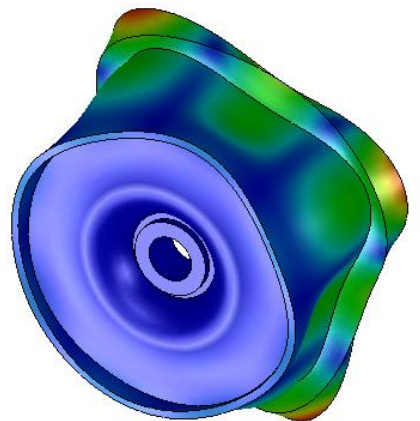


Figure 5.3.1.19 – Solidworks Mode 15.

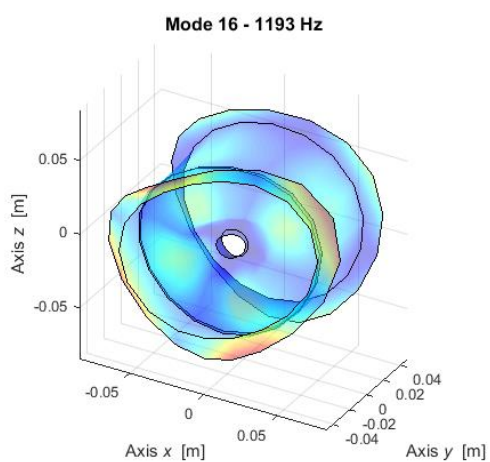


Figure 5.3.1.20 – LUPUS Mode 16.

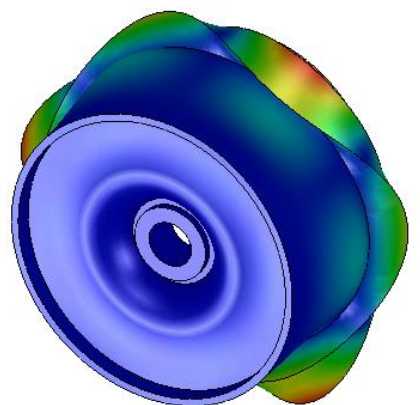


Figure 5.3.1.21 – Solidworks Mode 16.

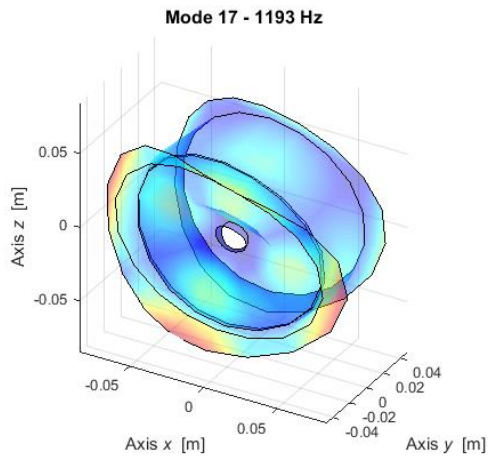


Figure 5.3.1.22 – LUPOS Mode 17.

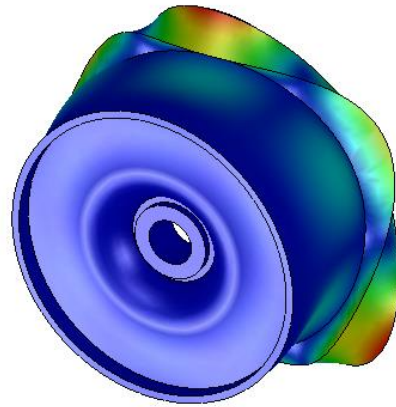


Figure 5.3.1.23 – Solidworks Mode 17.

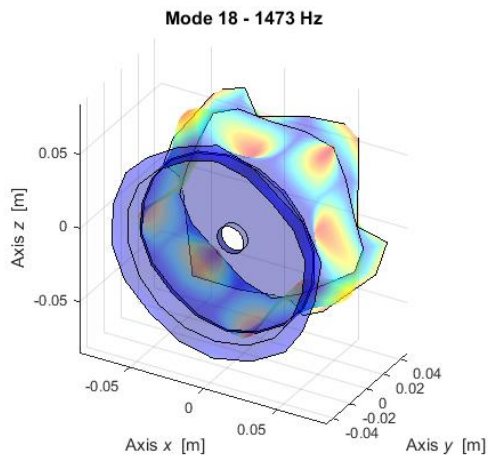


Figure 5.3.1.24 – LUPOS Mode 18.

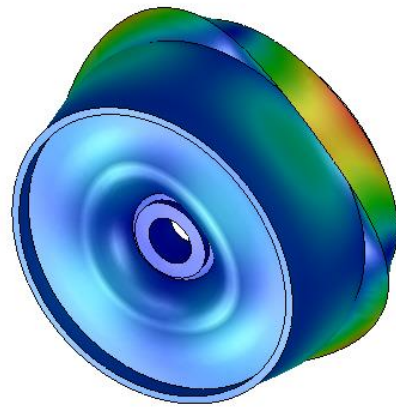


Figure 5.3.1.25 – Solidworks Mode 18.

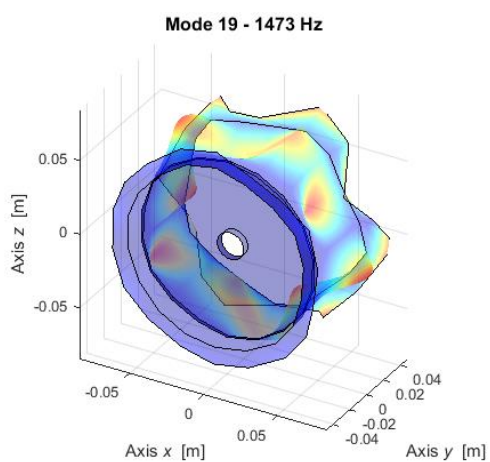


Figure 5.3.1.26 – LUPOS Mode 19.

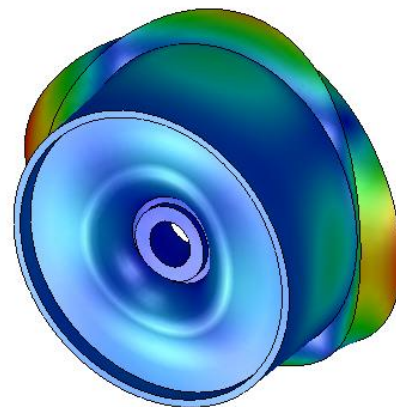


Figure 5.3.1.27 – Solidworks Mode 19.

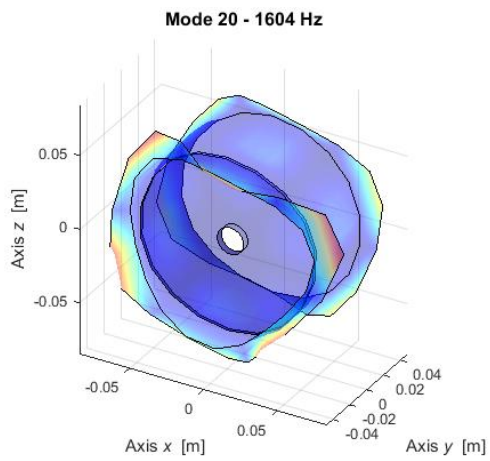


Figure 5.3.1.28 – LUPOS Mode 20.

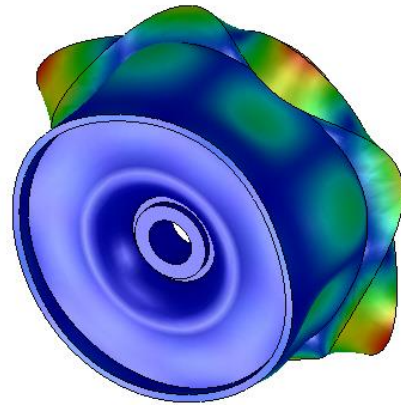


Figure 5.3.1.29 – Solidworks Mode 20.

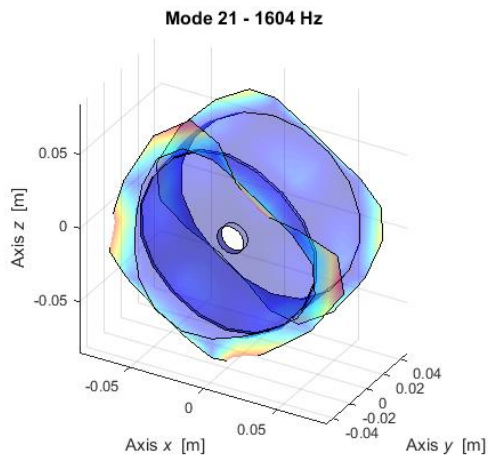


Figure 5.3.1.30 – LUPOS Mode 21.

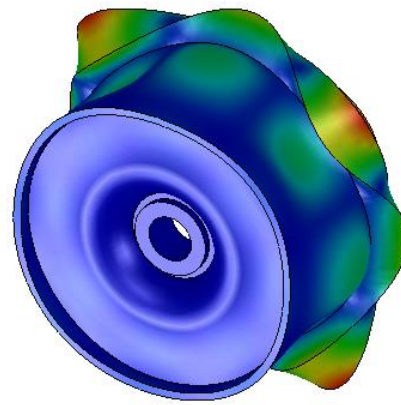


Figure 5.3.1.31 – Solidworks Mode 21.

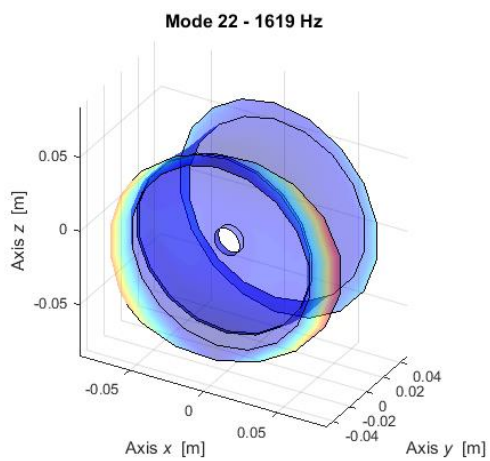


Figure 5.3.1.32 – LUPOS Mode 22.

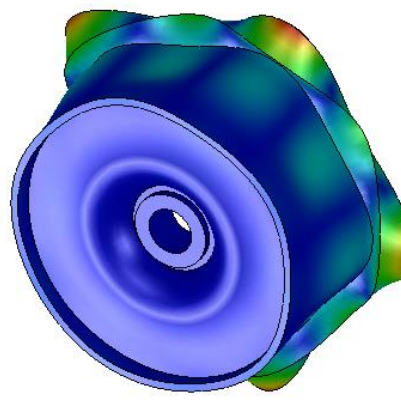


Figure 5.3.1.33 – Solidworks Mode 22.

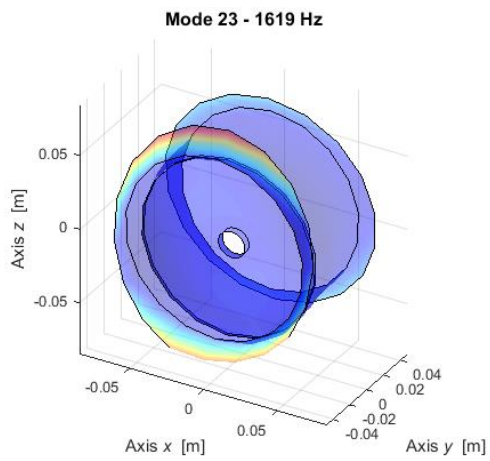


Figure 5.3.1.34 – LUPOS Mode 23.

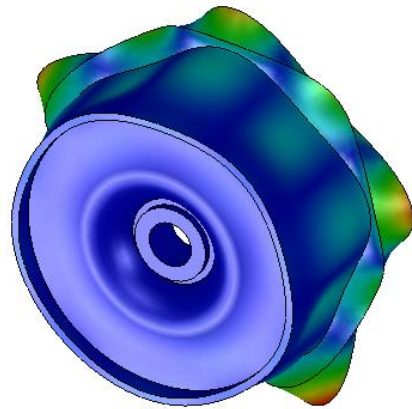


Figure 5.3.1.35 – Solidworks Mode 23.

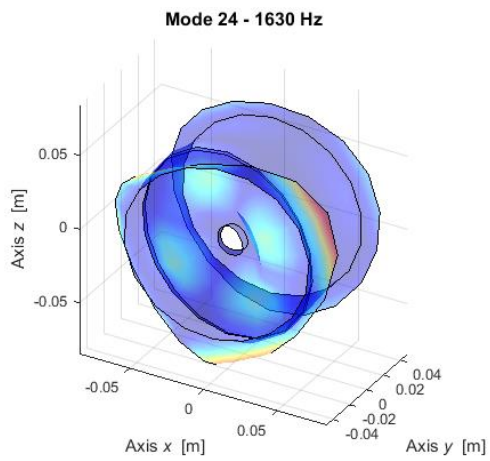


Figure 5.3.1.36 – LUPOS Mode 24.

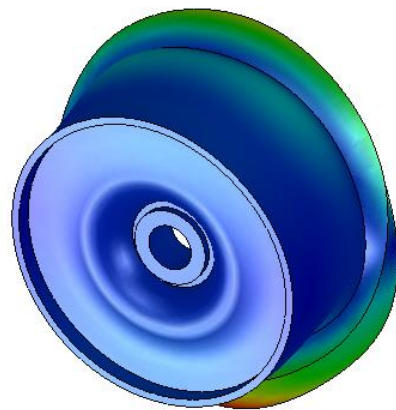


Figure 5.3.1.37 – Solidworks Mode 24.

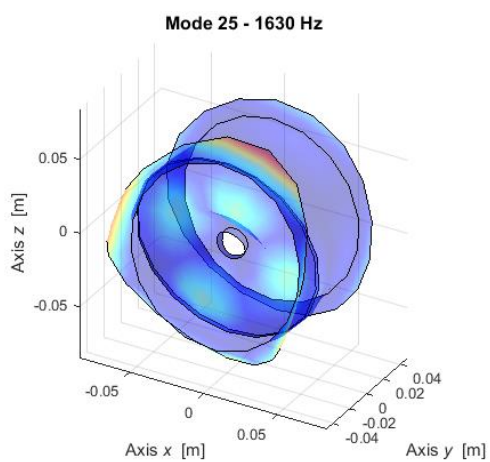


Figure 5.3.1.38 – LUPOS Mode 25.

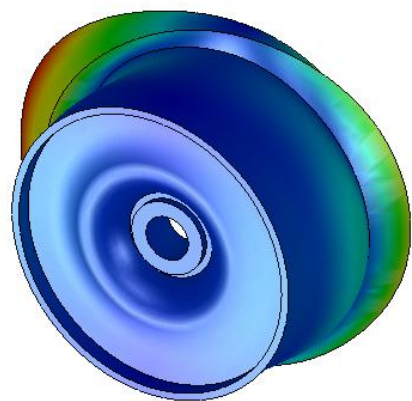


Figure 5.3.1.39 – Solidworks Mode 25.

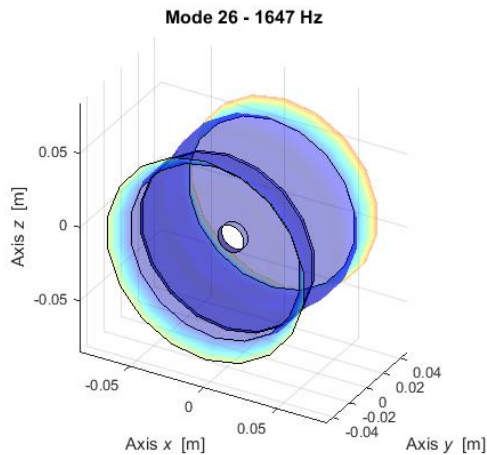


Figure 5.3.1.40 – LUPOS Mode 26.

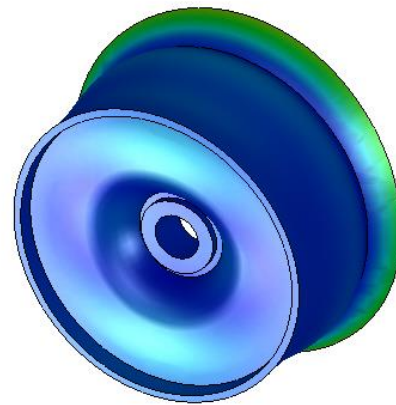


Figure 5.3.1.41 – Solidworks Mode 26.

5.3.2 Foam insert real modal analysis

In this case the wheel model is composed only by the foam insert. In the following analysis only the model geometry is changed. All the simulation parameters are the exact same of the one used for the entire wheel analysis. In Figure 5.3.2.1 the wheel model is shown. Table 5.3.2.1 shows some model geometric element, such as nodes and hexa element. Table 5.3.2.2 shows the first twenty flexible modes frequencies for both LUPOS and Solidworks. From Figure 5.3.2.2 to Figure 5.3.2.41 the modes are shown.

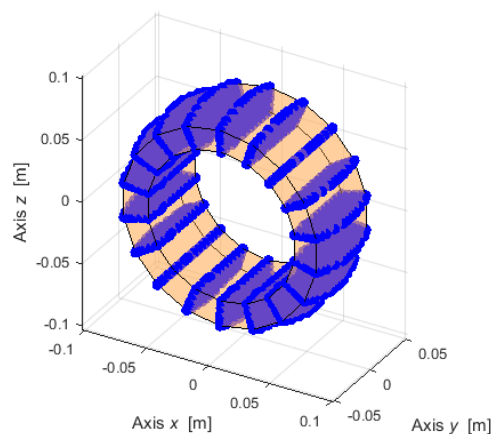


Figure 5.3.2.1 – Wheel model with foam only.

Table 5.3.2.1 –Model geometric element.

Element	Number
Geo	1746
Hex	1368

Table 5.3.2.2 –Modes frequency.

Mode	LUPOS	Description	Solidworks
------	-------	-------------	------------

	Frequency [Hz]		Frequency [Hz]
7	614	1 st Flexural	513.4
8	614	2 nd Flexural	513.4
9	871	3 rd Flexural	786
10	871	4 th Flexural	786
11	1735	5 th Flexural	1363
12	1735	6 th Flexural	1363
13	2202	7 th Flexural	1960
14	2202	8 th Flexural	1961
15	2237	1 st Axial	2154
16	2285	9 th Flexural	2235
17	2285	10 th Flexural	2235
18	2349	2 nd Axial	2347
19	3001	11 th Flexural	2416
20	3001	12 th Flexural	2416
21	3270	13 th Flexural	2842
22	3270	14 th Flexural	2844
23	3321	15 th Flexural	3220
24	3321	16 th Flexural	3220
25	3729	17 th Flexural	3224
26	3729	18 th Flexural	3225

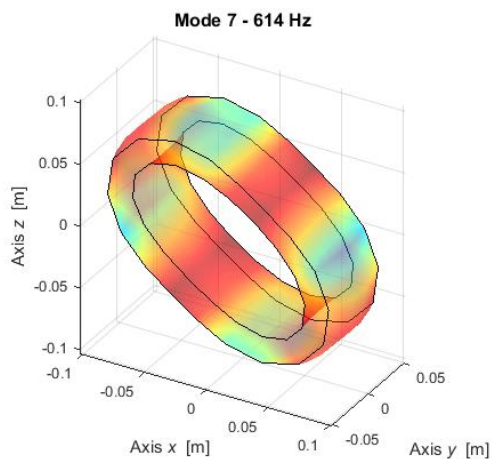


Figure 5.3.2.2 – LUPOS Mode 7.

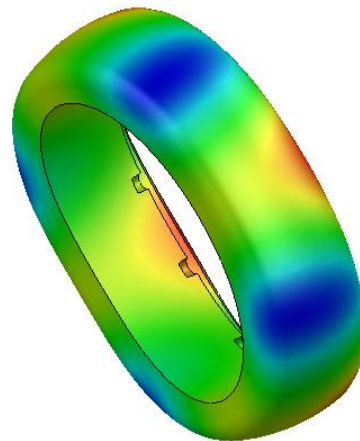


Figure 5.3.2.3 – Solidworks Mode 7.

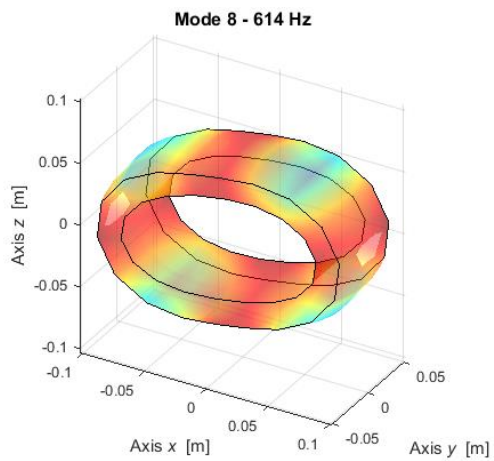


Figure 5.3.2.4 – LUPOS Mode 8.

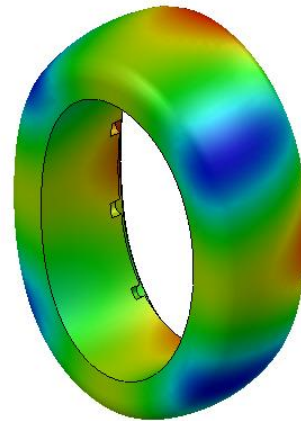


Figure 5.3.2.5 – Solidworks Mode 8.

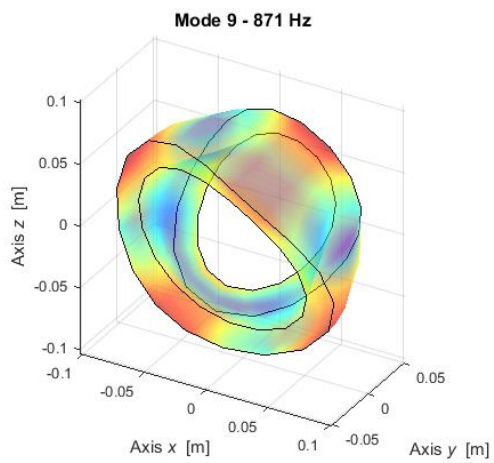


Figure 5.3.2.6 – LUPOS Mode 9.

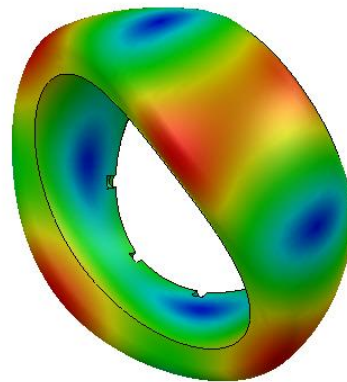


Figure 5.3.2.7 – Solidworks Mode 9.

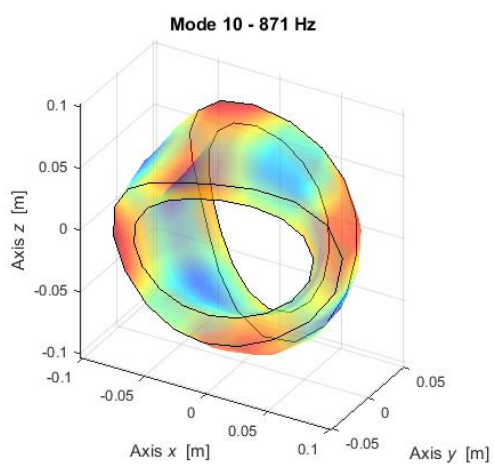


Figure 5.3.2.8 – LUPOS Mode 10.

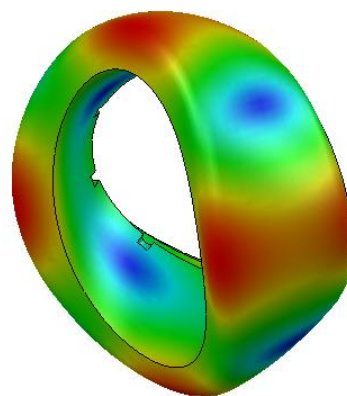


Figure 5.3.2.9 – Solidworks Mode 10.

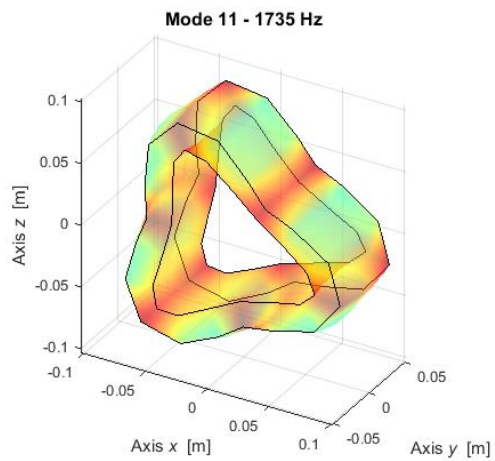


Figure 5.3.2.10 – LUPOS Mode 11.

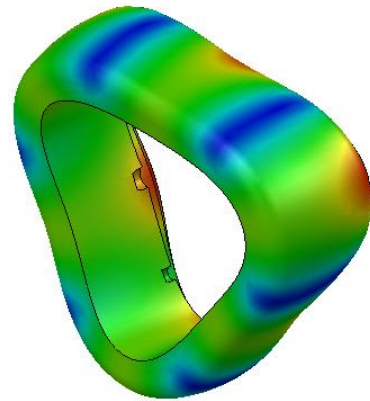


Figure 5.3.2.11 – Solidworks Mode 11.

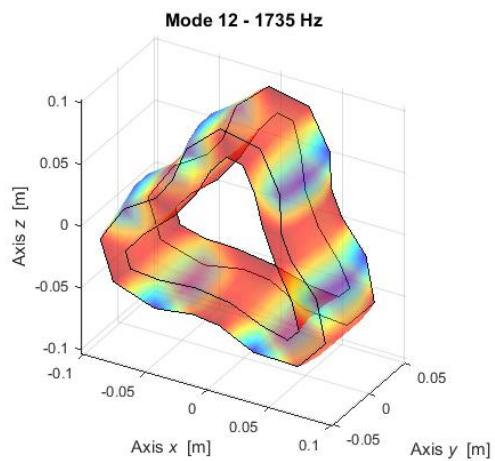


Figure 5.3.2.12 – LUPOS Mode 12.

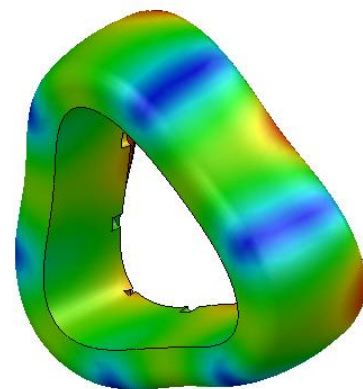


Figure 5.3.2.13 – Solidworks Mode 12.

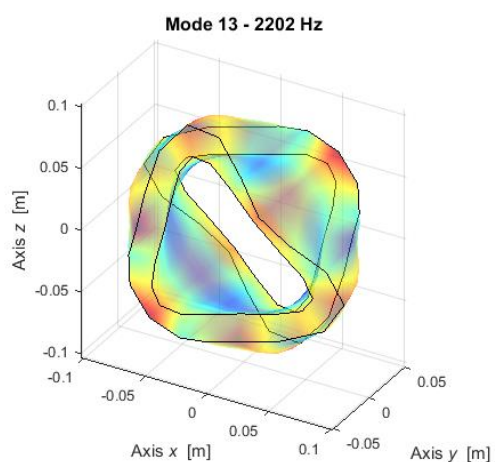


Figure 5.3.2.14 – LUPOS Mode 13.

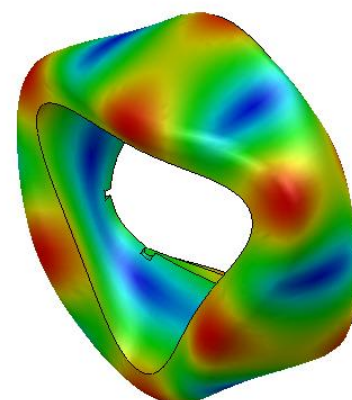


Figure 5.3.2.15 – Solidworks Mode 13

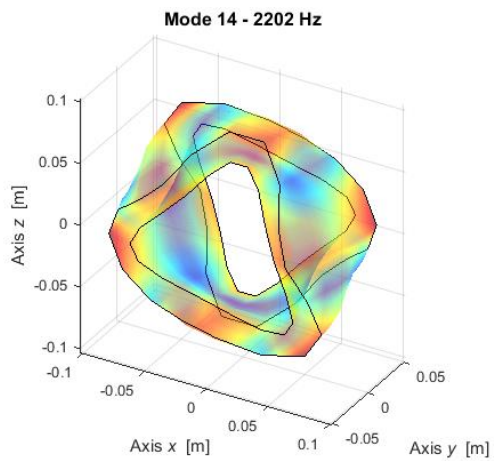


Figure 5.3.2.16 – LUPUS Mode 14.

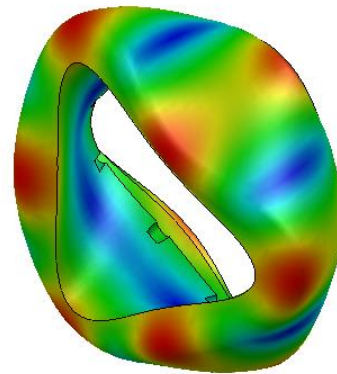


Figure 5.3.2.17 – Solidworks Mode 14.

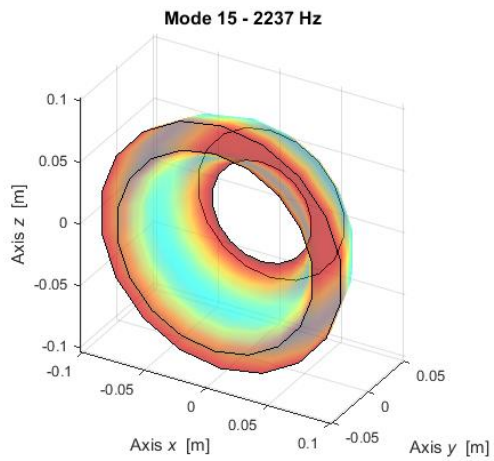


Figure 5.3.2.18 – LUPUS Mode 15.

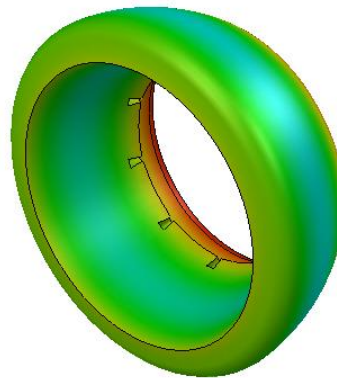


Figure 5.3.2.19 – Solidworks Mode 15.

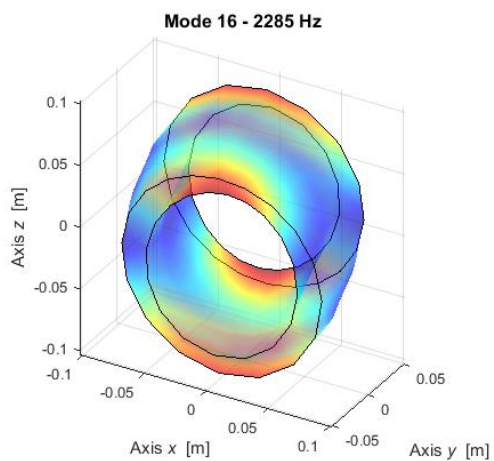


Figure 5.3.2.20 – LUPUS Mode 16.

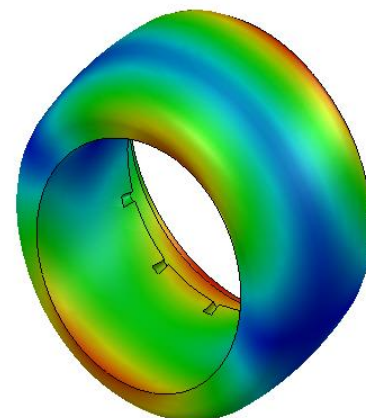


Figure 5.3.2.21 – Solidworks Mode 16.

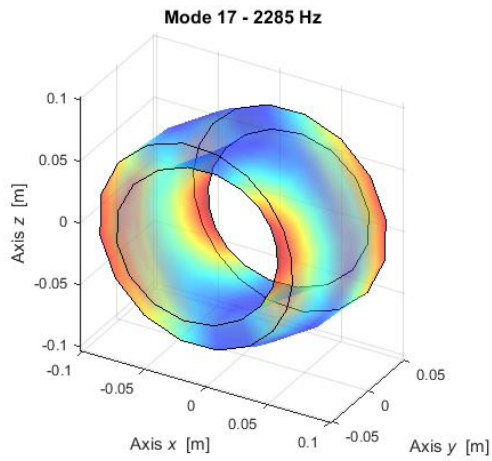


Figure 5.3.2.22 – LUPUS Mode 17.

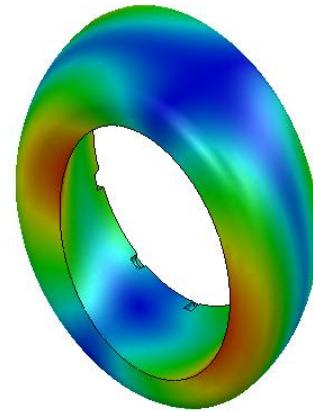


Figure 5.3.2.23 – Solidworks Mode 17.

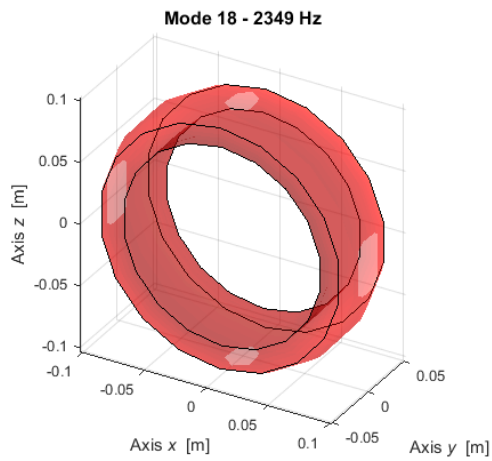


Figure 5.3.2.24 – LUPUS Mode 18.

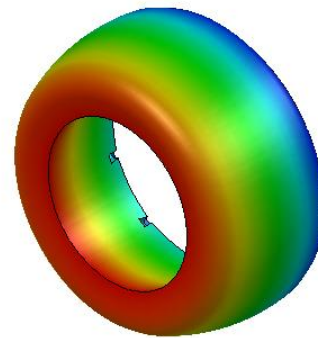


Figure 5.3.2.25 – Solidworks Mode 18.

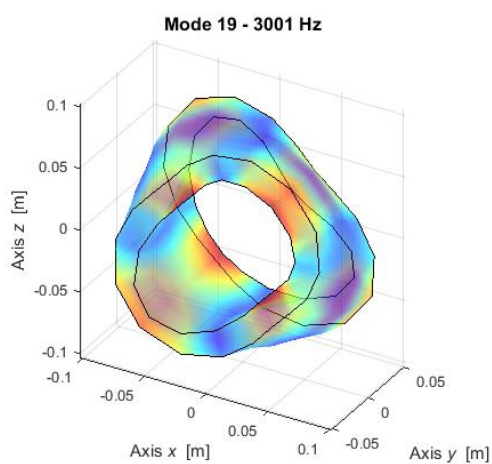


Figure 5.3.2.26 – LUPUS Mode 19.

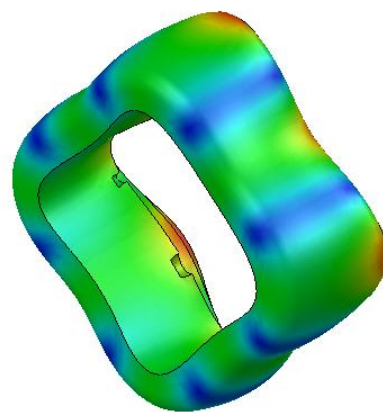


Figure 5.3.2.27 – Solidworks Mode 19.

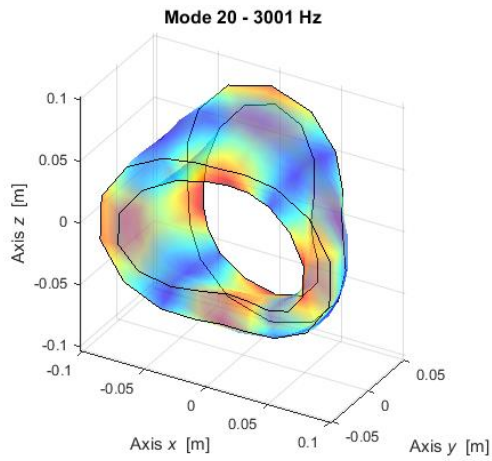


Figure 5.3.2.28 – LUPOS Mode 20.

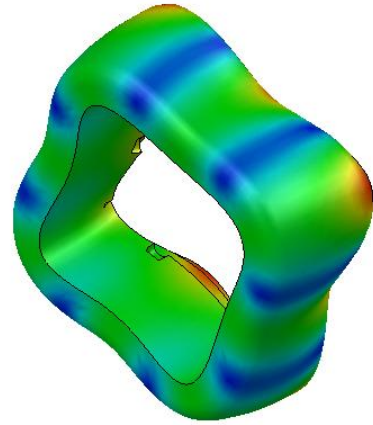


Figure 5.3.2.29 – Solidworks Mode 20.

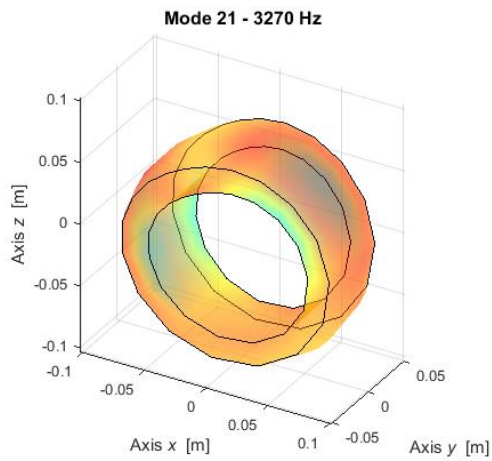


Figure 5.3.2.30 – LUPOS Mode 21.

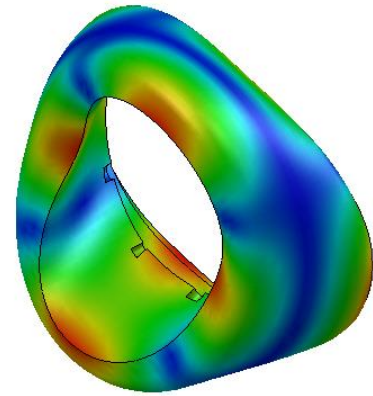


Figure 5.3.2.31 – Solidworks Mode 21.

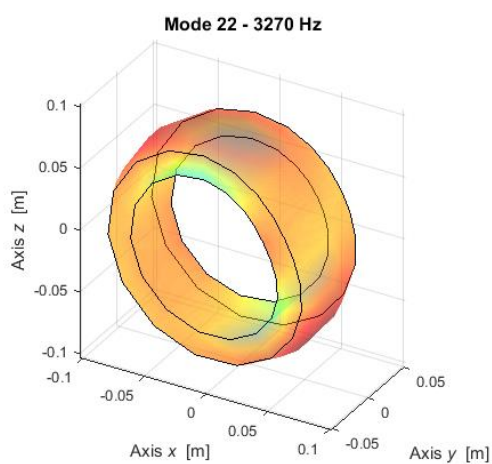


Figure 5.3.2.32 – LUPOS Mode 22.

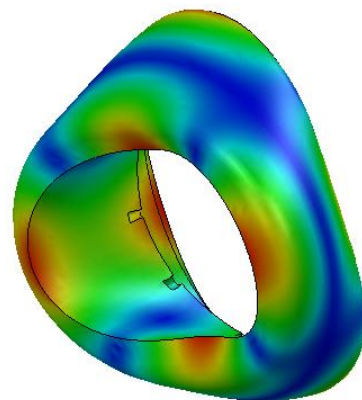


Figure 5.3.2.33 – Solidworks Mode 22.

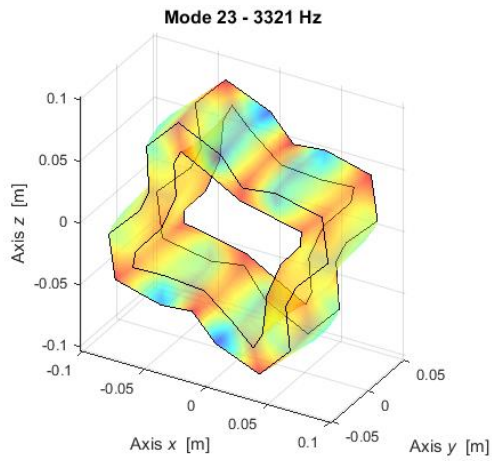


Figure 5.3.2.34 – LUPUS Mode 23.

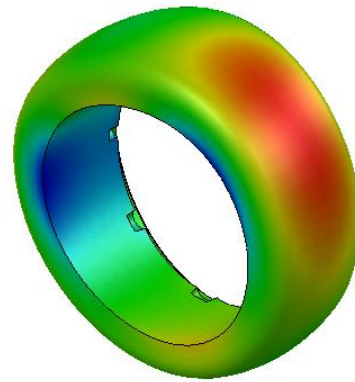


Figure 5.3.2.35 – Solidworks Mode 23.

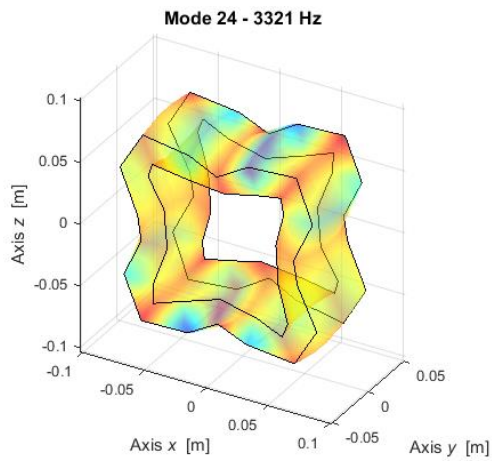


Figure 5.3.2.36 – LUPUS Mode 24.

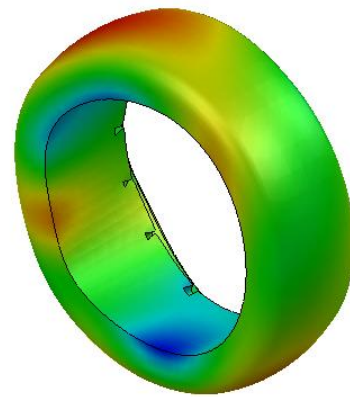


Figure 5.3.2.37 – Solidworks Mode 24.

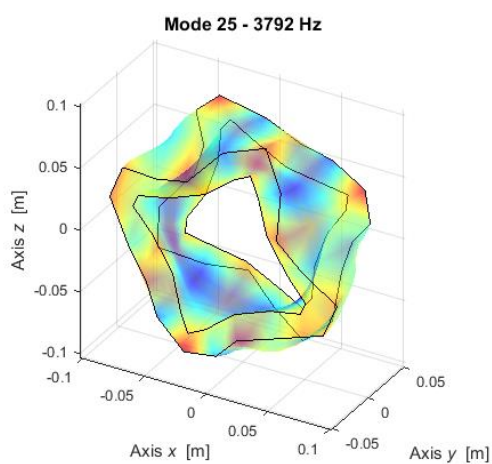


Figure 5.3.2.38 – LUPUS Mode 25.

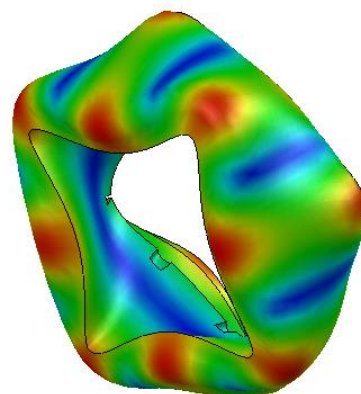


Figure 5.3.2.39 – Solidworks Mode 25.

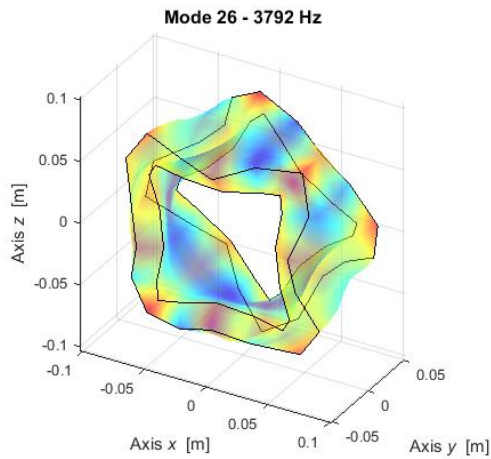


Figure 5.3.2.40 – LUPOS Mode 26.

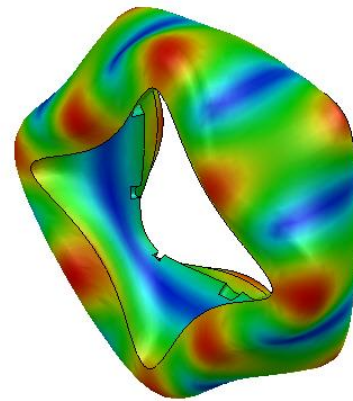


Figure 5.3.2.41 – Solidworks Mode 26.

5.3.3 Tyre real modal analysis

In this case the wheel model is composed only by the tyre. In the following analysis only the model geometry is changed. All the simulation parameters are the exact same of the one used for the entire wheel analysis. In Figure 5.3.3.1 the wheel model is shown. Table 5.3.3.1 shows some model geometric element, such as nodes, rigid joints, and shell elements. Table 5.3.3.2 shows the first twenty flexible modes frequencies for both LUPOS and Solidworks. From Figure 5.3.3.2 to Figure 5.3.3.41 the modes are shown.

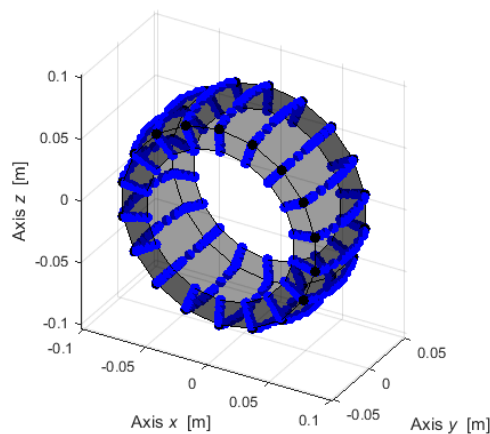


Figure 5.3.3.1 – Wheel model with tyre only.

Table 5.3.3.1 –Model geometric element.

Element	Number
Geo	486
Rjs	36
Sh4	432

Table 5.3.3.2 –Modes frequency.

Mode	LUPOS Frequency [Hz]	Description	Solidworks Frequency [Hz]
7	31.68	1 st Flexural	29.1
8	31.68	2 nd Flexural	29.2
9	34.72	3 rd Flexural	39.7
10	34.72	4 th Flexural	39.7
11	45.63	1 st Axial	44.3
12	46.86	5 th Flexural	50.4
13	46.86	6 th Flexural	50.4
14	49.88	7 th Flexural	67.3
15	49.88	8 th Flexural	67.6
16	52.23	9 th Flexural	69.6
17	52.23	10 th Flexural	70.1
18	52.24	2 nd Axial	70.3
19	52.67	11 th Flexural	76.2
20	52.67	12 th Flexural	76.3
21	62.46	13 th Flexural	83.1
22	62.46	14 th Flexural	83.2
23	63.6	15 th Flexural	85
24	63.6	16 th Flexural	85.2
25	79.07	17 th Flexural	108.3
26	79.07	18 th Flexural	108.3

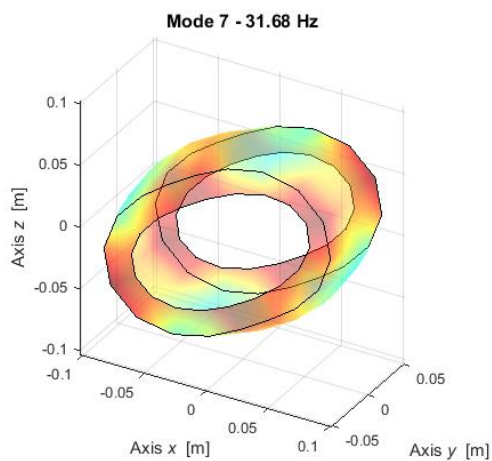


Figure 5.3.3.2 – LUPOS Mode 7.

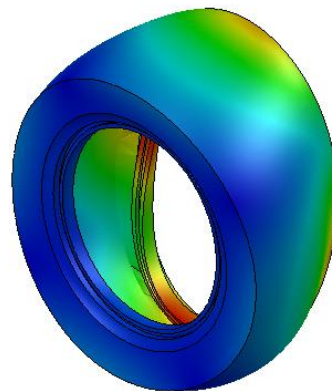


Figure 5.3.3.3 – Solidworks Mode 7.

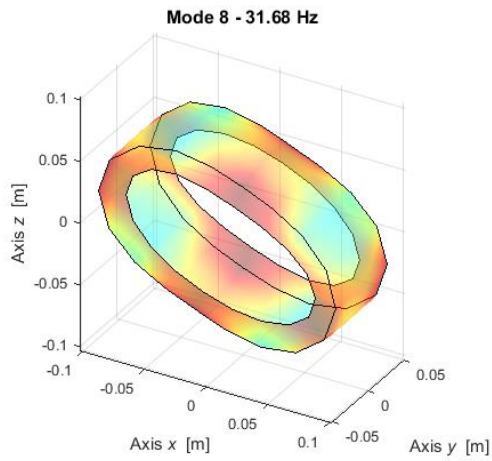


Figure 5.3.3.4 – LUPOS Mode 8.

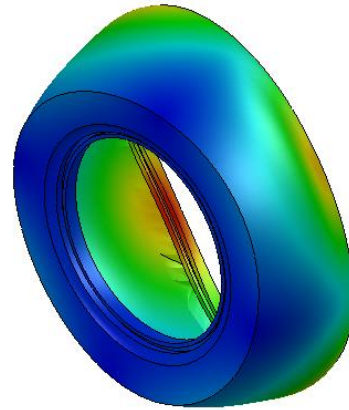


Figure 5.3.3.5 – Solidworks Mode 8.

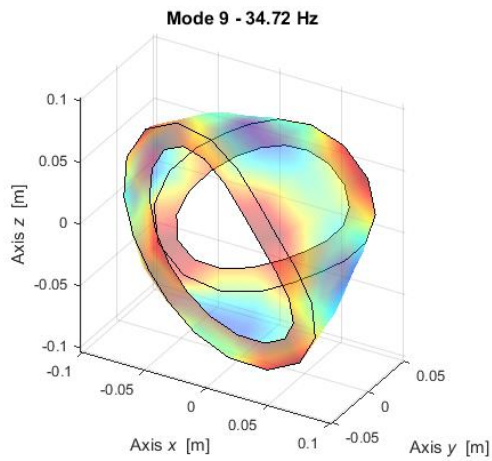


Figure 5.3.3.6 – LUPOS Mode 9.

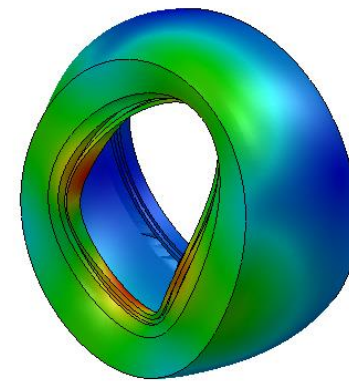


Figure 5.3.3.7 – Solidworks Mode 9.

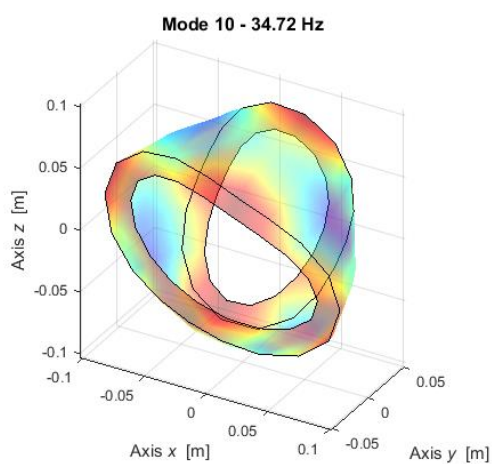


Figure 5.3.3.8 – LUPOS Mode 10.

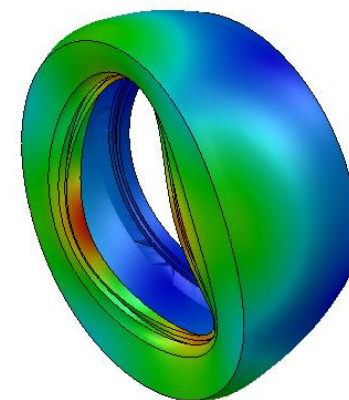


Figure 5.3.3.9 – Solidworks Mode 10.

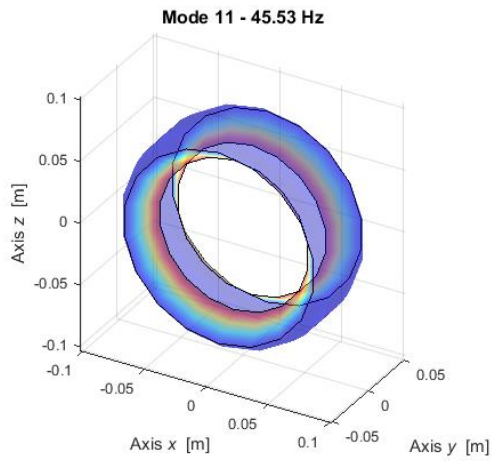


Figure 5.3.3.10 – LUPOS Mode 11.

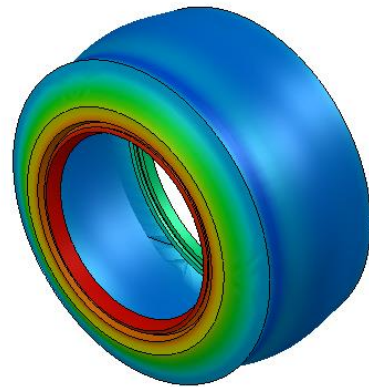


Figure 5.3.3.11 – Solidworks Mode 11.

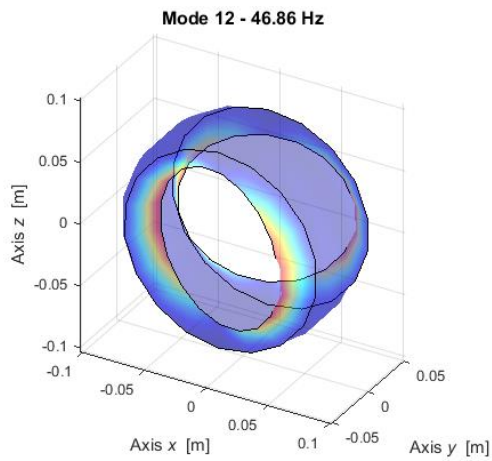


Figure 5.3.3.12 – LUPOS Mode 12.

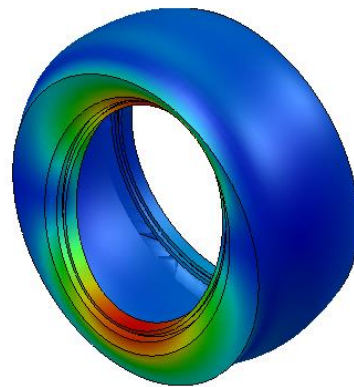


Figure 5.3.3.13 – Solidworks Mode 12.

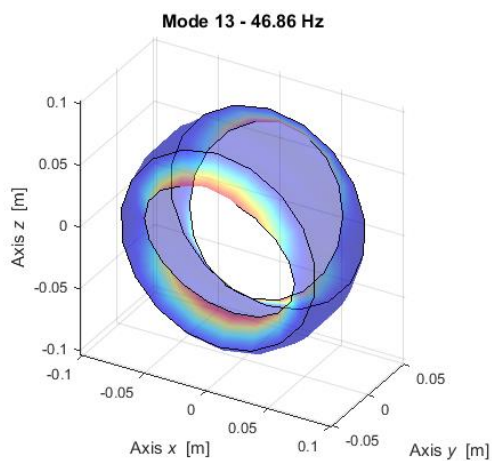


Figure 5.3.3.14 – LUPOS Mode 13.

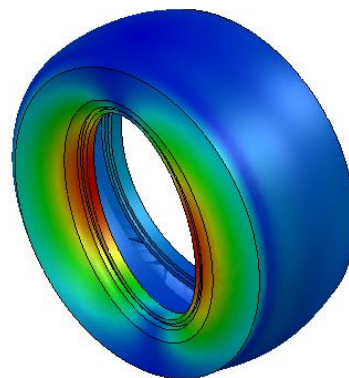


Figure 5.3.3.15 – Solidworks Mode 13

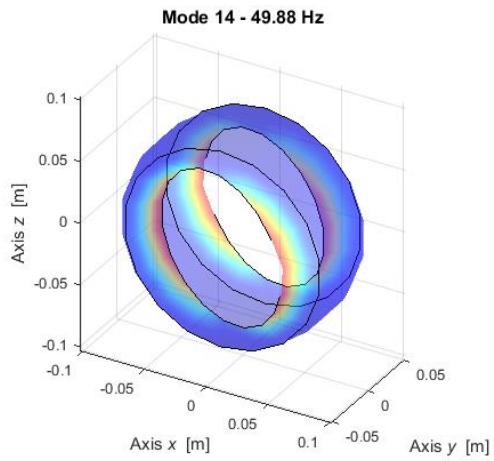


Figure 5.3.3.16 – LUPOS Mode 14.

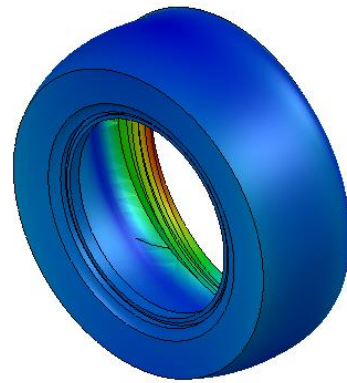


Figure 5.3.3.17 – Solidworks Mode 14.

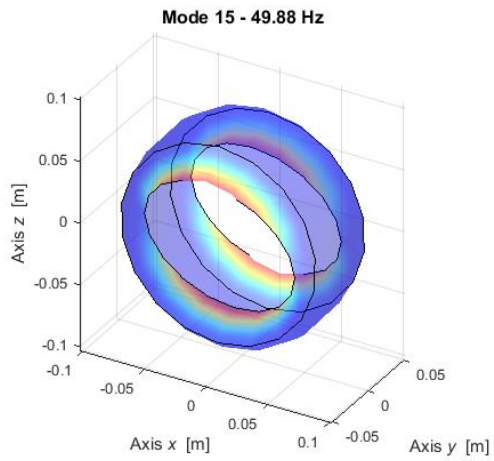


Figure 5.3.3.18 – LUPOS Mode 15.

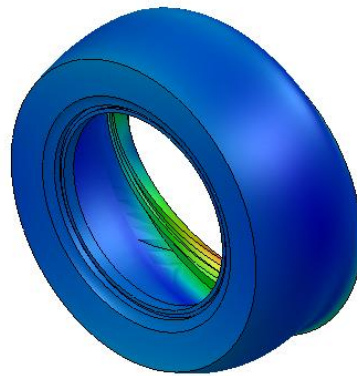


Figure 5.3.3.19 – Solidworks Mode 15.

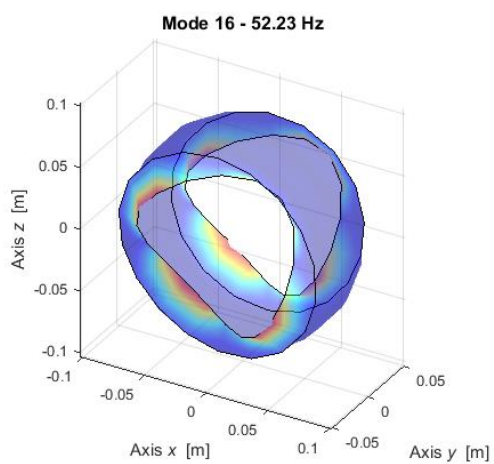


Figure 5.3.3.20 – LUPOS Mode 16.

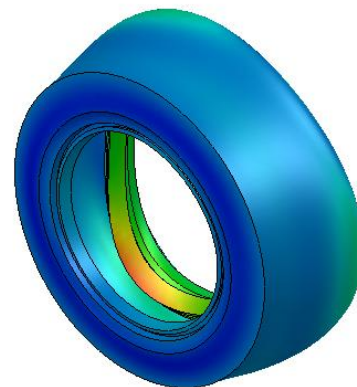


Figure 5.3.3.21 – Solidworks Mode 16.

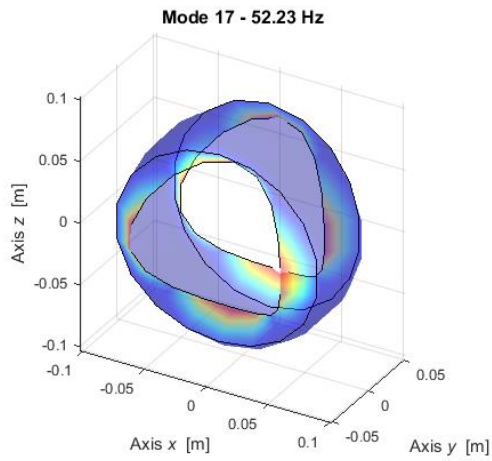


Figure 5.3.3.22 – LUPOS Mode 17.

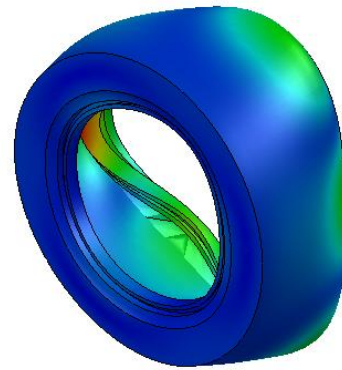


Figure 5.3.3.23 – Solidworks Mode 17.

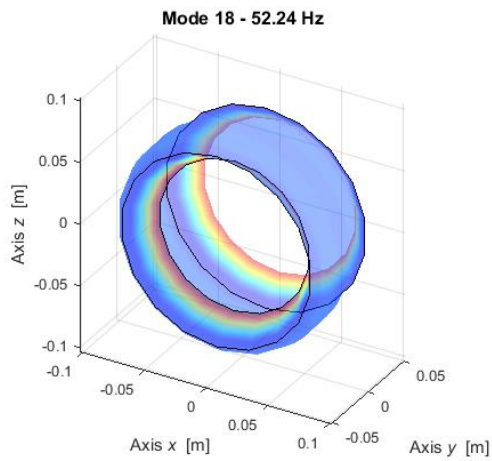


Figure 5.3.3.24 – LUPOS Mode 18.

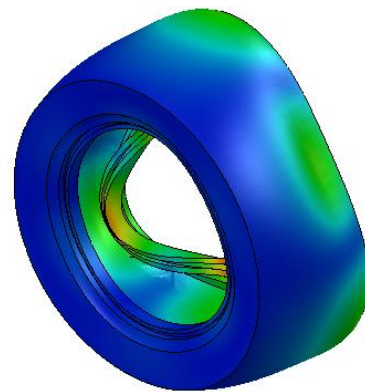


Figure 5.3.3.25 – Solidworks Mode 18.

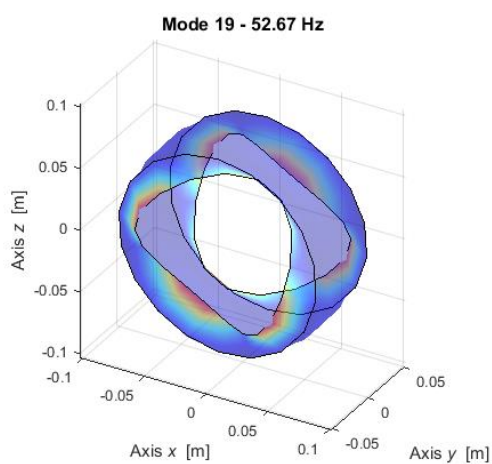


Figure 5.3.3.26 – LUPOS Mode 19.

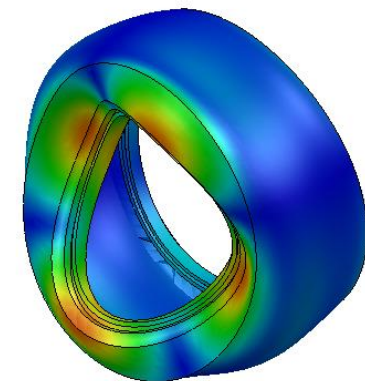


Figure 5.3.3.27 – Solidworks Mode 19.

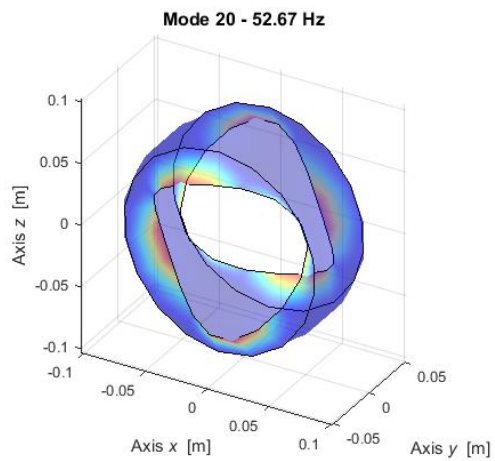


Figure 5.3.3.28 – LUPOS Mode 20.

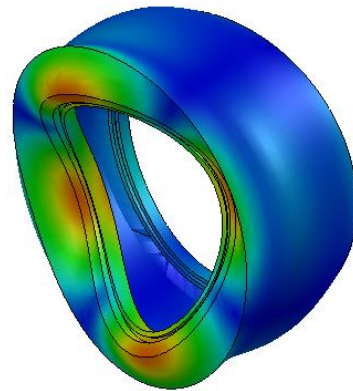


Figure 5.3.3.29 – Solidworks Mode 20.

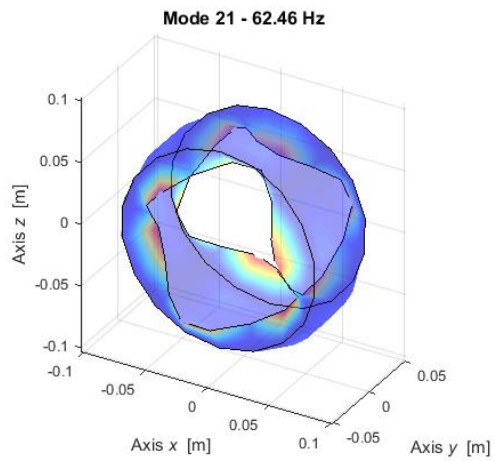


Figure 5.3.3.30 – LUPOS Mode 21.

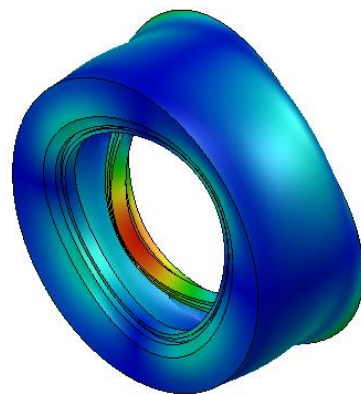


Figure 5.3.3.31 – Solidworks Mode 21.

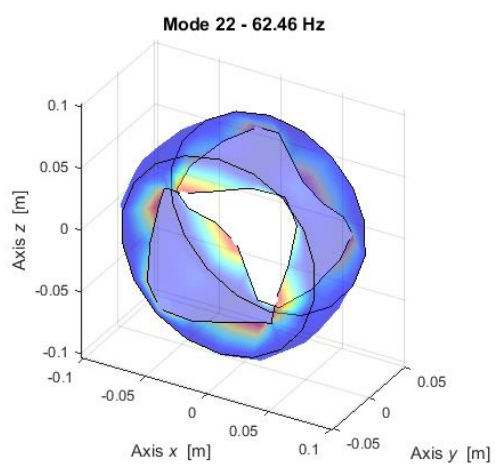


Figure 5.3.3.32 – LUPOS Mode 22.

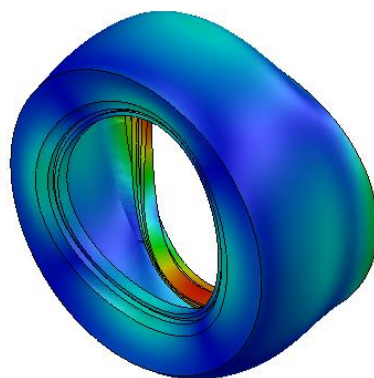


Figure 5.3.3.33 – Solidworks Mode 22.

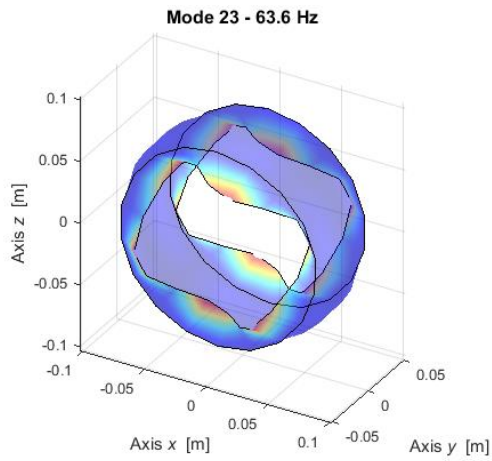


Figure 5.3.3.34 – LUPOS Mode 23.

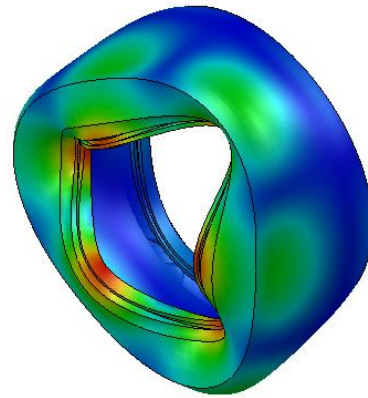


Figure 5.3.3.35 – Solidworks Mode 23.

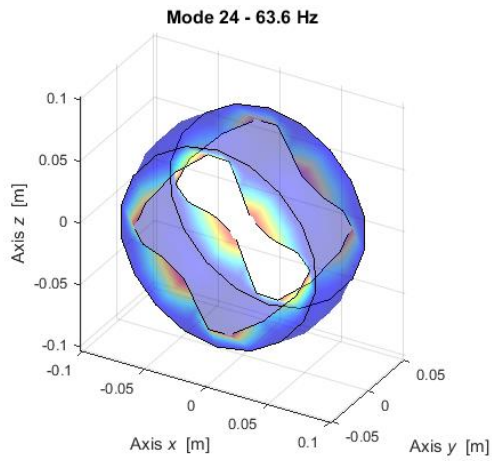


Figure 5.3.3.36 – LUPOS Mode 24.

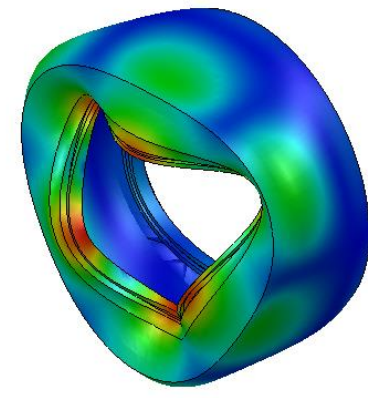


Figure 5.3.3.37 – Solidworks Mode 24.

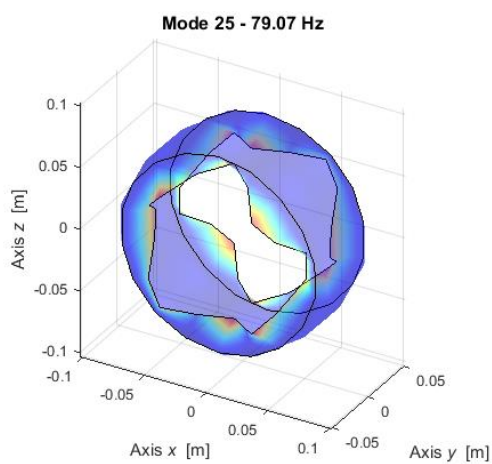


Figure 5.3.3.38 – LUPOS Mode 25.

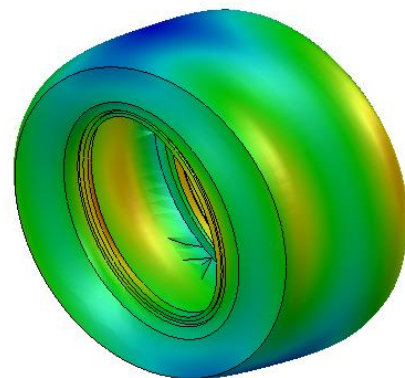


Figure 5.3.3.39 – Solidworks Mode 25.

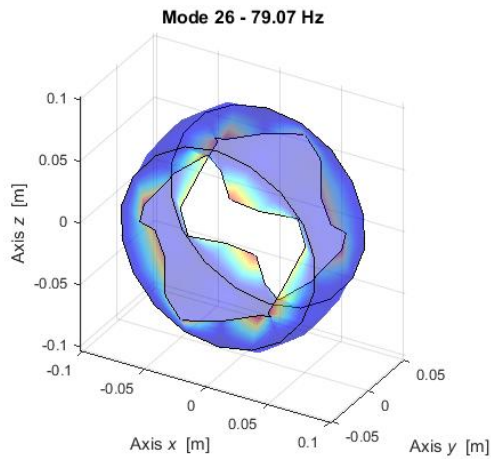


Figure 5.3.3.40 – LUPOS Mode 26.

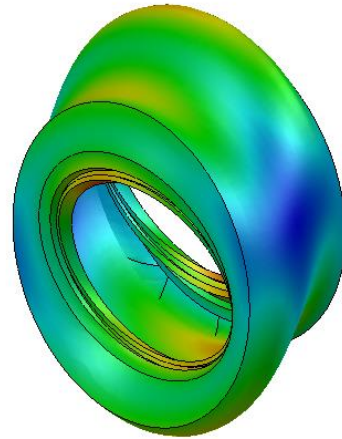


Figure 5.3.3.41 – Solidworks Mode 26.

5.4 Pinned real modal analysis

During the working condition the wheel is not free; it is in fact attached to the wheel hub. For this reason, also a pinned analysis is done to see if there are any differences.

For this analysis the inner disc nodes are linked to a fixed point that simulate the wheel hub attachment (Figure 5.4.1). Table 5.4.1 shows the first 20 modes frequency for both LUPOS and Solidworks. Figure 5.4.2 to Figure 5.4.41 show the modes deformation.

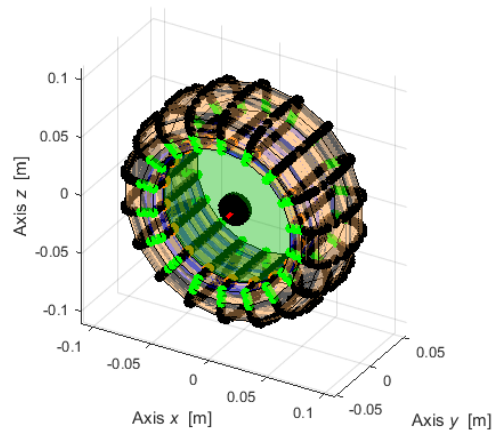


Figure 5.4.1 – Pinned wheel model.

Table 5.4.1 –Modes frequency.

Mode	LUPOS Frequency [Hz]	Description	Solidworks Frequency [Hz]
1	33.59	1 st Flexural	50
2	33.59	2 nd Flexural	50
3	80.75	1 st Axial	97
4	110.7	2 nd Axial	140
5	251	3 rd Flexural	324

6	251	4 th Flexural	330
7	593.7	5 th Flexural	487
8	593.7	6 th Flexural	488
9	934.4	7 th Flexural	969
11	934.4	8 th Flexural	969
11	1453	9 th Flexural	1092
12	1453	10 th Flexural	1096
13	1617	3 rd Axial	1349
14	1644	11 th Flexural	1356
15	1644	12 th Flexural	1365
16	1647	4 th Axial	1634
17	1836	13 th Flexural	1640
18	1836	14 th Flexural	1655
19	1843	15 th Flexural	1666
20	1843	16 th Flexural	1739

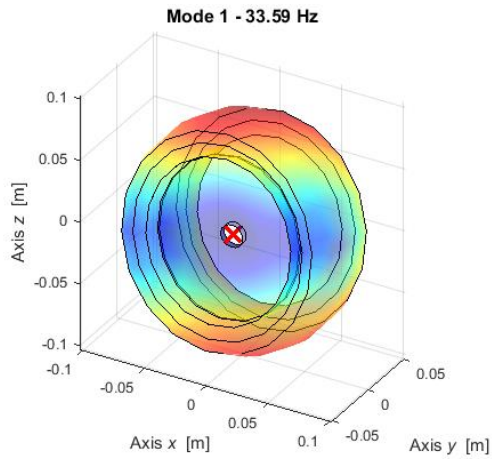


Figure 5.4.2 – LUPOS Mode 7.

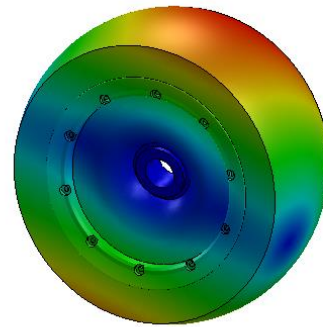


Figure 5.4.3 – Solidworks Mode 7.

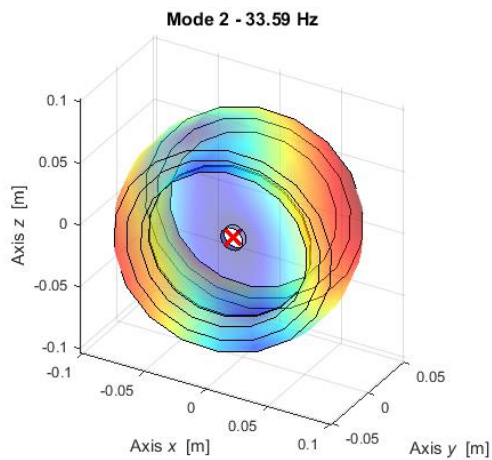


Figure 5.4.4 – LUPOS Mode 8.

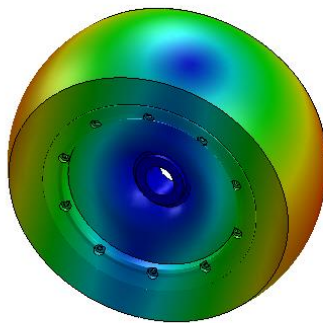


Figure 5.4.5 – Solidworks Mode 8.

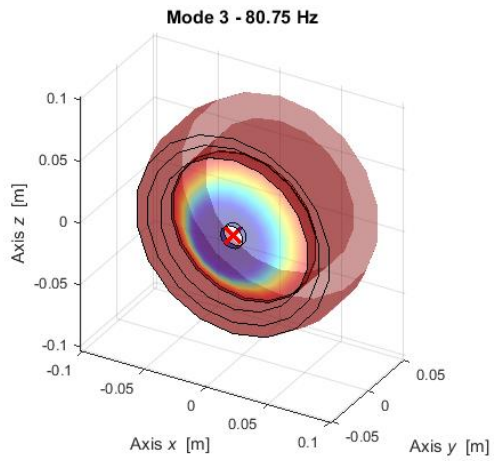


Figure 5.4.6 – LUPOS Mode 9.

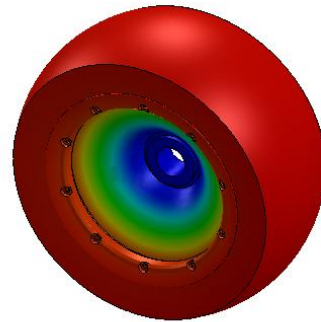


Figure 5.4.7 – Solidworks Mode 9.

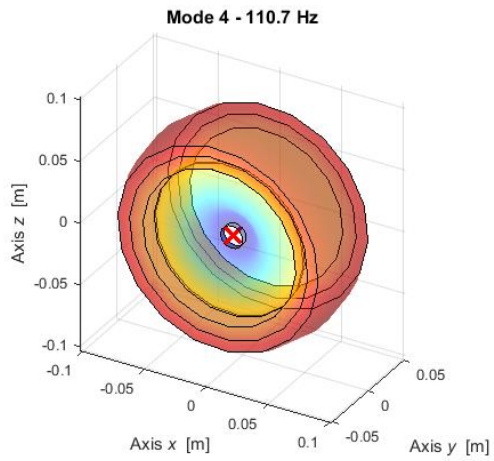


Figure 5.4.8 – LUPOS Mode 10.

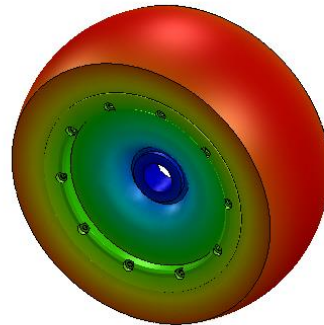


Figure 5.4.9 – Solidworks Mode 10.

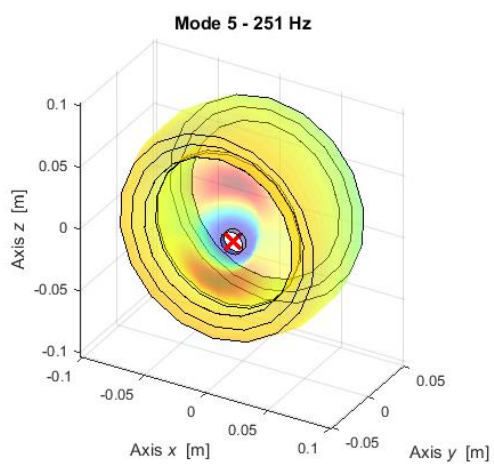


Figure 5.4.10 – LUPOS Mode 11.

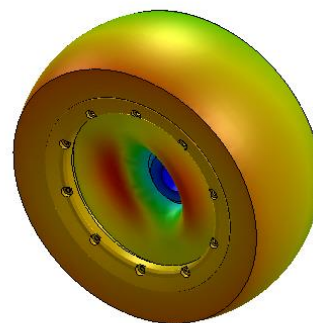


Figure 5.4.11 – Solidworks Mode 11.

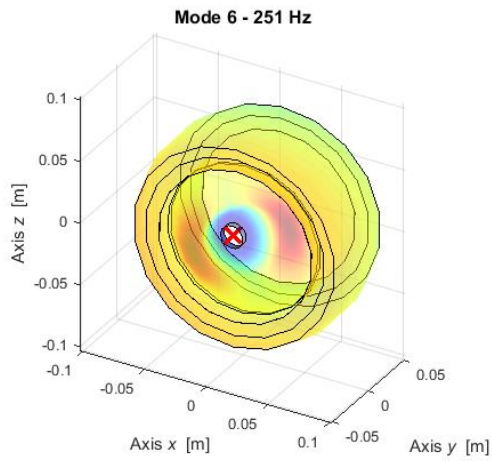


Figure 5.4.12 – LUPOS Mode 12.

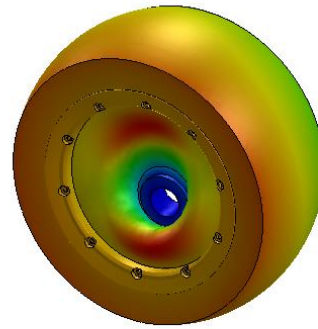


Figure 5.4.13 – Solidworks Mode 12.

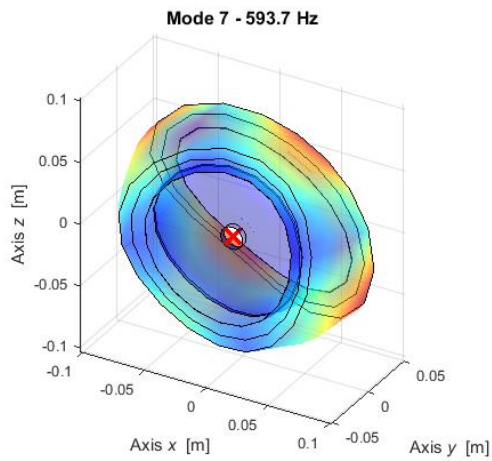


Figure 5.4.14 – LUPOS Mode 13.

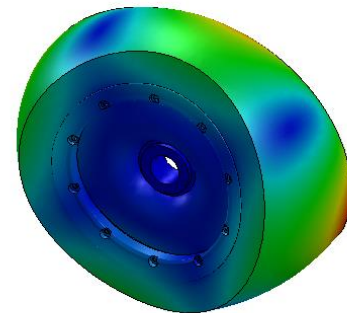


Figure 5.4.15 – Solidworks Mode 13

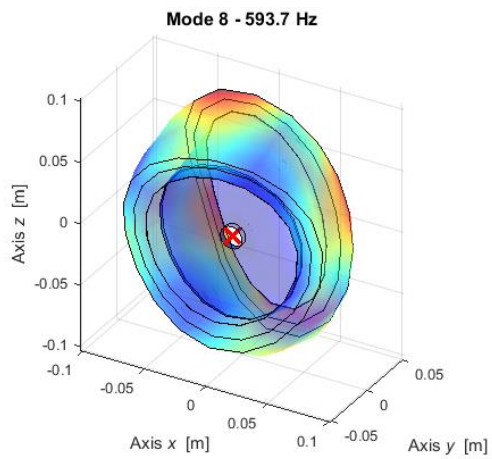


Figure 5.4.16 – LUPOS Mode 14.

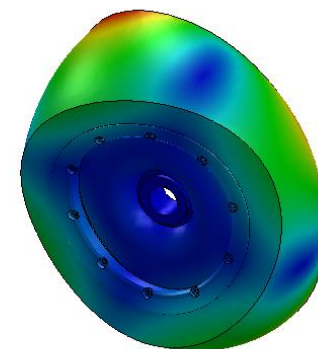


Figure 5.4.17 – Solidworks Mode 14.

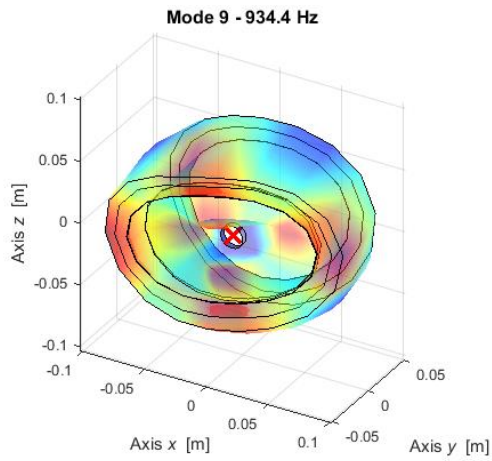


Figure 5.4.18 – LUPOS Mode 15.

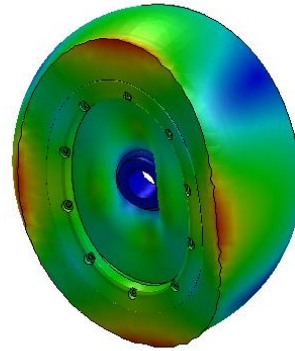


Figure 5.4.19 – Solidworks Mode 15.

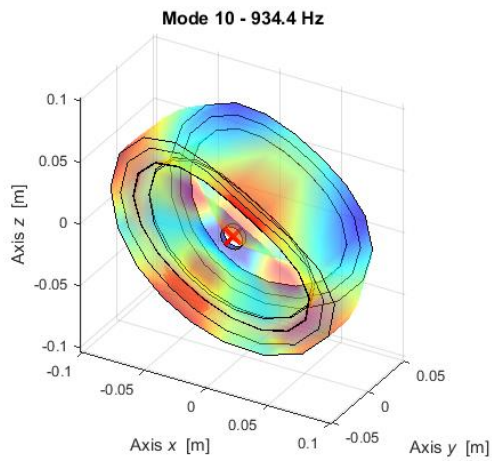


Figure 5.4.20 – LUPOS Mode 16.

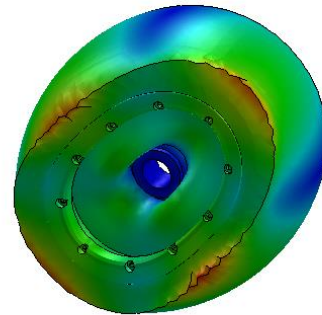


Figure 5.4.21 – Solidworks Mode 16.

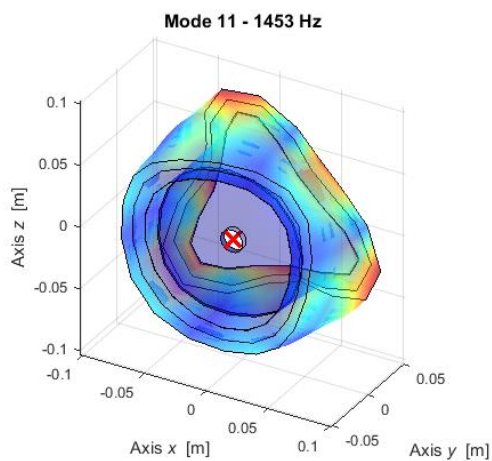


Figure 5.4.22 – LUPOS Mode 17.

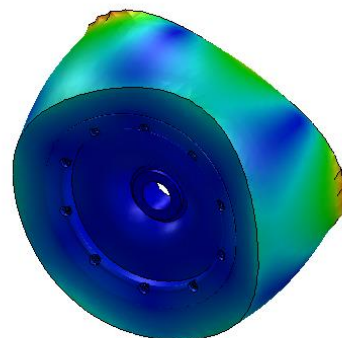


Figure 5.4.23 – Solidworks Mode 17.

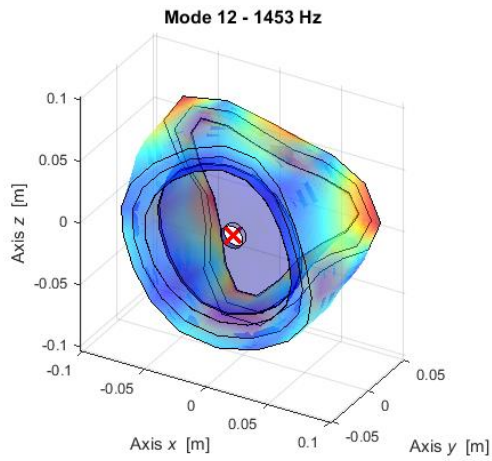


Figure 5.4.24 – LUPOS Mode 18.

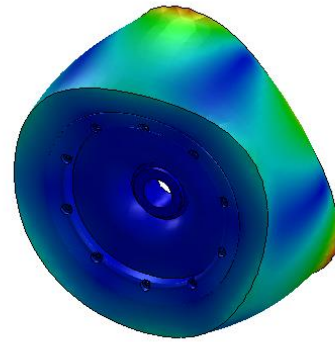


Figure 5.4.25 – Solidworks Mode 18.

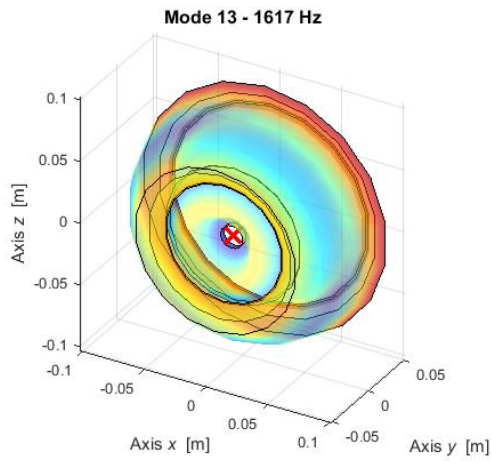


Figure 5.4.26 – LUPOS Mode 19.

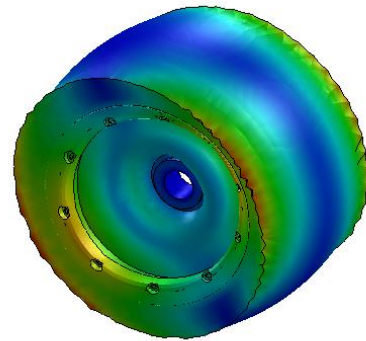


Figure 5.4.27 – Solidworks Mode 19.

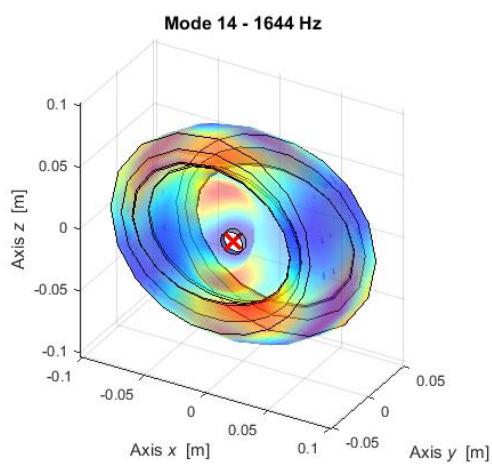


Figure 5.4.28 – LUPOS Mode 20.

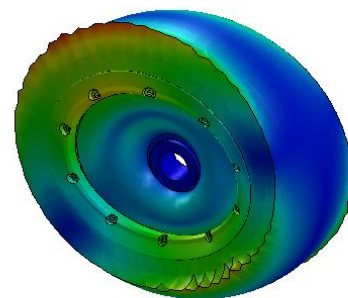


Figure 5.4.29 – Solidworks Mode 20.

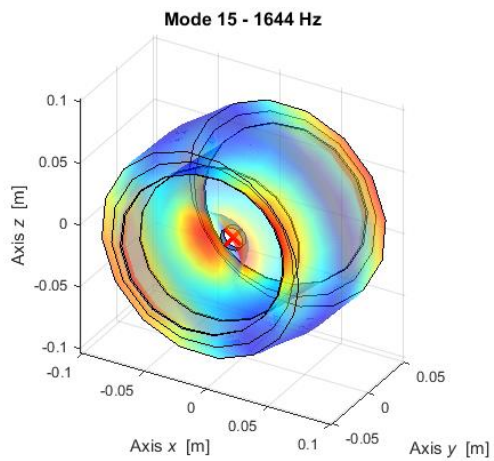


Figure 5.4.30 – LUPOS Mode 21.

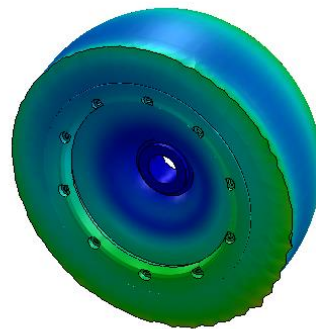


Figure 5.4.31 – Solidworks Mode 21.

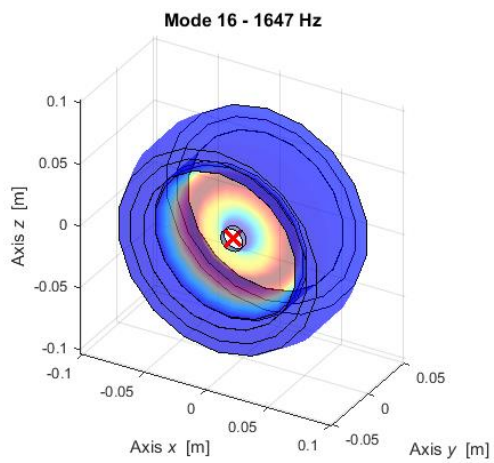


Figure 5.4.32 – LUPOS Mode 22.

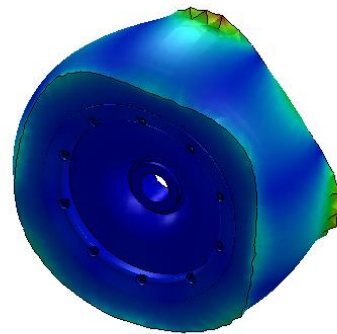


Figure 5.4.33 – Solidworks Mode 22.

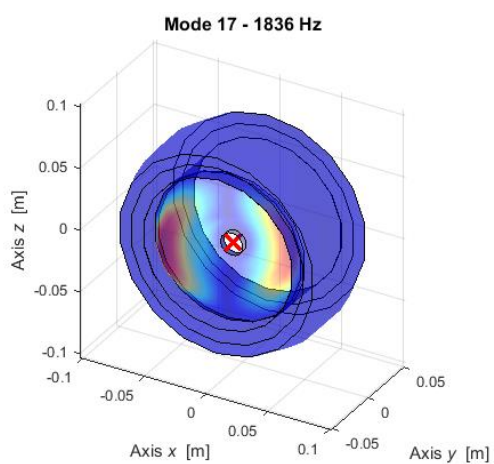


Figure 5.4.34 – LUPOS Mode 23.

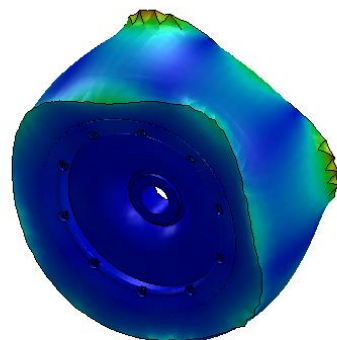


Figure 5.4.35 – Solidworks Mode 23.

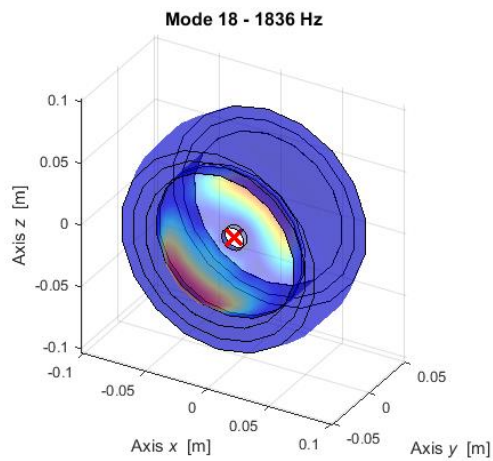


Figure 5.4.36 – LUPOS Mode 24.

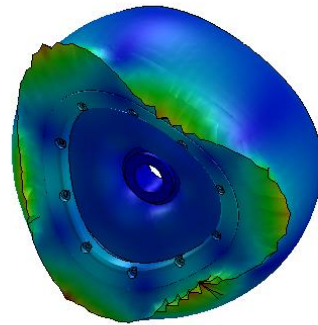


Figure 5.4.37 – Solidworks Mode 24.

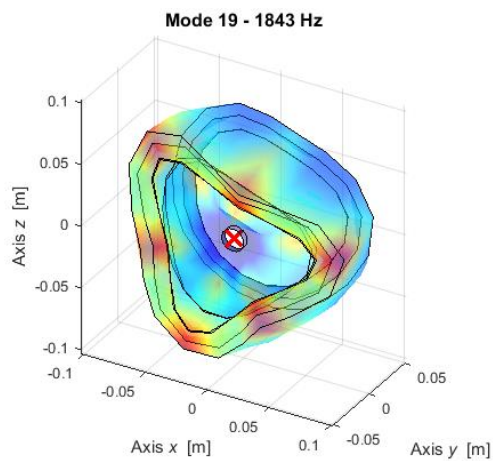


Figure 5.4.38 – LUPOS Mode 25.

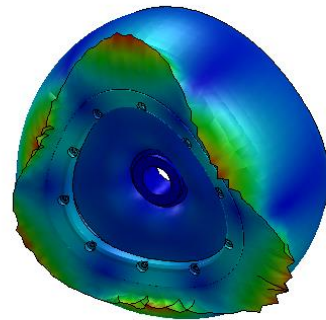


Figure 5.4.39 – Solidworks Mode 25.

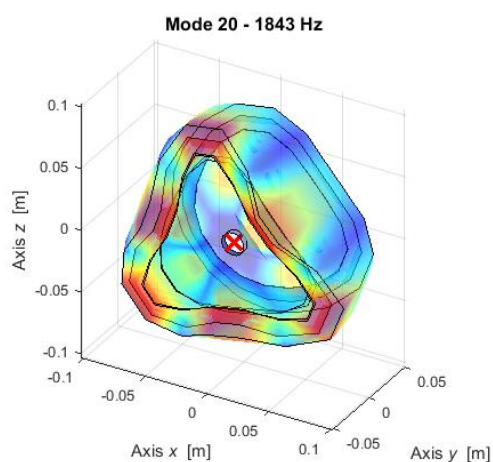


Figure 5.4.40 – LUPOS Mode 26.

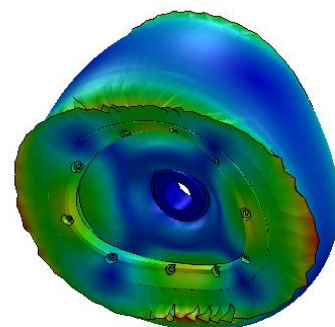


Figure 5.4.41 – Solidworks Mode 26.

5.5 Results comparison

As it is possible to see from the previous chapters, the resultant modes are quite different in both frequency values and deformations comparing the free and the pinned wheel study. The easiest thing to note is the fact that in the pinned configuration there are some modes at low frequency, while in the free one the first mode is over 400 Hz. At higher frequency the modes for the two configurations tend to be more similar or even perfectly equal.

Apart from these differences, the frequency results and the deformations of the two software simulations (Lupos and Solidworks) are quite the same for all the analysis.

Conclusions

In this paper, the wheel has been analysed both statically and dynamically. The tests lead to the estimation of the wheel stiffness for both the wheel configurations. These results could be useful for further study on this scale vehicle.

Other than this, the studied wheel has been dismantled and studied in each single component. Using Solidworks and Lupos it was possible to create a model that correspond well to the real wheel. Looking at the simulations results it is possible too see how both the software lead to the same response in term of natural frequencies.

These models, that have been useful for the stiffness estimation could be used for future testing. A complete Lupos vehicle study for example, could implement this wheel model directly as they are thanks to the optimization process developed in this paper.

In conclusion, the main aim of the thesis is achieved. The stiffnesses have been estimated and a model has been built for future tests.

Reference

- [1] De Giuseppe G., *Experimental setup for RC car suspensions*, MSc Thesis, I Facoltà di Ingegneria Politecnico di Torino, 2019.
- [2] <https://www.pcb.com/products?model=208c02> available in 2019-12.
- [3] <https://www.keyence.it/products/measure/laser-1d/lk-g5000/models/lk-h050/> available in 2019-12
- [4] <http://www.losi.com/Products/Default.aspx?ProdID=LOS05014T1> available in 2020-06-10
- [5] <http://www-mdp.eng.cam.ac.uk/web/library/enginfo/cueddatabooks/materials.pdf> available in 2020-07-13
- [6] <https://www.makeitfrom.com/material-properties/Epichlorohydrin-Copolymer-Rubber-ECO> available in 2020-07-13
- [7] Bonisoli, Prandina, Marcuccio, Esposito, Brino, Manca, Scapolan, Lisitano, Dimauro, Lomuscio, Venturini, Vella: *LUPOS - Lumped Parameters Open Source FEM code* - Tutorial – v.2020-06-16.